
Masters Theses

Student Theses and Dissertations

Summer 2013

3D seismic data interpretation of Boonsville Field, Texas

Aamer Ali Alhakeem

Follow this and additional works at: https://scholarsmine.mst.edu/masters_theses



Part of the [Geology Commons](#), and the [Geophysics and Seismology Commons](#)

Department:

Recommended Citation

Alhakeem, Aamer Ali, "3D seismic data interpretation of Boonsville Field, Texas" (2013). *Masters Theses*. 7122.

https://scholarsmine.mst.edu/masters_theses/7122

This thesis is brought to you by Scholars' Mine, a service of the Missouri S&T Library and Learning Resources. This work is protected by U. S. Copyright Law. Unauthorized use including reproduction for redistribution requires the permission of the copyright holder. For more information, please contact scholarsmine@mst.edu.

3D SEISMIC DATA INTERPRETATION OF BOONSVILLE FIELD, TEXAS

by

AAMER ALI ALHAKEEM

A THESIS

Presented to the Faculty of the Graduate School of the
MISSOURI UNIVERSITY OF SCIENCE AND TECHNOLOGY

In Partial Fulfillment of the Requirements for the Degree

MASTER OF SCIENCE IN GEOLOGY AND GEOPHYSICS

2013

Approved by

Dr. Kelly Liu

Dr. Stephen Gao

Dr. Yang Wan

© 2013

Aamer Ali Alhakeem

All Rights Reserved

ABSTRACT

The Boonsville field is one of the largest gas fields in the US located in the Fort Worth Basin, north central Texas. The highest potential reservoirs reside in the Bend Conglomerate deposited during the Pennsylvanian. The Boonsville data set is prepared by the Bureau of Economic Geology at the University of Texas, Austin, as part of the secondary gas recovery program. The Boonsville field seismic data set covers an area of 5.5 mi². It includes 38 wells data. The Bend Conglomerate is deposited in fluvio-deltaic transaction. It is subdivided into many genetic sequences which include depositions of sandy conglomerate representing the potential reserves in the Boonsville field. The geologic structure of the Boonsville field subsurface are visualized by constructing structure maps of Caddo, Davis, Runaway, Beans Cr, Vineyard, and Wade. The mapping includes time structure, depth structure, horizon slice, velocity maps, and isopach maps. Many anticlines and folds are illustrated. Karst collapse features are indicated specially in the lower Atoka. Dipping direction of the Bend Conglomerate horizons are changing from dipping toward north at the top to dipping toward east at the bottom. Stratigraphic interpretation of the Runaway Formation and the Vineyard Formation using well logs and seismic data integration showed presence of fluvial dominated channels, point bars, and a mouth bar. RMS amplitude maps are generated and used as direct hydrocarbon indicator for the targeted formations. As a result, bright spots are indicated and used to identify potential reservoirs. Petrophysical analysis is conducted to obtain gross, net pay, NGR, water saturation, shale volume, porosity, and gas formation factor. Volumetric calculations estimated 989.44 MMSCF as the recoverable original gas in-place for a prospect in the Runaway and 3.32 BSCF for a prospect in the Vineyard Formation.

ACKNOWLEDGMENTS

First and foremost, I would like to express my sincere gratitude to my advisor Dr. Kelly Liu for her continuous support and guidance during my research work. In addition, I would like to spread my deep appreciation and respect to my committee members Dr. Stephen Gao and Dr. Yang Wang; Dr. Stephen Gao for his great advices to end up with a perfect thesis, and Dr. Yang Wang for his informative adds to my petroleum geology understanding.

My thanks to the Saudi Ministry of Higher Education for the scholarship they honored me with to get my master degree. Accordingly, the thanks go to my technical advisor from Saudi Arabian Cultural Mission (SACM), Dr. Nabil Khoury. His help and support creates the best study environment in the US.

It is a great chance to thank all my colleagues in the Department of Geological Sciences and Engineering for motivating me. Thanks for all my officemates at McNutt B16 who made the lab such a friendly place. Special thanks to my colleague Mr. Abdulsaid Ibrahim for sharing helpful ideas.

I would like to thank my mother for giving me all the love that encourages me to the success. Finally, I send tons of thanks to my lovely wife, Mrs. Hashmiah Alsaedi for her continuous support and motivation.

TABLE OF CONTENTS

	Page
ABSTRACT.....	iii
ACKNOWLEDGMENTS	iv
LIST OF ILLUSTRATIONS.....	viii
LIST OF TABLES.....	xiii
NOMENCLATURE	xiv
 SECTION	
1. INTRODUCTION.....	1
1.1. AREA OF STUDY	1
1.2. PREVIOUS STUDIES.....	4
1.3. OBJECTIVES.....	5
2. REGIONAL GEOLOGY	6
2.1. FORT WORTH BASIN.....	6
2.2. GEOLOGICAL STRATIGRAPHY	10
2.2.1. Barnett Shale	12
2.2.2. The Bend Conglomerate.....	14
2.3. GEOLOGICAL STRUCTURES	17
2.4. PETROLEUM SYSTEM.....	18
2.4.1. Source Rock	18
2.4.2. Migration Pathways.....	18
2.4.3. Traps and Reservoirs	19
3. DATA AND METHOD	22

3.1. BOONSVILLE 3D SEISMIC DATA.....	22
3.2. METHOD	29
4. STRUCTURAL INTERPRETATION.....	30
4.1. INTRODUCTION	30
4.2. SYNTHETIC GENERATION.....	35
4.2.1. Time-Depth (T-D) Chart.	38
4.2.2. Acoustic Impedance (AI)	38
4.2.3. Wavelet.....	38
4.2.4. The Reflection Coefficient (RC).	40
4.3. SYNTHETIC MATCHING.....	40
4.4. HORIZON INTERPRETATION.....	43
4.4.1. Caddo and Davis	43
4.4.2. Runaway and Beans Cr	43
4.4.3. Vineyard and Wade	44
4.4.4. Updating T-D Chart.....	46
4.5. STRUCTURAL MAPPING	47
4.5.1. Time Structure Map.....	47
4.5.2. Average Velocity Map	54
4.5.3. Depth Map.....	61
4.5.4. Time to Depth Conversion.	71
5. STRATIGRAPHIC INTERPRETATION	73
5.1. HORIZON SLICE	73
5.2. ISOPACH MAP.....	78

5.2.1. Interval Velocity Map.	78
5.2.2. Isopach Map.	81
5.3. WELL LOG CORRELATION.....	83
6. RESERVOIR ESTIMATION	93
6.1. INTRODUCTION	93
6.2. ROOT-MEAN SQUARE AMPLITUDE	93
6.3. PETROPHYSICAL ANALYSIS	96
6.3.1. Volume of Shale (Vsh).....	98
6.3.2. Net to Gross Ratio (NGR)	100
6.3.3. Porosity (Φ).	100
6.3.4. Water Saturation (Sw)	102
6.3.5. Permeability (K)	102
6.3.6. Gas Formation Factor (Bg).....	103
6.4. VOLUMATRIC CALCULATION	106
7. CONCLUSION	108
BIBLIOGRAPHY.....	110
VITA	113

LIST OF ILLUSTRATIONS

Figure	Page
1.1. Location of the Boonsville field and the BEG/SGR project area in the north central of Texas (Hentz et al., 2012).....	2
1.2. Generalized post-Mississippian stratigraphic column for the Fort Worth Basin.....	3
2.1. A cross-section of a foreland basin system.....	7
2.2. Regional paleogeography of the southern mid-continent region during the Late Mississippian (325 Ma) showing the approximate position of the Fort Worth Basin close to the Island Chain resulted from the convergent collision between Laurussia and Gondwana.....	7
2.3. Tectonic and structural framework of the Fort Worth Foreland Basin.....	8
2.4. Paleogeology and structural elements of the Fort Worth Basin showing the depositional environment formed the Bend Conglomerate (Thomas et al., 2003).....	9
2.5. North-south and west-east cross sections through the Fort Worth Basin illustrating the structural position of the Barnett Shale between the Muenster Arch, Bend Arch, and Llano Uplift (Burner et al., 2011).....	10
2.6. Generalized subsurface stratigraphic section of the Bend Arch–Fort Worth Basin province showing the distribution of source rocks, reservoir rocks, and seal rocks of the Barnett-Paleozoic petroleum system (Pollastro et al., 2003).....	11
2.7. Structure contour map on top of the Barnett Shale, Bend arch–Fort Worth Basin. ..	13
2.8. Stratigraphic nomenclature used to define the Bend Conglomerate genetic sequences in the Boonsville field.....	15
2.9. Composite genetic sequence illustrating the key chronostratigraphic surfaces and typical facies successions.....	16
2.10. The major geological features bounding the Fort Worth Basin.....	20
2.11. Petroleum system event chart for Barnett-Paleozoic total petroleum system of the Fort Worth Basin, Texas.....	21

3.1. Basemap of the 3D seismic data set of the Boonsville field, north central Texas.	23
3.2. Chart showing the logs provided with each well.	26
4.1. Vertical seismic section of Crossline 147 showing a general view of the seismic data.	31
4.2. Time slice at 1.062 s showing a general view of the seismic data.	32
4.3. General view of the structural geology using the formation tops.	33
4.4. The interpretation work flow.	34
4.5. Synthetic seismogram generation for Well BY18D, illustrating all the components used and the synthetic seismogram generated.	36
4.6. Synthetic seismogram generation for Well 14 (BY15), illustrating all the components used and the synthetic seismogram generated.	37
4.7. Extracted wavelets and their amplitude spectra for Wells 15 and 14.	39
4.8. Seismic section of Crossline 151 with the generated synthetic seismograms from Well 15 (BY18D).	41
4.9. Seismic section of Crossline 152 with the generated synthetic seismograms from Well 15 (BY18D) (green), and Well 14 (BY15) (blue).	42
4.10. Seismic section of Inline112 showing the horizon picking for: Caddo (MFS90) in blue, Davis (MFS70) in pink, Runaway (MFS53) in yellow, Beans Creek (MFS40) in light brown, Vineyard (MFS20) in green, and Wade (MFS10) in dark green.	45
4.11. Time structure map of the Caddo top (MFS90) showing a dipping toward north.	48
4.12. Time structure map of the Davis top (MFS70) showing a dipping toward north.	49
4.13. Time structure map of the Runaway top (MFS53) showing a dipping toward north-east.	50
4.14. Time structure map of the Beans Creek top (Runaway bottom) (MFS40) showing a dipping toward north-east.	51

4.15. Time structure map of the Vineyard top (MFS20) showing a dipping toward east.	52
4.16. Time structure map of the Wade top (Vineyard bottom) (MFS10) showing a dipping toward east.	53
4.17. Illustration showing the method to compute the parameters from the well formation top and the seismic time structure in order to calculate the average velocity.....	54
4.18. Average velocity map of the Caddo (MFS90).....	55
4.19. Average velocity map of the Davis (MFS70).....	56
4.20. Average velocity map of the Runaway (MFS53).....	57
4.21. Average velocity map of the Beans Cr top (Runaway base) (MFS40).....	58
4.22. Average velocity map of the Vineyard (MFS20).	59
4.23. Average velocity map of the Wade top (Vineyard base) (MFS10).	60
4.24. The Caddo (MFS90) depth map in TVD from the seismic datum (ft) showing that the layer is dipping toward north.	62
4.25. The Davis (MFS70) depth map in TVD from the seismic datum (ft) showing that the layer is dipping toward north.	63
4.26. The Runaway (MFS53) depth map in TVD from the seismic datum (ft) showing that the layer is dipping toward north-east.	64
4.27. The Bean Cr (MFS40) depth map in TVD from the seismic datum (ft) showing that the layer is dipping toward north-east.....	65
4.28. The Vineyard (MFS20) depth map in TVD from the seismic datum (ft) showing that the layer is dipping toward north-east.	66
4.29. The Wade (MFS10) depth map in TVD from the seismic datum (ft) showing that the layer is dipping toward east.	67
4.30. 3D structure depth view for all the targeted formations.	68

4.31. 3D depth structure view of the Runaway Formation top (MFS53) and base (MFS40).....	69
4.32. 3D depth structure view of the Vineyard Formation top (MFS20) and base (MFS10).....	70
4.33. Vertical seismic section in depth.	72
5.1. The Runaway top (MFS53) horizon slice indicating a channel by the high amplitudes.....	74
5.2. Horizon slice for the Beans Cr (MFS40), base of Vineyard, indicating a channel flowing toward southwest.....	75
5.3. Top Vineyard (MFS20) horizon slice showing a channel indicated by the high amplitudes from the south to north.	76
5.4. Horizon slice of the Wade (MFS10), the Vineyard Base showing the effect of karst collapse features at the base of the Bend Conglomerate near the Wells 6, 8, 18, 27, 33, and 35.....	77
5.5. Illustration showing the method to compute the parameters from the well formation tops and the seismic time structure in order to calculate the interval velocity.....	78
5.6. The Runaway Formation interval velocity map.....	79
5.7. The Vineyard Formation interval velocity map.....	80
5.8. The Runaway Formation isopach map showing the formation thickness varying from 22 ft to 183 ft.....	81
5.9. The Vineyard Formation isopach map showing the formation thickness varying from 34 ft to 230 ft.....	82
5.10. GR and Rt logs showing in the basemap for the Runaway Formation.....	84
5.11. GR and Rt logs showing in the basemap for the Vineyard Formation.	85
5.12. Well log correlation for the Runaway Formation.....	86
5.13. Well log correlation for the Runaway Formation.....	87

5.14. SP-Rt log from the Well 2 showing in the seismic section for the Runaway Formation.	88
5.15. GR (green) and Rt (blue) logs from the Well 19 showing in the seismic section of crossline 199.	89
5.16. Rt logs for the Wells 2, 4 and 37 plotted in the seismic section.	90
5.17. Well log correlation for the Vineyard Formation.	91
5.18. Well logs placed in the vertical seismic section for the Vineyard Formation.	92
6.1. RMS amplitude map of the Runaway Formation with the depth structural contour of the Runaway top.	94
6.2. RMS amplitude map of the Vineyard Formation with the depth structural contour of the Vineyard top.	95
6.3. Logs generated from the Rt (RILD) log of the Well 2.	97
6.4. SP logs for the Wells 2 and 16 showing examples for calculating the SPcln by 7% cut off and calculating SPsh by 10% cut off.	99
6.5. Well 2 logs generated from the petrophysical analysis showing the shale volume (Vsh) and effective porosity (PHIE).	104
6.6. Well 16 logs generated from the petrophysical analysis showing the shale volume (Vsh) and effective porosity (PHIE).	105

LIST OF TABLES

Table	Page
2.1. The Bend Conglomerate reservoir properties (Hardage et al., 1996)	17
3.1. Coordinators defining the study area in the Boonsville field (Hardage et al., 1996)	24
3.2. Vibroseis velocity survey in the Billie Yates 18D well (Hardage et al., 1996)	25
3.3. Dynamite velocity survey in the Billie Yates 18D well (Hardage et al., 1996)	25
3.4. Well data and formation tops of MFS depths (ft) measured relative to KB (Hardage et al., 1996).....	28
3.5. The SMT Kingdom Suite 8.6 modules used in the study	29
4.1. Updated T-D charts generated from the horizon picks and the formation tops.....	46
6.1. Calculated reservoir properties from the Runaway Formation.....	96
6.2. Calculated reservoir properties from the Vineyard Formation	96
6.3. Petrophysical parameters calculated for both Runaway and Vineyard Formations	107
6.4. The results of the volumetric calculations for both Runaway and Vineyard Formations.	107

NOMENCLATURE

Symbol	Description
3D	Three Dimensional
AI	Acoustic Impedance
bb1	Barrel
BEG	Bureau of Economic Geology
CALI	Caliper
CC	Correlation Coefficient
CS	Check Shot
DT	Delta-t Sonic
GR	Gamma Ray
GRI	Gas Research Institute
KB	Kelly Bushing
LL3	Laterolog 3 Resistivity
LL8	Laterolog 8 Resistivity
LAT	Laterolog Resistivity
LN	Long Normal Resistivity
LVM	Local Varying Mean
mi ²	Mile Square
MICRO	Micro Log
MLP	Multi-Layer Perception
MSFL	Micro Spherically Focused Log
NPHI	Compensated Neutron
TWT	Two Way Time
PEF	Photo Electric Effect
RILD	Deep Induction Resistivity
RILM	Medium Induction Resistivity
RC	Reflection Coefficient
RHOB	Bulk Density
SFL	Spherically Focused Resistivity
SGR	Secondary Gas Recovery
SN	Short Normal (16") Resistivity

SRD	Seismic Reference Datum
Tcf	Trillion Cubic Feet
HST	Highstand
LST	Lowstand
TST	Transgressive

1. INTRODUCTION

1.1. AREA OF STUDY

The Boonsville field is located, primarily, within both Wise County and Jack County in Texas (Figure 1.1). It encompasses approximately 2300 mi² in the Fort Worth Basin, North central Texas (Hardage et al., 1996). This field is considered as one of the largest gas fields in the United States, especially, from the Bend Conglomerate group, which was deposited during the Atoka Stage of the Middle Pennsylvanian period (Hardage et al., 1996) (Figure 1.2). As of January 2011, the lower Atoka reservoirs, collectively, produced more than 3.2 tcf (trillion cubic feet) of natural gas and more than 36.3 million bbl (barrel) of oil from more than 5700 wells (IHS Energy, Inc., 2011).

A 3D seismic exploration acquisition was conducted in the Boonsville field for a Secondary Gas Recovery (SGR) program which was funded by the U.S. Department of Energy and the Gas Research Institute (GRI) from 1993 to 1996. The exploration covered a total area of 26 mi² (Hardage et al., 1996).

The Bureau of Economic Geology (BEG) at the University of Texas, Austin prepared a Boonsville 3D seismic data set as part of the SGR, supported by the GRI. This data is a result of three companies who operated the area of SGR and worked side by side with BEG. The companies are Arch Petroleum, Enserch, and OXY, those who paid 90% of the 3D seismic Data acquisition and processing cost (Hardage et al., 1996).

The primary targeted reservoirs in the Boonsville field are in the Bend Conglomerate Formation (Hardage et al., 1996). These reservoirs hold high content of gas and some oil. During the Atoka stage, the Bend Conglomerate was deposited in a fluvio-deltaic transition environment (Hardage et al., 1996). An important feature in this

field is karst collapse zones, which occurred as a result of collapsing of the deep Ellenburger carbonate formation (Hardage et al., 1996).

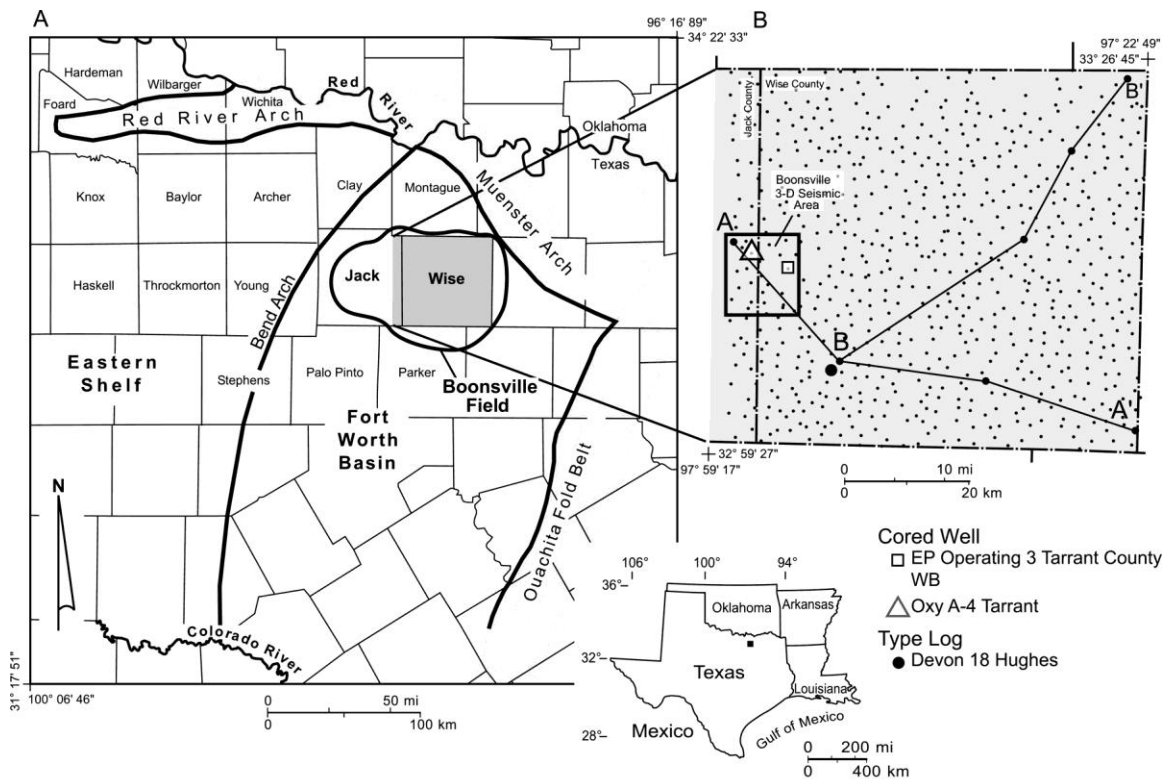


Figure 1.1. Location of the Boonsville field and the BEG/SGR project area in the north central of Texas (Hentz et al., 2012).

SYSTEM		SERIES	GROUP OR FORMATION
K		UNDIVIDED	
P		WOLFCAMPIAN	Cisco Group
IP	UPPER	VIRGILIAN	Canyon Group
		MISSOURIAN	
	MIDDLE	DES MOINESIAN	Strawn Group
		ATOKAN	Atoka Group
	LOWER	MORROWAN	Marble Falls and Canyon Formation
MISSISSIPPIAN			

Gas from Bend Conglomerate

Figure 1.2. Generalized post-Mississippian stratigraphic column for the Fort Worth Basin. In the Boonsville field, the Bend Conglomerate which is shown during Atokan series, is equivalent to the Atoka Group (Hardage et al., 1996).

1.2. PREVIOUS STUDIES

Boonsville field, which lies in the Fort Worth Basin in the north-central of Texas, is one of the largest gas reserves in US. It contains many potential formations within a complete petroleum system. As a result, many studies were conducted using the Boonsville 3D seismic data set.

Since 1985, Hardage and colleagues (Hardage et al., 1996) have conducted extensive studies for the Boonsville field. These studies include the seismic interpretations and reservoir characterization in the Bend Conglomerate. The studies resulted both geologic understanding and petrophysical analysis to the Boonsville field. Discontinuous and thin reservoirs were identified. In addition, some approaches were developed to characterize the reservoir geometries for the gas reserves. The effects of the carbonate karst collapse were also recognized.

Using core data, seismic data, and well logs, Maharaj et al. (2009) identified the facies in Atoka based on lithological relationships. The study divided Atoka into twelve parasequences and identified point bars and channels.

Hentz et al. (2012) mapped sandstone distribution of the depositional facies using the well log chronostratigraphic framework. This study provided depositional geometries of Atoka. It suggested that the Bend includes braided fluvial deposits, braid-plain deposits, and river-dominated deltas.

1.3. OBJECTIVES

The objective of this study is to provide a geological visualization of the Boonsville field subsurface by correlating the regional geological data, geophysical seismic data, well logs, well test data, and well production history. Geologic subsurface structures were visualized for six horizons within the Bend Conglomerate. The horizons are Caddo, Davis, Runaway, Beans Creek, Vineyard, and Wade. Various maps such as time structure, horizon slice, velocity, depth structure, and isopach were constructed. Moreover, the seismic data volume was converted from time to depth domain for better correlation with well logs.

Another objective includes stratigraphic interpretation to identify different geological features for both the Runaway and Vineyard Formations. Studying the horizon slices, isopach maps, and well logs were useful to interpret the stratigraphic features such as fluvial dominated channels, point bars, and mouth bar sandstone deposits.

Reservoirs estimation is conducted for the Runaway and the Vineyard Formations. First, RMS amplitude maps were generated as a direct hydrocarbon indicator to show bright spots. Then, petrophysical analyses were implemented for both formations to conduct the reservoir properties and to calculate petrophysical parameters including the gross, net pay, NGR, water saturation, shale volume, porosity, and gas formation factor. Two prospects are identified for both formations. Finally, volumetric prospect calculations were performed to estimate the amount of the recoverable original gas in-place (ROGIP) for the Runaway Formation and the Vineyard Formation.

2. REGIONAL GEOLOGY

2.1. FORT WORTH BASIN

Fort Worth Basin is a part of the foreland basin system (Figure 2.1). This basin was formed during Late Paleozoic episode deformed along the Ouachita Fold-Thrust belt (Figure 2.2). It has an area of approximately 15000 mi² (Walper, 1982; Thompson, 1988) and elongates north-south parallel to the Ouachita Thrust fault located in the south-east of the basin. The Fort Worth Basin is bounded by the Muenster Arch to the east-north, the Red River Arch to the north-west, the structural Bend Arch to the west, and the Precambrian Llano uplift to the south (Figure 2.3).

The Fort Worth Basin deposited during the formation of Pangea as a foredeep basin within the foreland basin system (Walper, 1982) (Figure 2.1). In Early Paleozoic, carbonate deposition from Cambro-Ordovician followed by erosion during the Middle Paleozoic. The basin is developed between the Ouachita Thrust Belt and the Bend Arch during the tectonic plate convergence between Laurussia plate and Gondwana plate (Figures 2.2 and 2.3). During Mississippian-Pennsylvanian, the Ouachita Thrust Belt developed as a result of plate convergence when the continental margin was approaching the subduction zone (Figure 2.3). Subsequently during Pennsylvanian, the Fort Worth Basin formed when layering sequence deposited on the continental margin (Walper, 1982) (Figure 2.4).

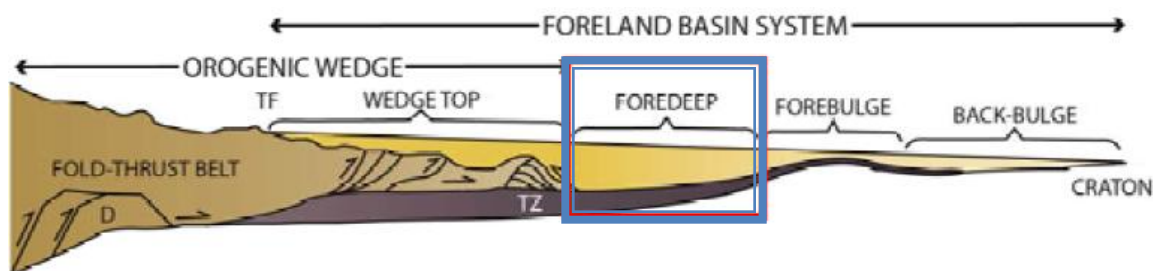


Figure 2.1. A cross-section of a foreland basin system. The Fort Worth Basin is considered as a foredeep basin within a foreland basin system (Modified from DeCelles and Giles, 1996).

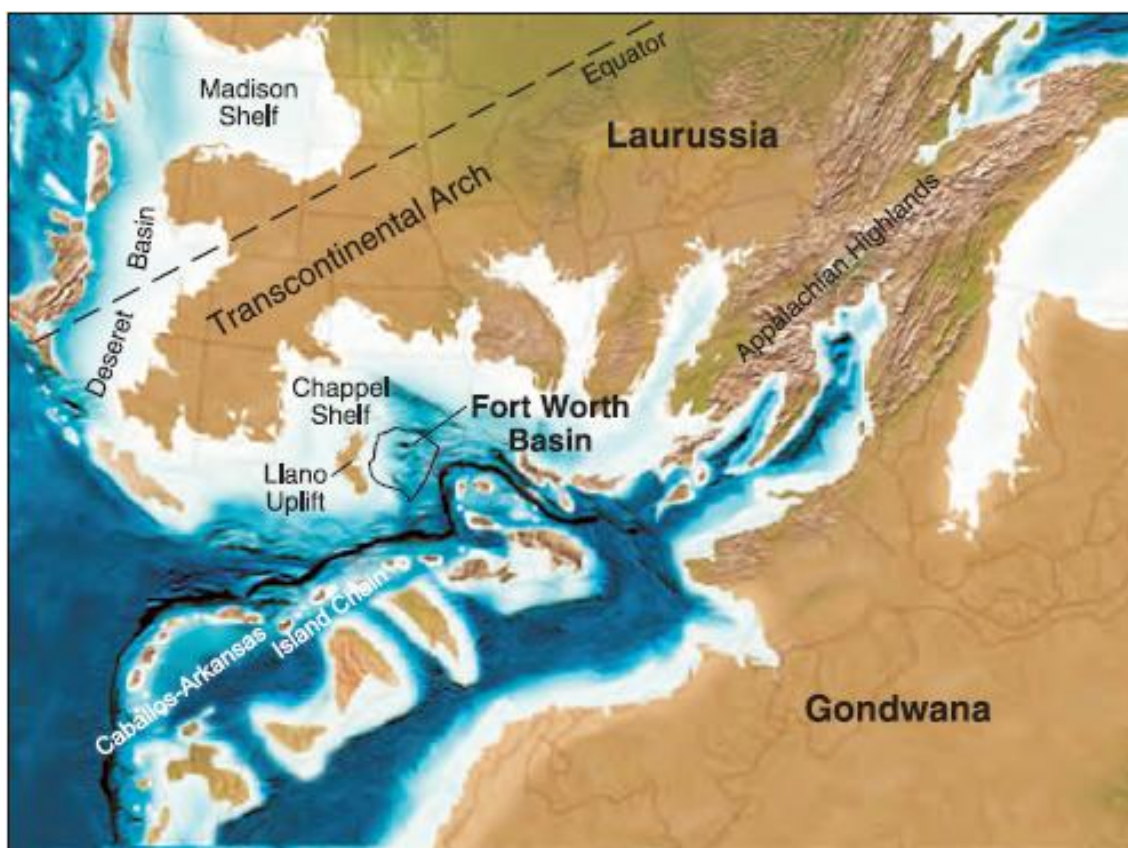


Figure 2.2. Regional paleogeography of the southern mid-continent region during the Late Mississippian (325 Ma) showing the approximate position of the Fort Worth Basin close to the Island Chain resulted from the convergent collision between Laurussia and Gondwana. Llano Uplift and the Arch equator are shown. They played important role in the evaluation of the Fort Worth Basin (Burner et al., 2011).

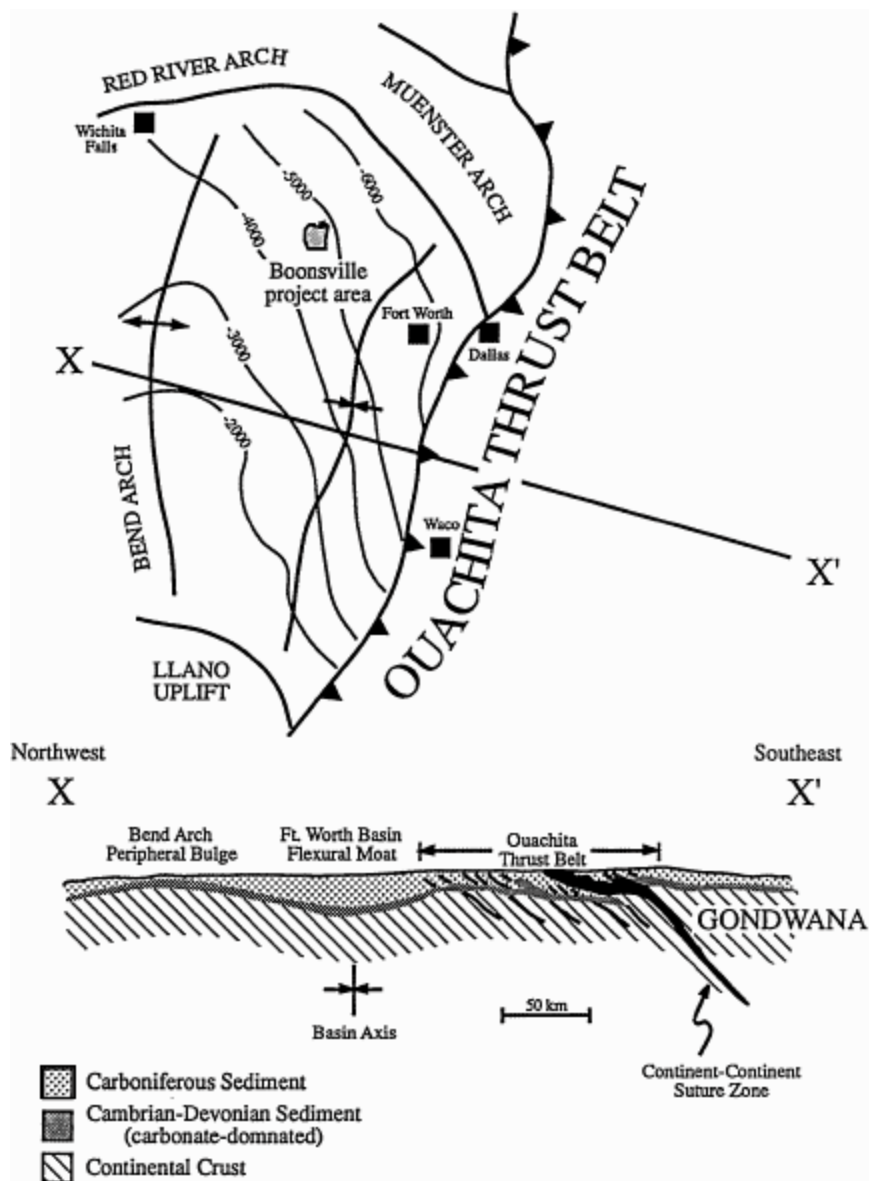


Figure 2.3. Tectonic and structural framework of the Fort Worth Foreland Basin. The contour map above represents the depth below sea level of the top of the Marble Falls Formation. The cross section shows the subduction zone between Laurussia and Gondwana (Hardage et al., 1996).

During Early Atoka, the Muenster Arch was the primary sediment source that formed and served the Fort Worth Basin. In addition, the Ouachita Fold Belt and the Bend Arch also fed the Fort Worth Basin as sediment sources (Figure 2.4). They deformed the Fort Worth Basin into the warped shape (Thomas, 2003). The Llano Uplift, worked as the main structure that twisted the formations of the Fort Worth Basin to its present structure and dip (Figure 2.5). The Llano Uplift, worked as the main structure that twisted the formations of the Fort Worth Basin to its present structure and dip (Figure 2.5). The Fort Worth Basin is shallow, and dipping toward the north, with a maximum depth of 12000 ft along the Ouachita (Burner et al., 2011) (Figure 2.5).

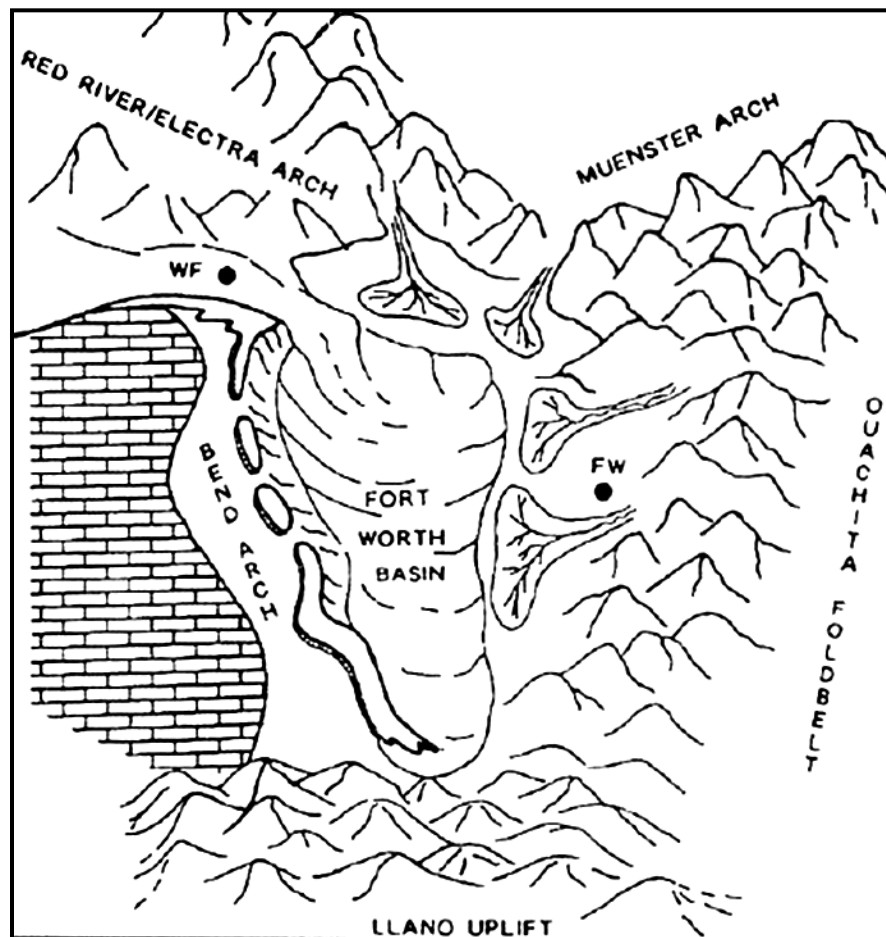


Figure 2.4. Paleogeology and structural elements of the Fort Worth Basin showing the depositional environment formed the Bend Conglomerate (Thomas et al., 2003).

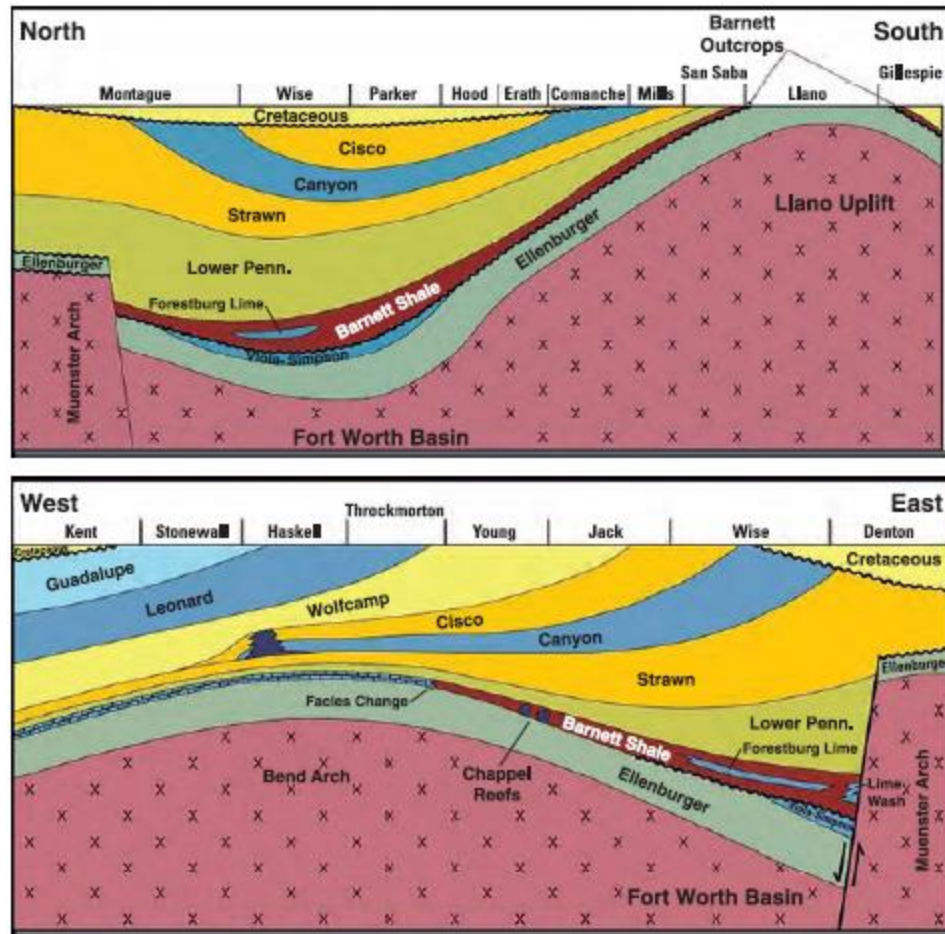


Figure 2.5. North-south and west-east cross sections through the Fort Worth Basin illustrating the structural position of the Barnett Shale between the Muenster Arch, Bend Arch, and Llano Uplift (Burner et al., 2011).

2.2. GEOLOGICAL STRATIGRAPHY

During the Pennsylvanian Period, different sequences of sedimentary deposition were accumulated in the Fort Worth Basin. Depositions of 6000 – 7000 ft consist mainly of clastics and carbonates. However, accumulations from Ordovician – Mississippian comprise about 4000 – 5000 ft of carbonates and shales (Burner et al., 2011; Thompson, 1988) (Figure 2.6).

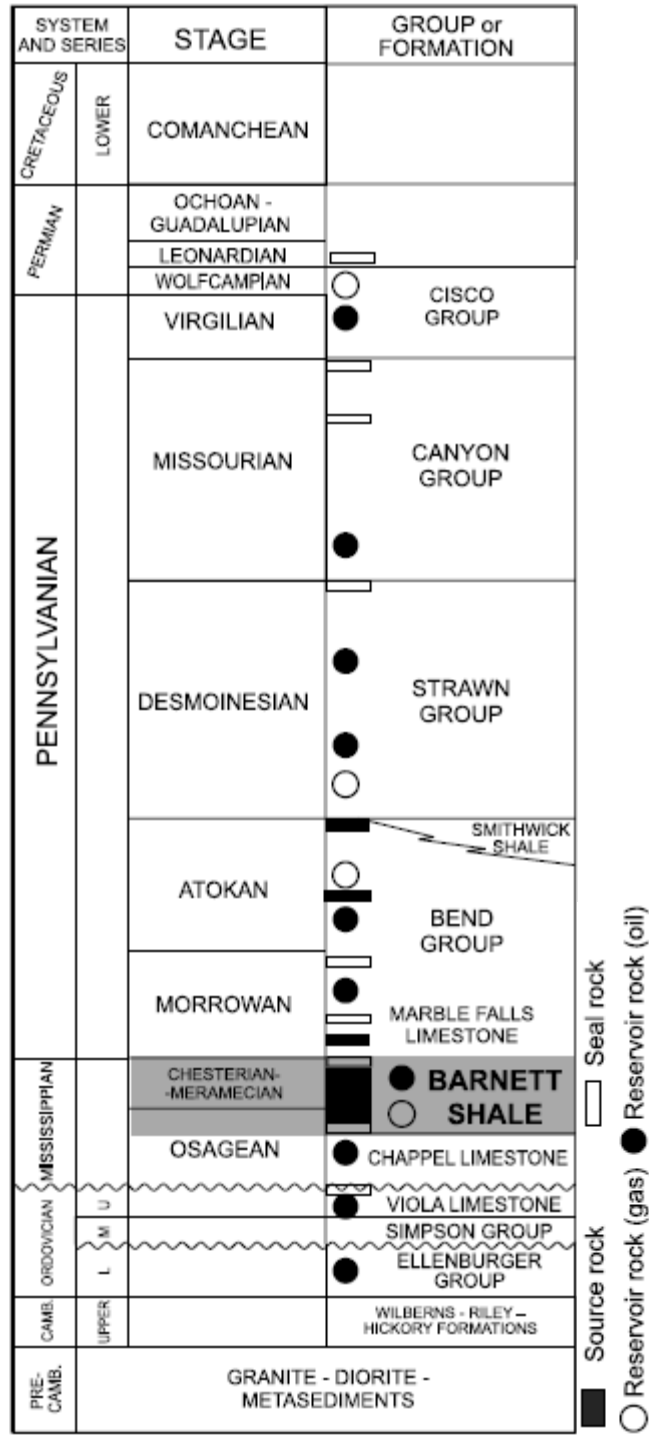


Figure 2.6. Generalized subsurface stratigraphic section of the Bend Arch-Fort Worth Basin province showing the distribution of source rocks, reservoir rocks, and seal rocks of the Barnett-Paleozoic petroleum system (Pollastro et al., 2003).

2.2.1. Barnett Shale Barnett Shale is an important Formation in the Fort Worth Basin. It plays a critical role in forming different gas fields in the northern part of Texas (Pollastro et al., 2007). Barnett shale consists of the Mississippian petroliferous black shale (Burner et al., 2011). It is considered to be a primary Kerogen kitchen in the Fort Worth Basin (Pollastro et al., 2007). It feeds the Pennsylvanian clastic reservoirs in the Boonsville field. Moreover, Barnett Shale represents an unconventional hydrocarbon play where the main elements of a petroleum system are found. Kerogen source, reservoir, and seal coincide in the same Formation. As a result, Barnett Shale is targeted itself (e.g., the Newark East field, where the Formation is 300-500 ft thick and 6500-8500 ft deep (Burner et al., 2011) (Figure 2.7).

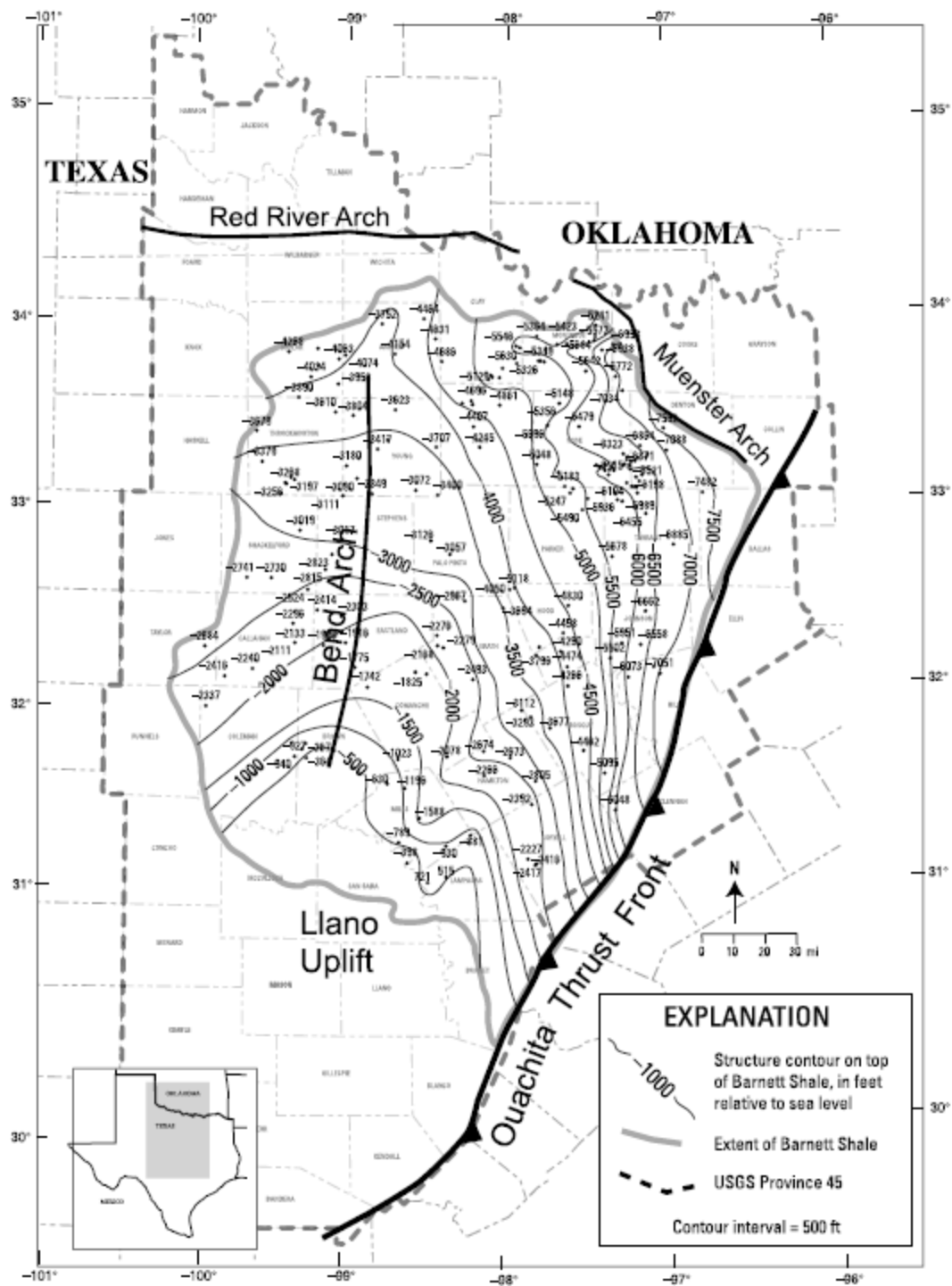


Figure 2.7. Structure contour map on top of the Barnett Shale, Bend arch–Fort Worth Basin. Contour interval equals 500 ft (152 m). The map also shows the distribution of the Barnett Shale (Pollastro et al., 2007).

2.2.2. The Bend Conglomerate. The Bend Conglomerate is an interval of the Atoka group deposited in the Fort Worth Basin during the Middle Pennsylvanian. It consists of many genetic sequences characterized by Conglomerate depositions (Figure 2.8). It is deposited in fluvial – deltaic transition environment (Hardage et al., 1996). Each genetic sequence represents one relative base level cycle. Each cycle is characterized by highstand (HST), lowstand (LST), and transgressive (TST) system tracts. Reservoir sandstone facies, regularly, arise in the LST. The Bend includes braided fluvial deposits, braid-plain deposits, and river-dominated deltas (Hentz et al., 2012). These environments resulted high porous, thin, and discontinuous formations of Conglomerate sandstone formed within a genetic sequences shown by a stratigraphic nomenclature in Figure 2.8. The Bend Conglomerate genetic sequence of depositional environment is identified by Galloway (1989) termed as following: the Maximum Flooding Surface (MFS), the Flooding Surface (FS), and the Erosional Surface (ES) (Figure 2.9). The Bend begins at the Caddo Formation and ends at the Vineyard Formation. There are erosional surfaces between the formations giving a precise definition of the clastic reservoirs. Because of their high productivity, both the Caddo and Vineyard Formations are the main target zones in the Boonsville field (Hardage et al., 1996). Table 2.1 lists the Bend Conglomerate reservoir properties.

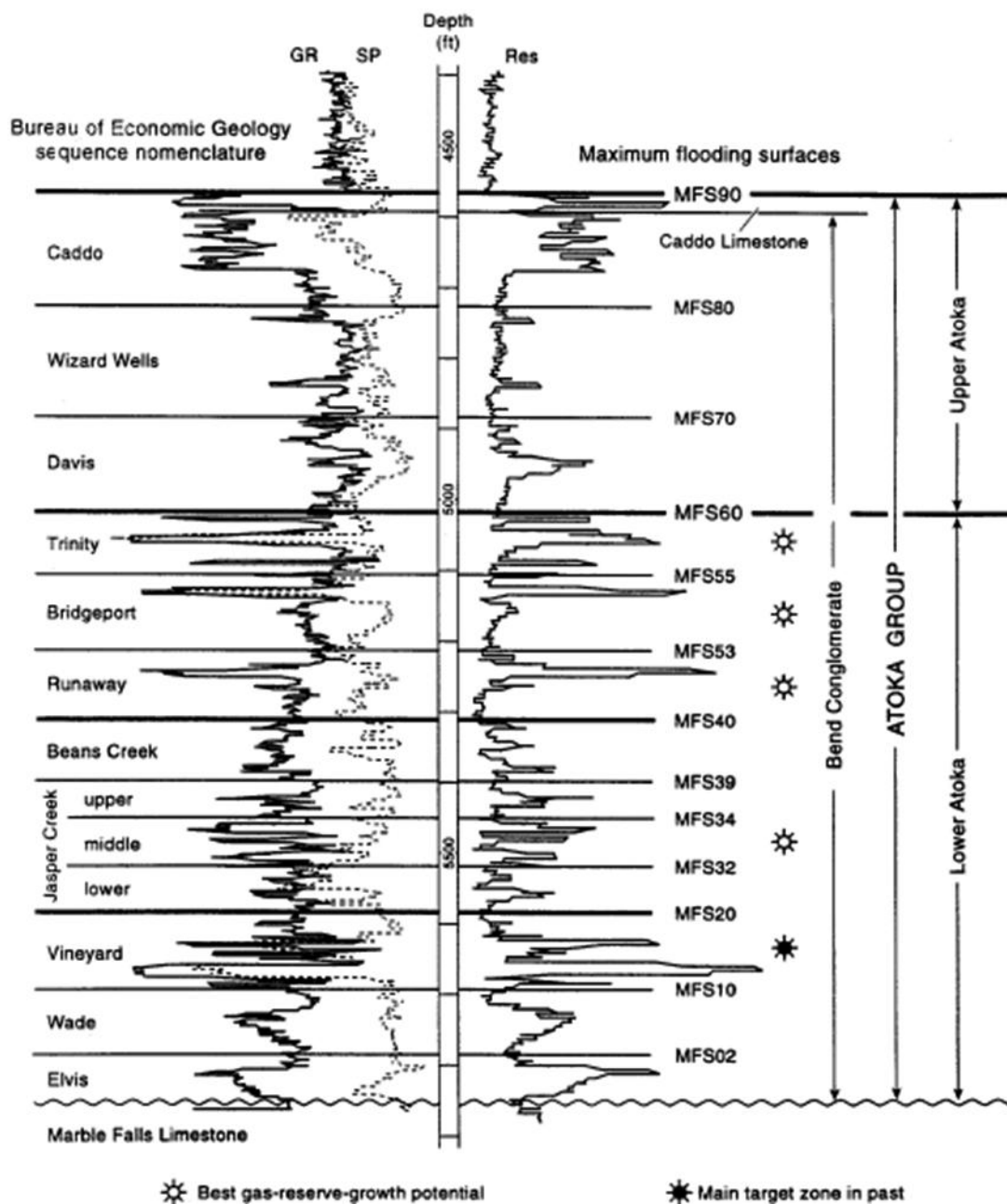


Figure 2.8. Stratigraphic nomenclature used to define the Bend Conglomerate genetic sequences in the Boonsville field. As defined by the Railroad Commission of Texas, the Bend Conglomerate is the interval from the base of the Caddo Limestone to the top of the Marble Falls Limestone (Hardage et al., 1996).

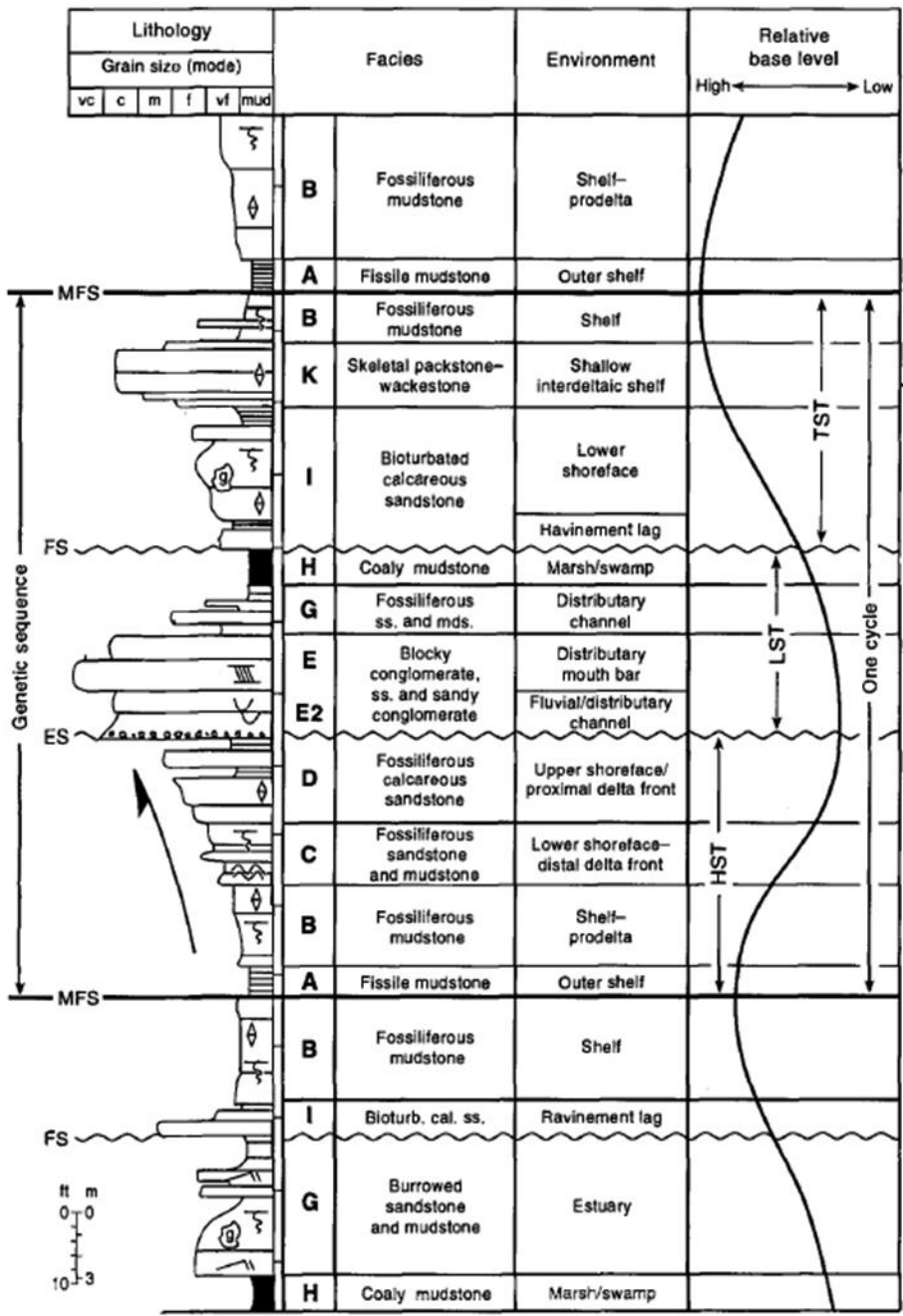


Figure 2.9. Composite genetic sequence illustrating the key chronostratigraphic surfaces and typical facies successions. It is constructed from the actual core data spanning four Bend Conglomerate sequences. One relative base level cycle is commonly represented by HST, LST, and TST systems tracts. Cycles begin and end with MFS and typically contains one or more ES and FS, which are commonly ravinement surfaces (Hardage et al., 1996).

Table 2.1. The Bend Conglomerate reservoir properties (Hardage et al., 1996)

Property/item	Typical values
Depth	4500 to 6000 ft
Initial pressures	1400 to 2200 psi – somewhat underpressured
Temperature	150°F
Gas gravity	0.65 to 0.75
Gross thickness	900 to 1300 ft
Net thickness	Multiple pays from a few ft to 20–30 ft each
Permeability	Varies from <0.1 md to >10 md; 0.1 to 5 md typical
Porosity	5 to 20 %
Production	From 10 Mmscf to 8 Bscf; 1.5 Bscf Median

2.3. GEOLOGICAL STRUCTURES

The Boonsville field was developed with different types of structural features, which are the result of either tectonic activity or solution weathering. An important structural feature in this area is the Mineral Wells Fault. It runs northeast-southwest with a length of more than 65 mi. In addition, there are many high-angle normal faults, karst fault chimneys, and local subsidence in the Boonsville field (Hardage et al., 1996). This is related to the karst development and solution collapse in the underlying Ordovician Ellenburger Group (Hardage et al., 1996). The karst collapse features extend vertically upward 2500 - 3500 ft through the strata of Barnett, Marble falls, and the Atoka group with diameters ranging from 1640 to 3940 ft (McDonnell et al., 2007).

2.4. PETROLEUM SYSTEM

The Boonsville field is a result of a complete petroleum system occurring north of the Fort Worth Basin. It consists of mature source rocks, migration pathways, reservoir rocks, and seals. The petroleum system elements in the Boonsville field are described as following:

2.4.1. Source Rock. The Barnett Shale is proved to be the primarily source rock for the hydrocarbon accumulation in the Bend Conglomerate (Hardage et al., 1996; Pollastro et al., 2003) (Figure 2.6). Figure 2.10 illustrates the distribution of the Barnett Shale in the Fort Worth Basin and the location of the Boonsville field. The Barnett Shale consists of shale and limestone. The shale properties are dense, organic-rich, soft, thin-bedded, petroliferous, and fossiliferous. The limestone properties are hard, black, finely crystalline, petroliferous, and fossiliferous. The Barnett kerogen is type II, with a minor admixture of type III (Burner et al., 2011) (Figure 2.11).

2.4.2. Migration Pathways. There are some major faults proven to be the hydrocarbon migration pathways in the Boonsville field. The Mineral Wells Fault system is a suggested pathway to migrate the hydrocarbon from the Barnett Shale up to Atoka. In addition, karst features are approved as high efficient pathways (Hardage et al., 1996; Pollastro et al., 2007). These features extend in the Fort Worth Basin through the Mississippian to the Pennsylvanian strata. Accordingly, the karst collapses connect the Barnett Shale and other thin shale beds in the Atoka to the Bend Conglomerate reservoirs. These karst collapses work as high efficient migration pathways for the hydrocarbon.

2.4.3. Traps and Reservoirs. The Bend Conglomerate consists of porous and permeable conglomerate sandstone formations. Point bars and channel depositions are part of the genetic sequences of the Bend. These depositions are bounded by erosional sequences. High potential reservoirs are founded in the following main zones of the Bend: Caddo, Davis, Runaway, and Vineyard (Hardage et al., 1996) (Figure 2.8). Shale and mudstone layers are deposited at the end of LST. These layers bound different sandstone formations of the Bend Conglomerate (Figure 2.9).

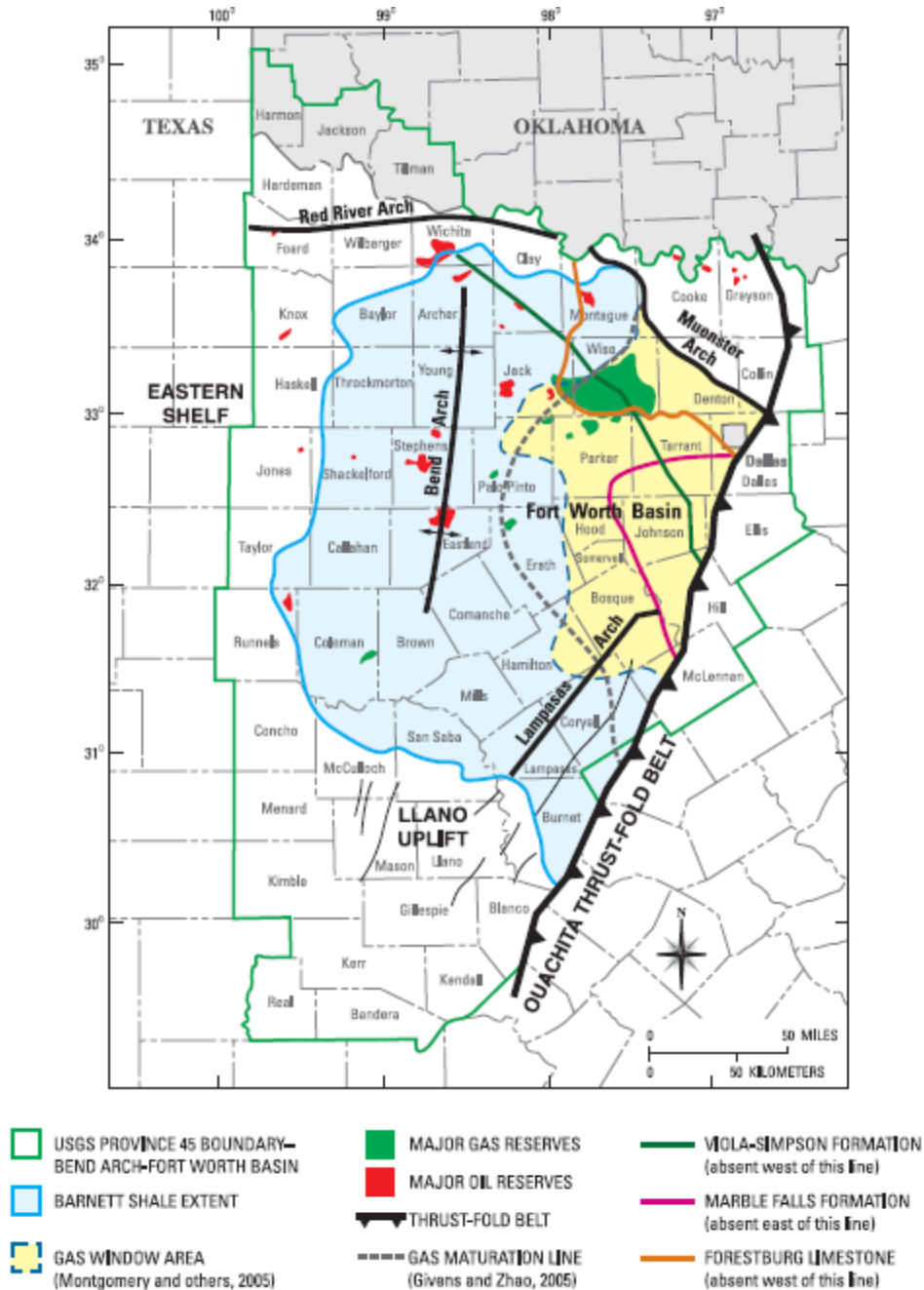


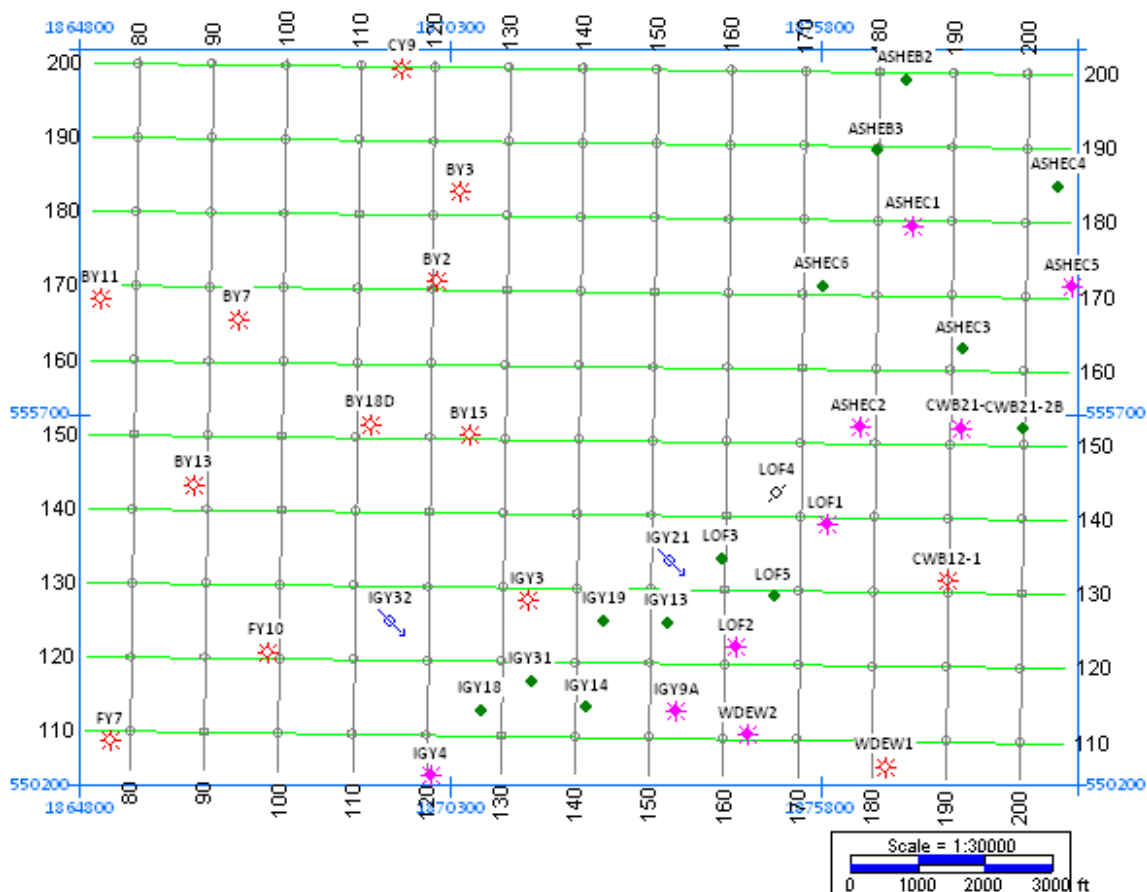
Figure 2.10. The major geological features bounding the Fort Worth Basin. The blue color outlines the extent of the Barnett Shale. The gas reserve north of the Fort Worth Basin (green) represents the Boonsville field (Burner et al., 2011).

3. DATA AND METHOD

3.1. BOONSVILLE 3D SEISMIC DATA

The data used in this project is the BEG/SGR 3D seismic data set of the Boonsville field, north central Texas. This data includes a 3D seismic survey, 38 wells, well logs, formation tops, production test data, checkshots, and a Vertical Seismic Profile (VSP). The 3D seismic data covers an area of 5.5 mi² out of 26 mi², the total SRG Boonsville study area (Figure 3.1). The source for the seismic survey was 10 oz directional explosives and the sampling rate was 1 ms. The survey source and receiver lines were staggered, allowing for a high-fold number, with 110 X 110-ft bins (Hardage et al., 1996). The 3D seismic volume was processed by Trend Technology of Midland, Texas. Hardage (1996) summarized the seismic processing sequence as following:

1. Surface and subsurface maps
2. Geometry definition and application
3. Prefilter 17-250 Hz
4. Surface-consistent deconvolution
5. Refraction statics: Seismic datum = 900 ft, velocity = 8000 ft/s
6. Velocity analysis
7. Refraction statics: Seismic datum = 900 ft, velocity = 8000 ft/s
8. CDP stack
9. Automatic residual statics: Iterate 6 times
10. Velocity analysis
11. Normal moveout
12. Spectral balance
13. CDP residual statics
14. CDP stack (55- and 110-ft bins)
15. Interpolate missing CDPs at edges of data volume (55-ft bins only)
16. 3-D migration



Well Symbol	
	Gas Well
	Water Injection Well
	Abandoned
	Oil Well
	Oil & Gas Well

Figure 3.1. Basemap of the 3D seismic data set of the Boonsville field, north central Texas. 38 wells are illustrated. Well names, numbers, and types are indicated.

This 3D seismic volume consists of 110 ft stacking bins. Trace (Inline,X) values increase from west to east and line (Crossline,Y) values increase from south to north. The northeast corner is located at Trace 206, Line 201. The southwest corner of the survey is located at Trace 74, Line 105. The longitude and latitude values for the four corners of the survey were translated to X and Y values for the North Central Texas Zone (4202) of the U. S. State Plane Coordinate System and the 1927 North American Datum. Table 3.1 lists the corners, starting in the southwest corner and moving clockwise. The Boonsville 3D seismic SEG Y file text header is listed as following:

Line number in bytes 9 – 12 105 – 201

Trace number in bytes 21 – 24 74 – 206

97 lines with 133 traces each

32 bit IBM Floating point data

Samples at 1 millisecond sampling rate

The maximum amplitude value is 149035.5.

The minimum amplitude value is 32029.25.

The average amplitude value is 63670.67.

Table 3.1. Coordinators defining the study area in the Boonsville field (Hardage et al., 1996)

Trace	Line	Longitude	Latitude	X Location	Y Location
74	105	-97.94162	33.17897	1864886	550461
74	201	-97.94132	33.20800	1865021	561020
206	201	-97.89384	33.20766	1879540	560838
206	105	-97.89416	33.17863	1879406	550279

The 38 well data includes various logs such as resistivity, gamma ray, SP, sonic, neutron, and density logs. Billie Yates 18D well is provided with the vibroseis-source VSP data and explosive (dynamite) checkshots as seen in Tables 3.2 and 3.3. Figure 3.2 shows types of logs included in each well. The resistivity and SP are the most log type available.

Table 3.2. Vibroseis velocity survey in the Billie Yates 18D well (Hardage et al., 1996)

Level	Depth KB (ft)	Vertical Depth from SRD (ft)	Measured one-way time (ms)	Vertical one-way time from source (ms)	Vertical one-way time from SRD (ms)
1	1000	8850	123	115.9	97
2	2000	1850	212.8	209.5	190.6
3	2500	2350	258.2	255.6	236.7
4	3000	2850	300.9	298.8	279.9
5	3500	3350	342.5	340.7	321.9
6	4000	3850	385.3	383.8	364.9
7	4500	4350	426.2	424.9	406
8	5000	4850	467.9	466.7	447.8
9	5500	5350	508.3	508.2	489.2
10	5700	5550	524.7	523.7	504.8

Table 3.3. Dynamite velocity survey in the Billie Yates 18D well (Hardage et al., 1996)

Level	Depth KB (ft)	Vertical Depth from SRD (ft)	Measured one-way time (ms)	Vertical one-way time from source (ms)	Vertical one-way time from SRD (ms)
1	1000	850	117.4	107.3	91.1
2	2000	1850	205.2	200.4	184.2
3	2500	2350	250.3	246.6	230.3
4	3000	2850	291.5	288.5	272.2
5	3500	3350	332.7	330.1	313.8
6	4000	3850	374.4	372.2	356
7	4500	4350	414.8	412.9	396.7
8	5000	4850	456.2	454.5	438.2
9	5500	5350	485.4	493.8	477.6
10	5723	5573	514.3	512.8	496.5

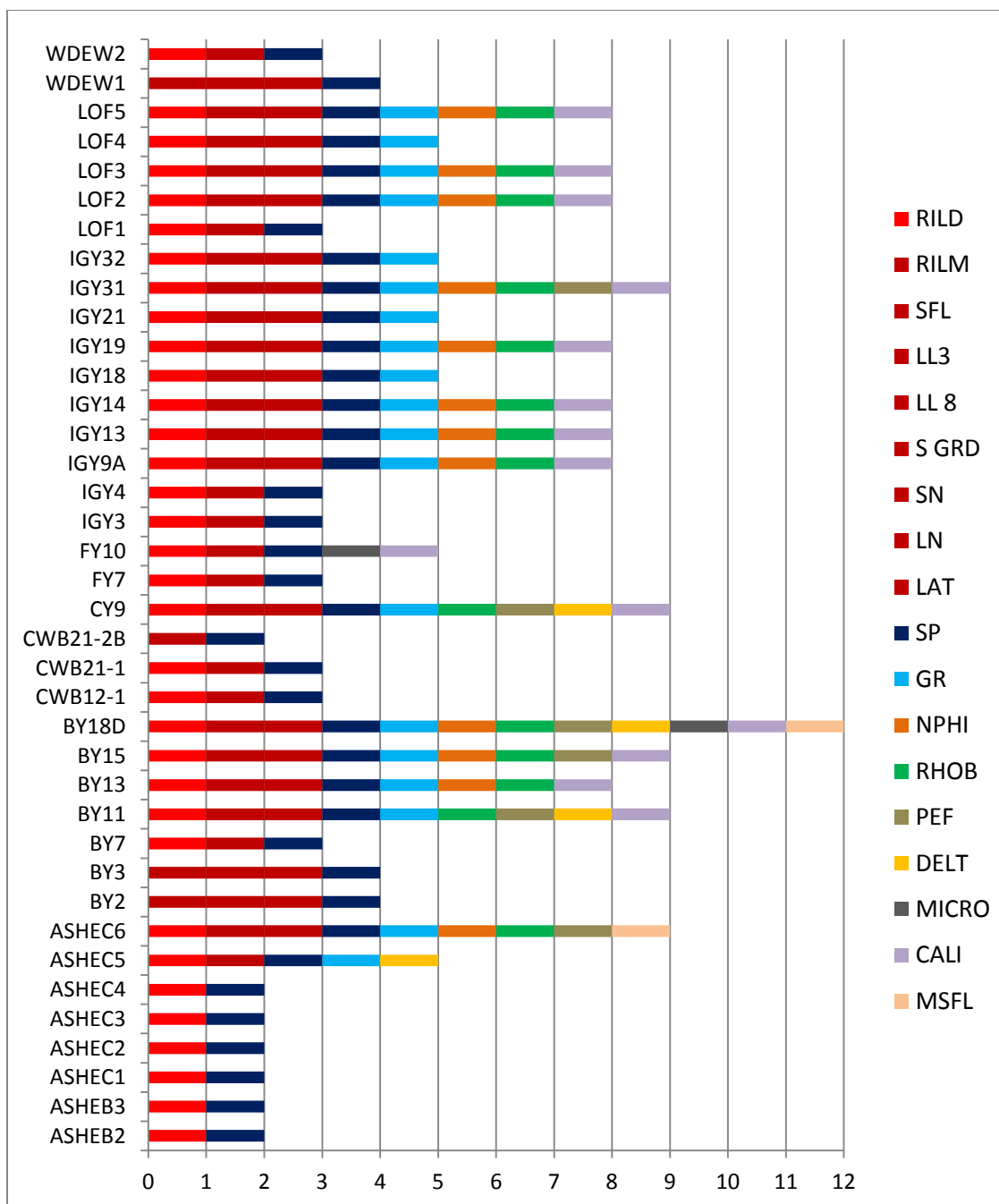


Figure 3.2. Chart showing the logs provided with each well. Red color indicates resistivity logs. All wells have resistivity log and SP log. Log abbreviations can be found in the nomenclature page.

Formation tops are provided for the wells. All the MFS, FS, and ES top depths are provided for all formations in the Bend Conglomerate. Table 3.4 lists the genetic sequence boundaries of MFS depths in each well for the formations that are interpreted in this study, depths from Kelly Bushing (KB).

Table 3.4. Well data and formation tops of MFS depths (ft) measured relative to KB
(Hardage et al., 1996)

Well#	Well name	KB datum	MFS90	MFS70	MFS53	MFS40	MFS20	MFS10
1	ASHEB2	1032	4833	5159	5393	5557	5737	5874
2	ASHEB3	1040	4820	5140	5380	5549	5735	5850
3	ASHEC1	943	4697	5023	5276	5431	5627	5758
4	ASHEC2	867	4588	4922	5194	5356	5576	5703
5	ASHEC3	879	4596					
6	ASHEC4	892	4691	5032	5302	5460	5648	5778
7	ASHEC5	900	4631	4977	5243	5390	5594	5715
8	ASHEC6	959	4724	5041	5294	5465	5672	5807.5
9	BY2	1030	4757	5070	5315	5462	5671	
10	BY3	1023	4777	5083	5316	5464	5666	
11	BY7	994	4709	5030	5269	5405	5591	5718
12	BY11	984	4701	5021	5253	5398	5577	5694
13	BY13	1042	4723	5048	5300	5440	5623	5743
14	BY15	1072	4770	5085	5341	5489	5689	5805
15	BY18D	1040	4735	5055	5299	5451	5647	
16	CWB12-1	847	4521	4853	5129	5292	5502	5645.9
17	CWB21-1	866	4584	4940	5219	5380	5599	5741.8
18	CWB21-2B	888	4613	4969	5254	5407	5634	5762
19	CY9	980.5	4765	5080	5322	5466	5642	5754.1
20	FY7	1046	4742	5066	5356	5506	5710	5828
21	FY10	1047	4724	5048	5309	5450	5641	5782
22	IGY3	1075	4766	5084	5351	5511	5707	5833
23	IGY4	1085	4785	5105	5393	5541	5750	5876
24	IGY9A	857	4532	4856	5135	5290	5498	5630.6
25	IGY13	873	4551					
26	IGY14	887	4565					
27	IGY18	1089	4781					
28	IGY19	905	4595					
29	IGY21	890	4578					
30	IGY31	962	4636					
31	IGY32	1074	4766					
32	LOF1	861	4571	4910	5184	5353	5565	5704
33	LOF2	855	4551	4885	5175			
34	LOF3	869	4565					
35	LOF4	875	4602					
36	LOF5	856	4563					
37	WDEW1	854	4479	4806	5088	5248	5458	5603
38	WDEW2	952	4512	4830	5110	5269	5489	5625.7

3.2. METHOD

The main software used in this study is the SMT KINGDOM Suite 8.6 that provides integrated geological and geophysical interpretation in 2D and 3D. It is useful for integrating seismic data with well data in a geological based interpretation. It consists of many modules. Table 3.5 below shows the list of the SMT KINGDOM Suite 8.6 modules that are used in this study and their uses.

Table 3.5. The SMT Kingdom Suite 8.6 modules used in the study

Modules	Features
SynPAK	Synthetic generation, seismic matching, synthetic display, cross-plot
2d/3dPAK	Horizon interpretation, fault Interpretation, gridding, contouring, create time maps
VuPAK	Import, view, display, integrate, analyze microseismic, horizon picking, dynamic filtering
VelPAK	Constructing velocity models, depth conversion
EarthPAK	Cross section, log calculations, mapping, facies modeling, composite log, petrophysics log and formation top aliasing

4. STRUCTURAL INTERPRETATION

4.1. INTRODUCTION

The seismic data was reviewed to gain a general understanding of the structural features characterizing the geological background of the study area. Both the seismic vertical sections (Figure 4.1) and the seismic horizontal sections (Figure 4.2) were studied to obtain an overall view of the structural impression on the targeted horizons. Additionally, both the well logs and the formation tops provide a general indication of the structural characterization (Figure 4.3).

The well data is utilized to correlate the 3D seismic volume with the well data to precisely identify the horizons of the study. Two formations within the Bend Conglomerate group were targeted in this study: the Runway Formation, bounded by MFS53 (top) and MFS40 (bottom), and the Vineyard Formation, bounded by MFS20 (top) and MFS10 (bottom). Figure 2.5 illustrates the BEG stratigraphic column of the Bend Conglomerate showing the order of the Runway and the Vineyard in comparison with other formations of the Bend. The work flow of the interpretations is illustrated in Figure 4.4.

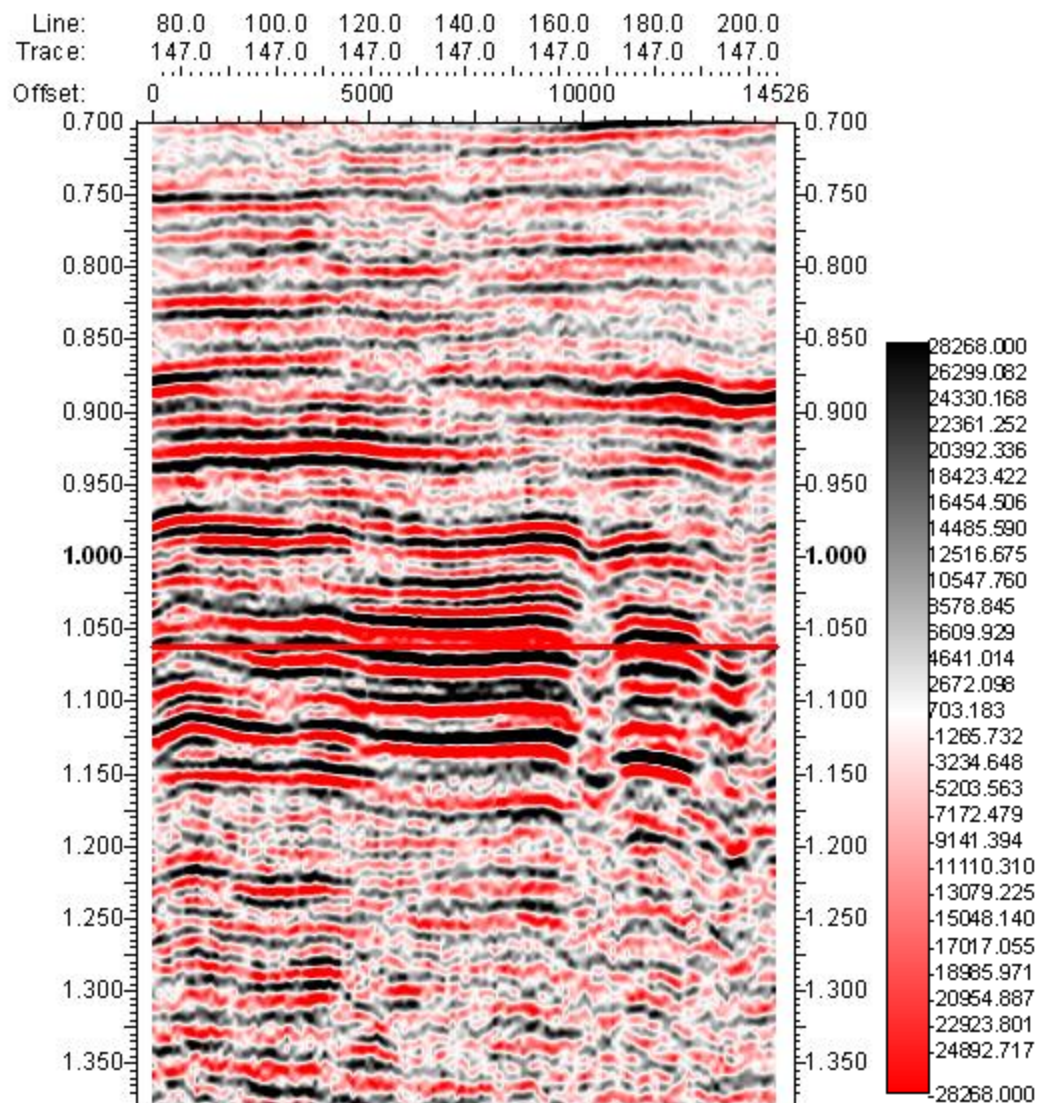


Figure 4.1. Vertical seismic section of Crossline 147 showing a general view of the seismic data. At offsets 10000 and 13500, karst collapse features can be observed. The color bar shows the amplitude information. High amplitudes between 0.875 s and 1.15 indicate the Bend Conglomerate interval. The red line at 1.062 s represents the horizon section shown in Figure 4.2

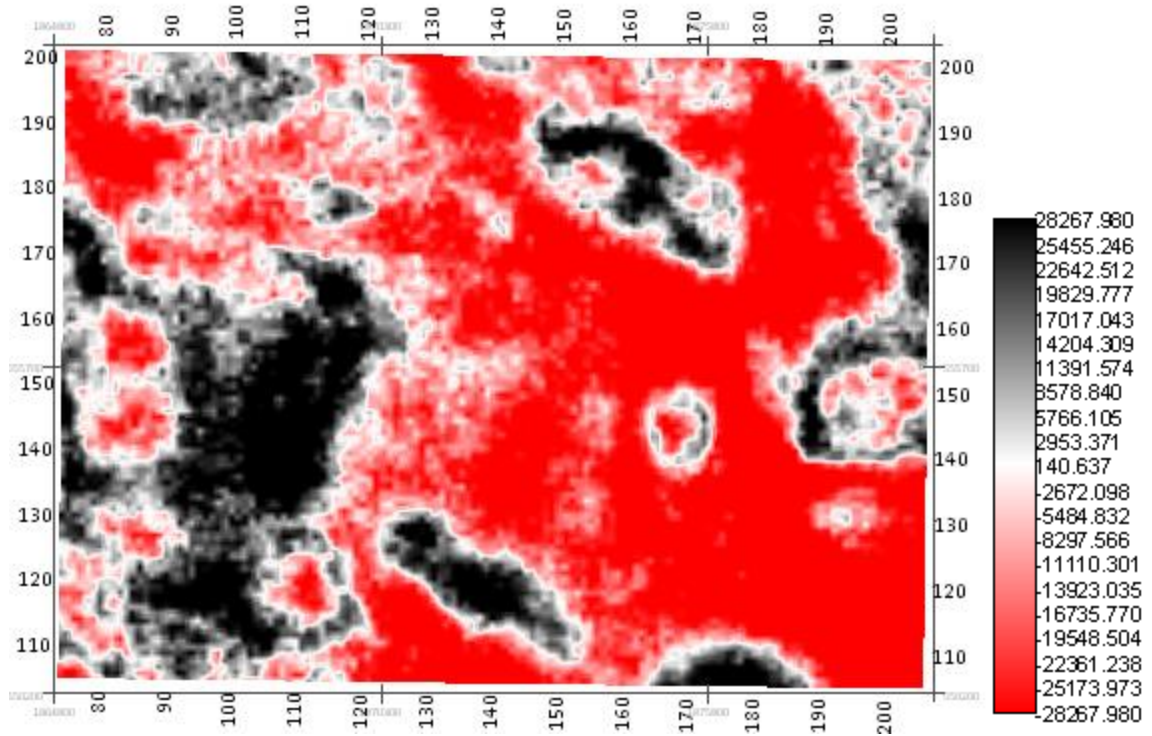


Figure 4.2. Time slice at 1.062 s showing a general view of the seismic data. Karst collapse features are observed by the black circles. The color bar shows the amplitude information.

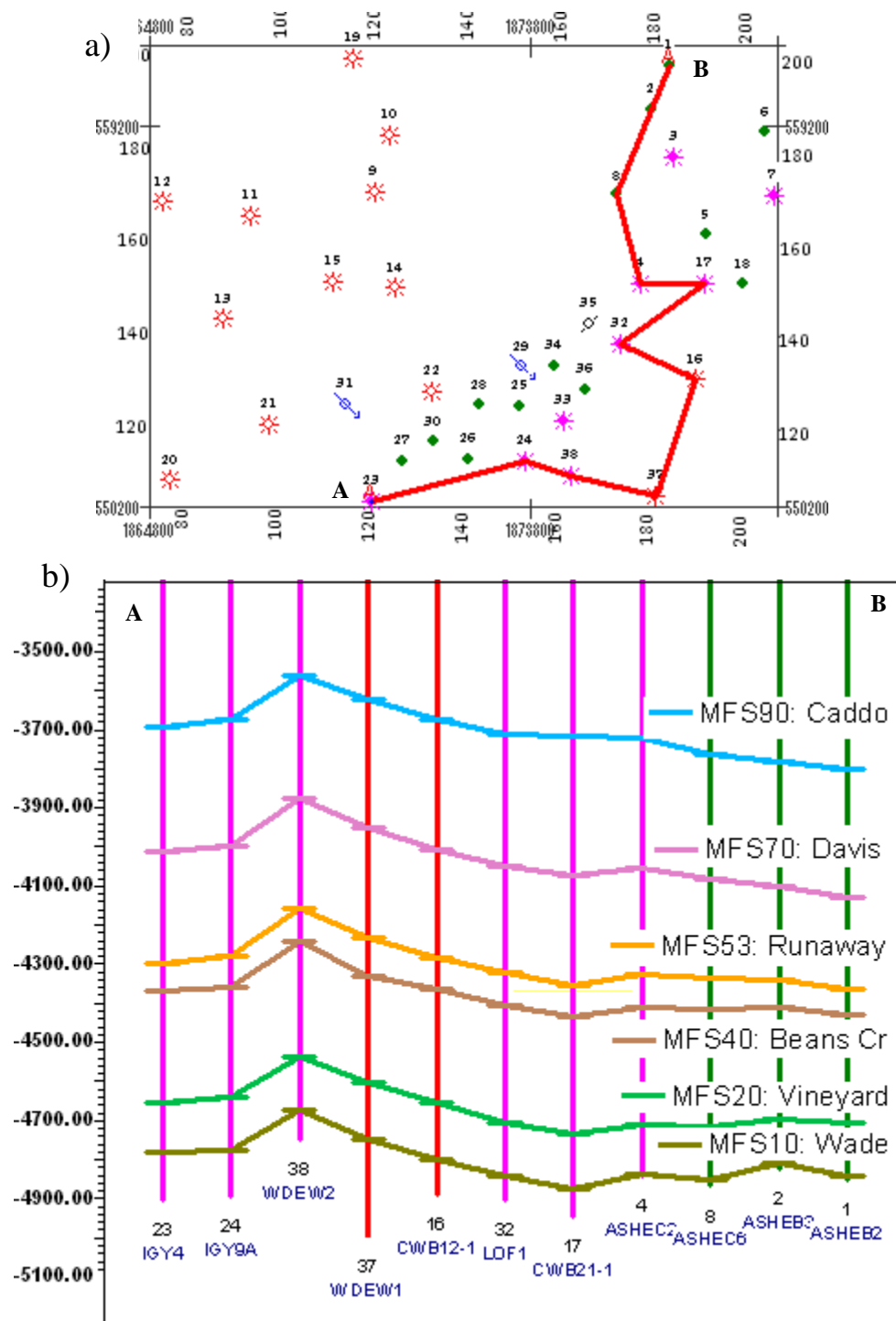


Figure 4.3. General view of the structural geology using the formation tops. a) The arbitrary line A-B in the basemap, b) Well cross section for A-B and the formation tops of the Bend Conglomerate. The depth is subsea in ft. A general south-north dipping, fold near well 17, and an anticline near well 38 are shown.

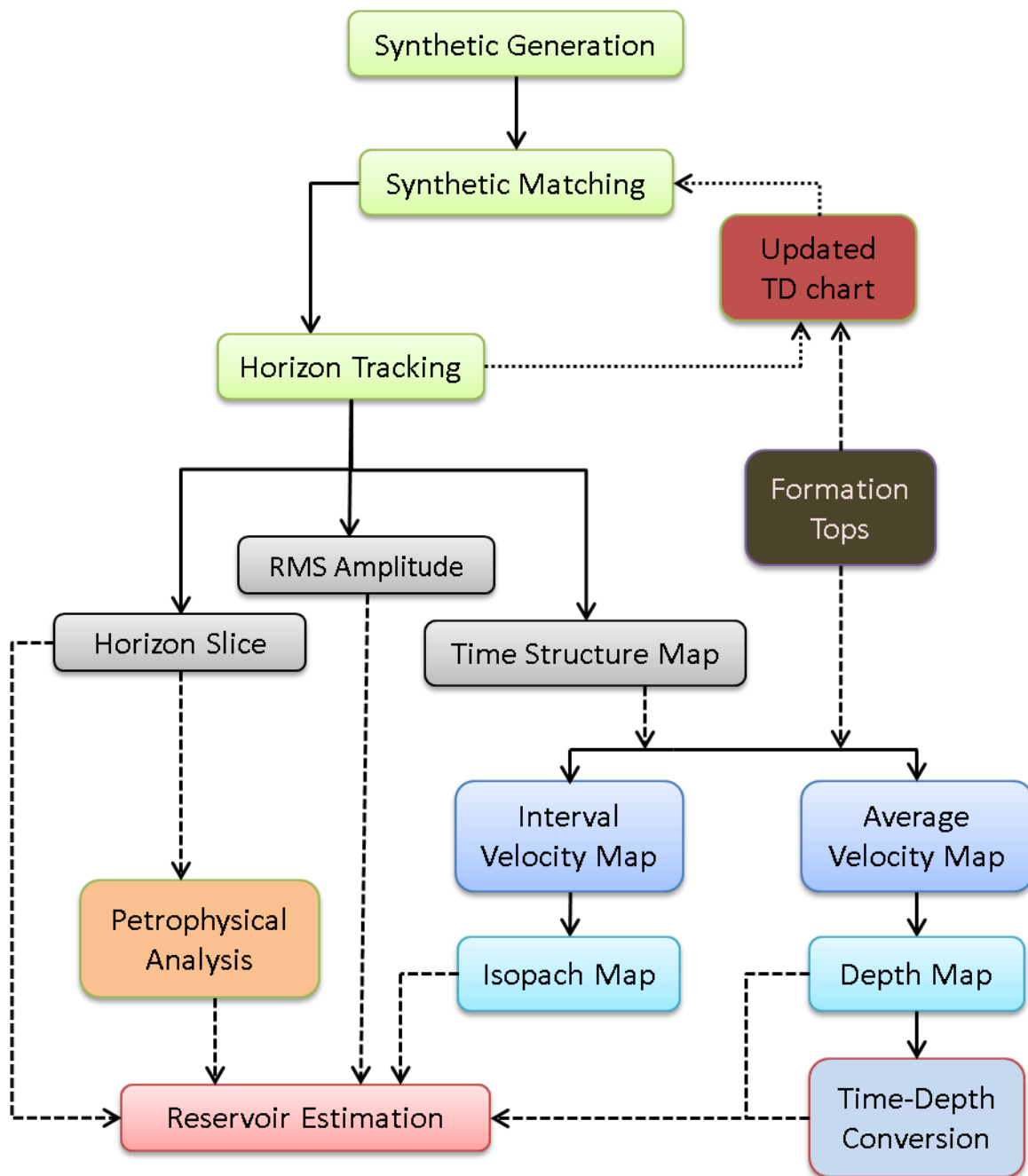


Figure 4.4. The interpretation work flow.

4.2. SYNTHETIC GENERATION

A synthetic seismogram is a simulated seismic response computed from well data. It is a suitable tool for correlating geological data from well logs with seismic data. The seismic data is displayed in time values. Synthetic seismogram provides both time and depth values for accurate reflection events verification. The components needed to generate a synthetic seismogram include Time-Depth (TD) chart, velocity log, density log (RHOB), acoustic impedance (AI), reflection coefficient (RC), and wavelet. Figures 4.5 and 4.6 illustrate all the components used to generate synthetic seismograms for Well 15 (BY18D) and Well 14 (BY15). Following are the description of each of the components:

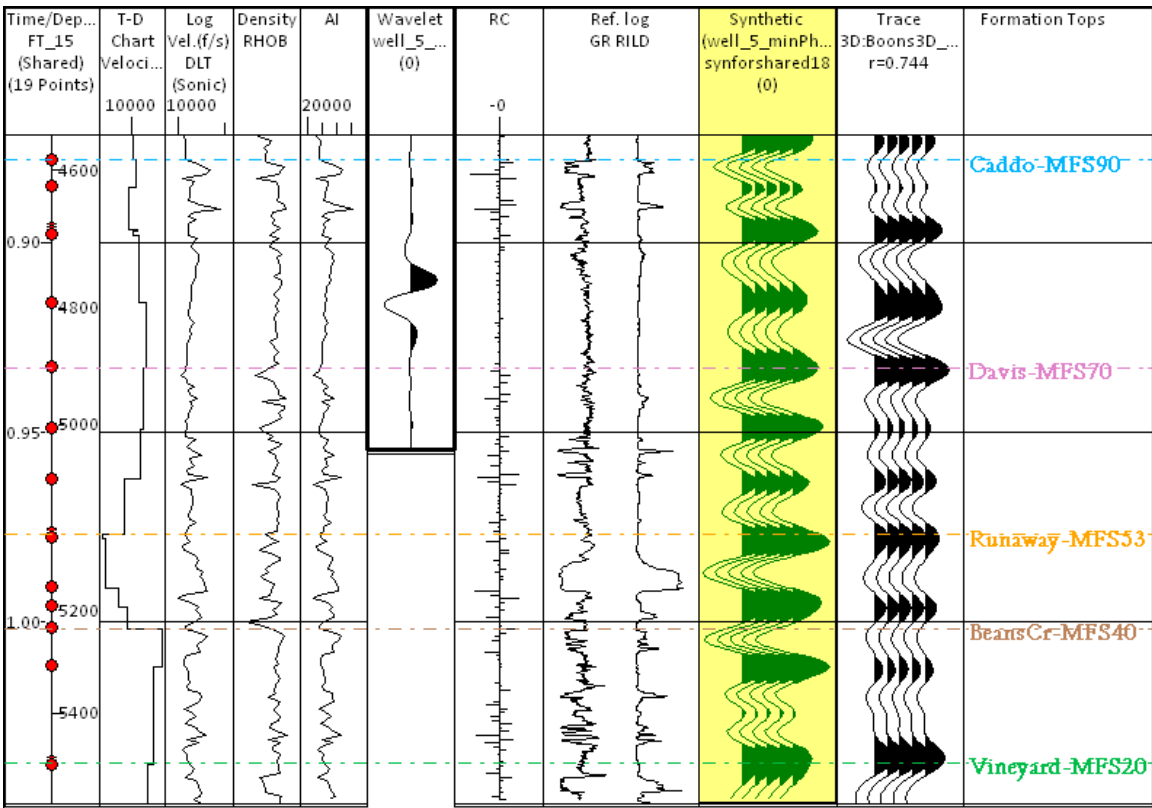


Figure 4.5. Synthetic seismogram generation for Well BY18D, illustrating all the components used and the synthetic seismogram generated. The cross correlation coefficient between the seismic trace and the synthetic seismogram (γ) value is 0.744 indicating a good matching between the synthetic seismogram and the seismic trace. The formations listed are the MFS formation tops from Hardage et al. (1996) shown in Table 3.4.

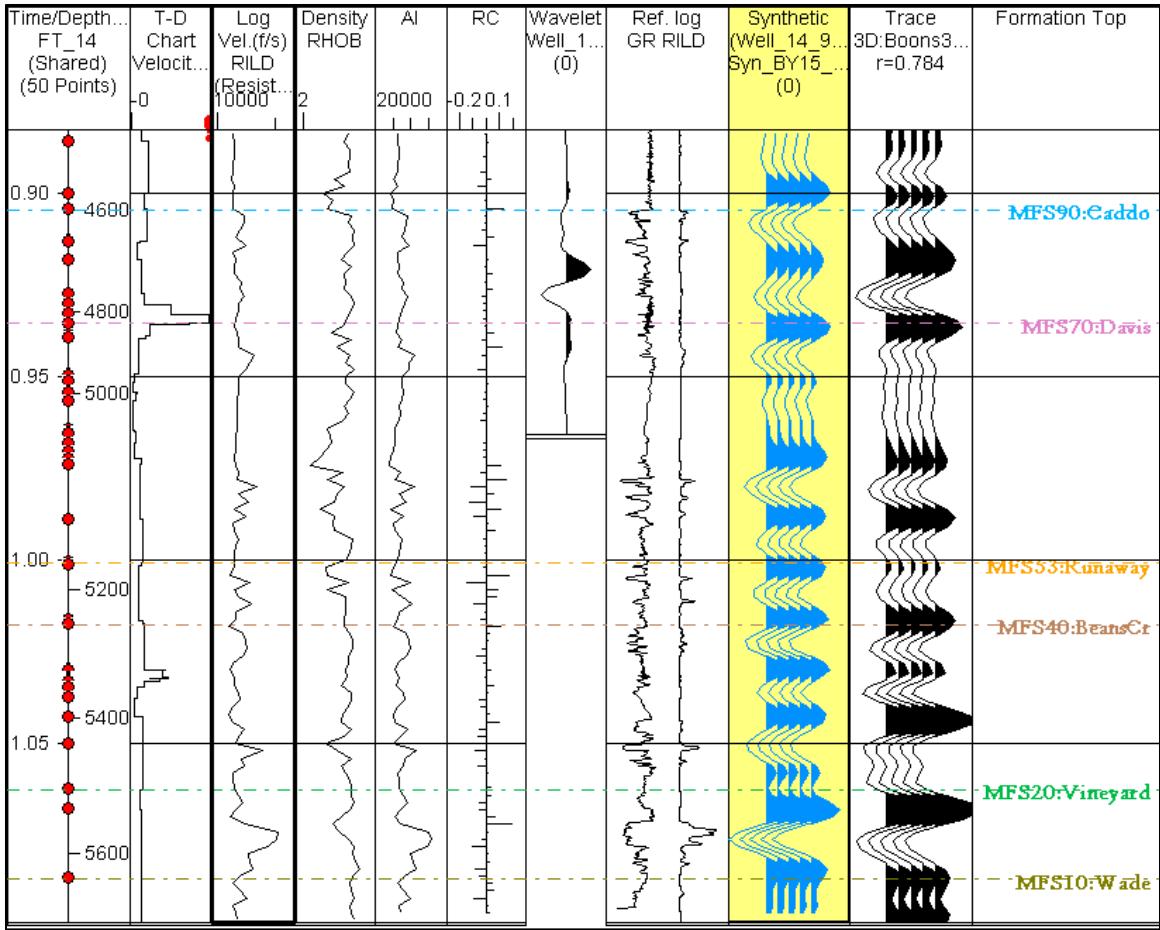


Figure 4.6. Synthetic seismogram generation for Well 14 (BY15), illustrating all the components used and the synthetic seismogram generated. The cross correlation coefficient between the seismic trace and the synthetic seismogram (γ) value is 0.784 indicating a good matching between the synthetic seismogram and the seismic trace. The formations listed are the MFS formation tops from Hardage et al. (1996) shown in Table 3.4.

4.2.1. Time-Depth (T-D) Chart. Time-Depth chart is used to connect depth of well logs to time in the seismic section. The T-D chart was generated for Well BY18D through the checkshots, which utilized both explosive and vibroseis sources (Tables 3.2 and 3.3). For better results, the T-D chart was integrated with the sonic log (DLT), which records the travel times of an emitted wave from the source to receivers. For other wells, the T-D chart was built using the Well BY18D checkshots, integrated with their logs.

4.2.2. Acoustic Impedance (AI). Acoustic Impedance is the product of the velocity and the density log values at a specific layer. The velocity log is a record of the wave speed along the well formations. It can be measured directly from DLT. The density log (RHOB) is combined with the DLT to compute the acoustic impedance as a function of depth. The velocity relates mathematically to both the density (by Gardner's correlation) and the resistivity (by Faust's correlation). Thus, it can be measured from either density logs or resistivity logs. For Well BY18D, the velocity log is measured using the sonic log. Other wells, such as Well BY15, are not provided with the sonic logs. In such situation, either density or resistivity logs are used to obtain the velocity information.

4.2.3. Wavelet. The wavelet is computed from the seismic traces surrounding the well. In this study, wavelets are extracted for Wells BY18D and BY15 from the surrounding seismic traces up to 110 ft away (Figure 4.7).

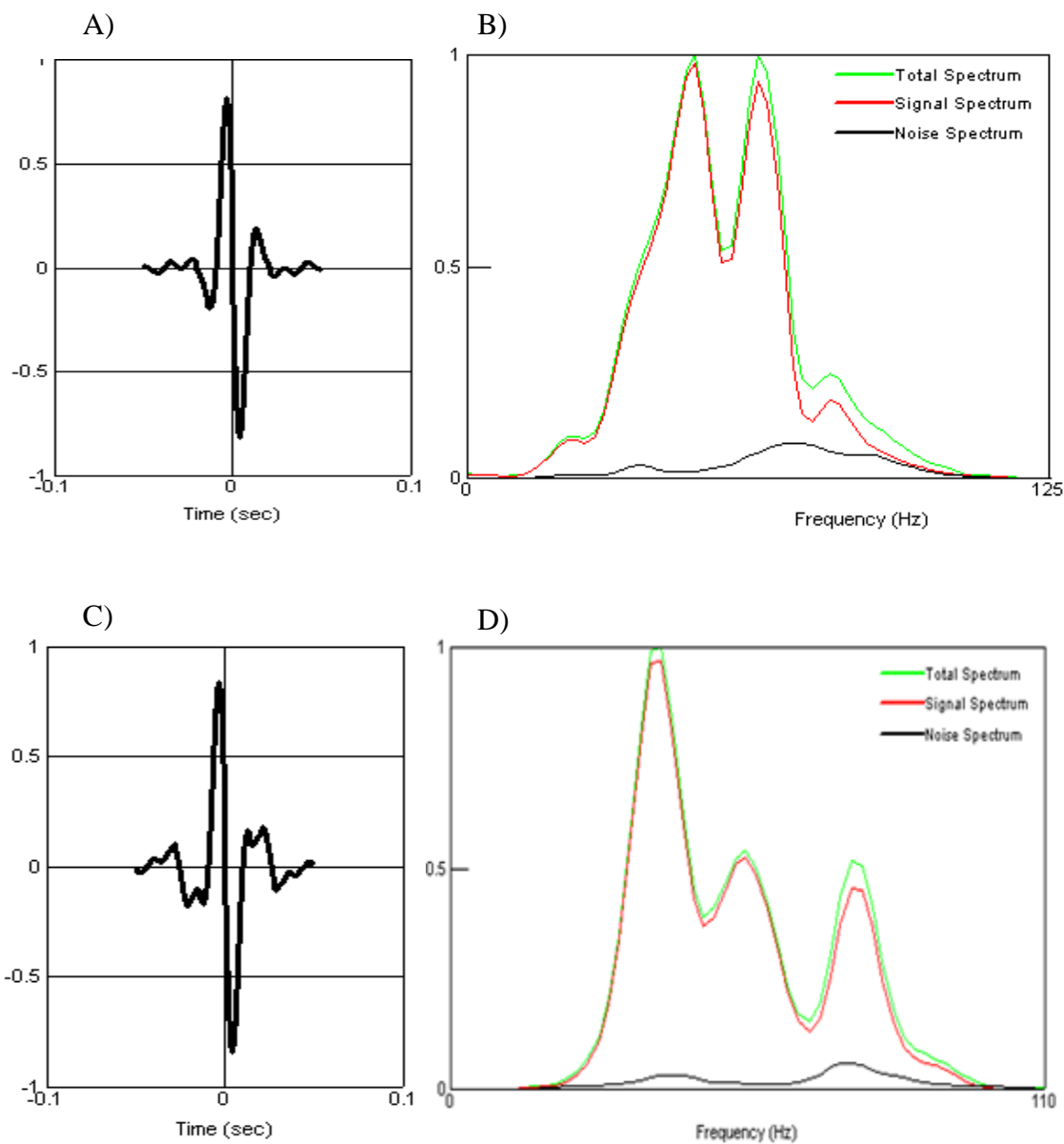


Figure 4.7. Extracted wavelets and their amplitude spectra for Wells 15 and 14. A) Extracted 90° phase wavelet for Well 15 (BY18D) with a sampling interval of 0.001 s and length 0.1 s. B) The amplitude spectra for the wavelet (green), the noise (black) and the signal (red). C) Extracted 90° phase wavelet for Well 14 (BY15) with a sampling interval of 0.001 s and length 0.1 s. D) The amplitude spectra plot for the wavelet (green), the noise (black), and the signal (red).

4.2.4. The Reflection Coefficient (RC). The reflection coefficient is a measure of the AI contrast at a formation bed boundary. It is expressed mathematically as:

$$RC = \frac{AI_2 - AI_1}{AI_2 + AI_1} \quad (1)$$

The reflection coefficient is computed for each time sample. Hence, a sequence of coefficients is generated as a reflection coefficient series (Figure 4.5).

The reflection coefficient series is convolved with the wavelet extracted to generate the synthetic seismogram. Finally, the synthetic seismogram is matched with nearby survey traces so that well log features can be tied to the seismic data.

4.3. SYNTHETIC MATCHING

After the synthetic seismogram is generated, it must be matched with the real seismic data. In order to do this, a seismic trace was extracted for each well from the nearest seismic traces around the wells. This extracted trace represented the real seismic data to be used in the synthetic matching. The synthetic trace could be shifted, stretched, or squeezed to obtain the best matching results. The SynPak calculates the cross-correlation coefficient (γ) between the seismic trace and the synthetic seismogram during the synthetic editing. The cross-correlation coefficient ranges between -1.0 (perfectly out of phase) and $+1.0$ (perfectly matched in shape). The γ values are $+0.744$ and $+0.784$ for Well 15 (BY18D) and Well 14 (BY15) respectively, indicating convincing matches (Figures 4.5 and 4.6). The synthetic seismograms for both wells are overlying the real seismic data after synthetic matching (Figures 4.8 and 4.9).

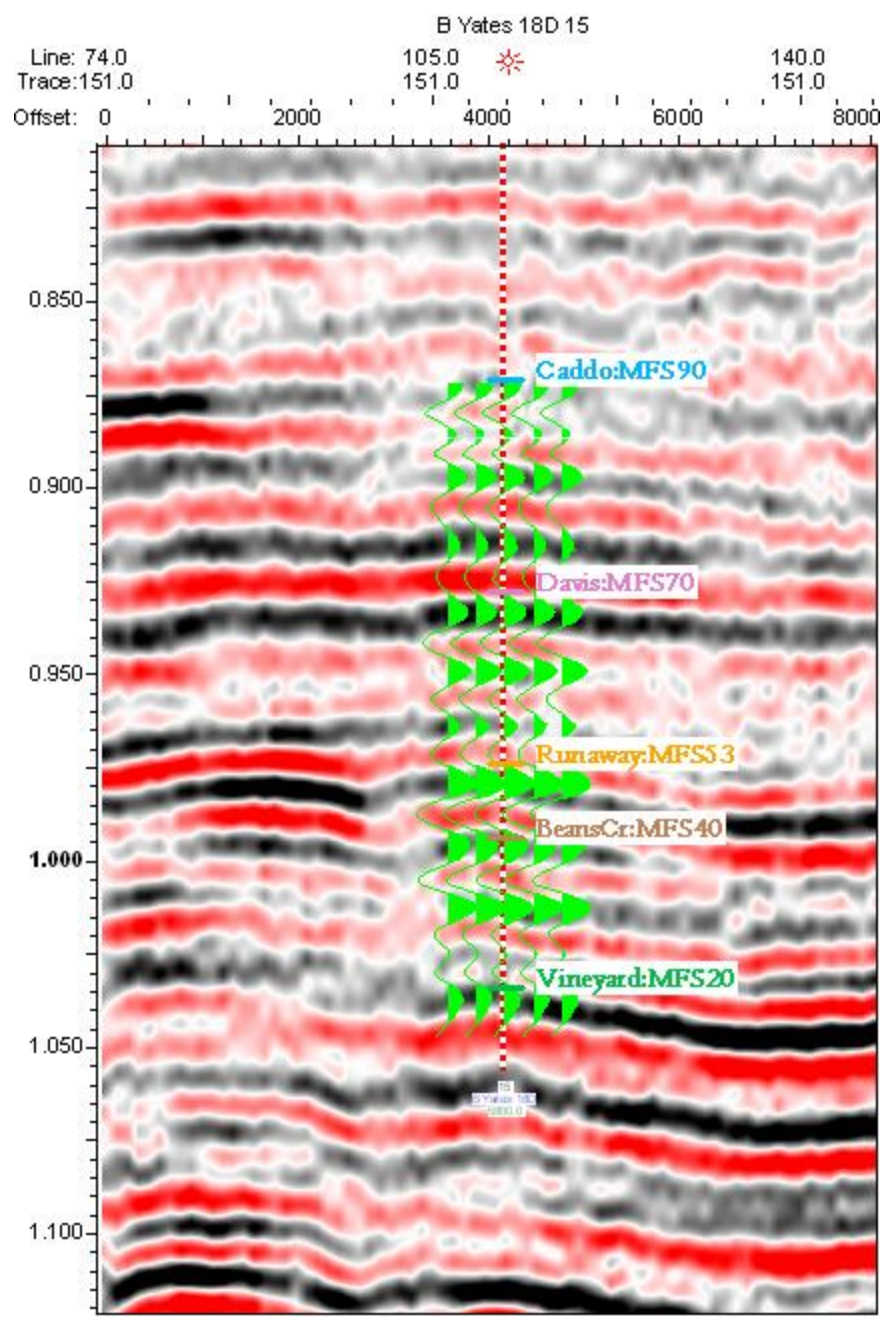


Figure 4.8. Seismic section of Crossline 151 with the generated synthetic seismograms from Well 15 (BY18D). The formation top of Wade (MFS10) is not provided for this well. The synthetic seismogram helps successfully to identify the horizons for each of the formation tops targeted.

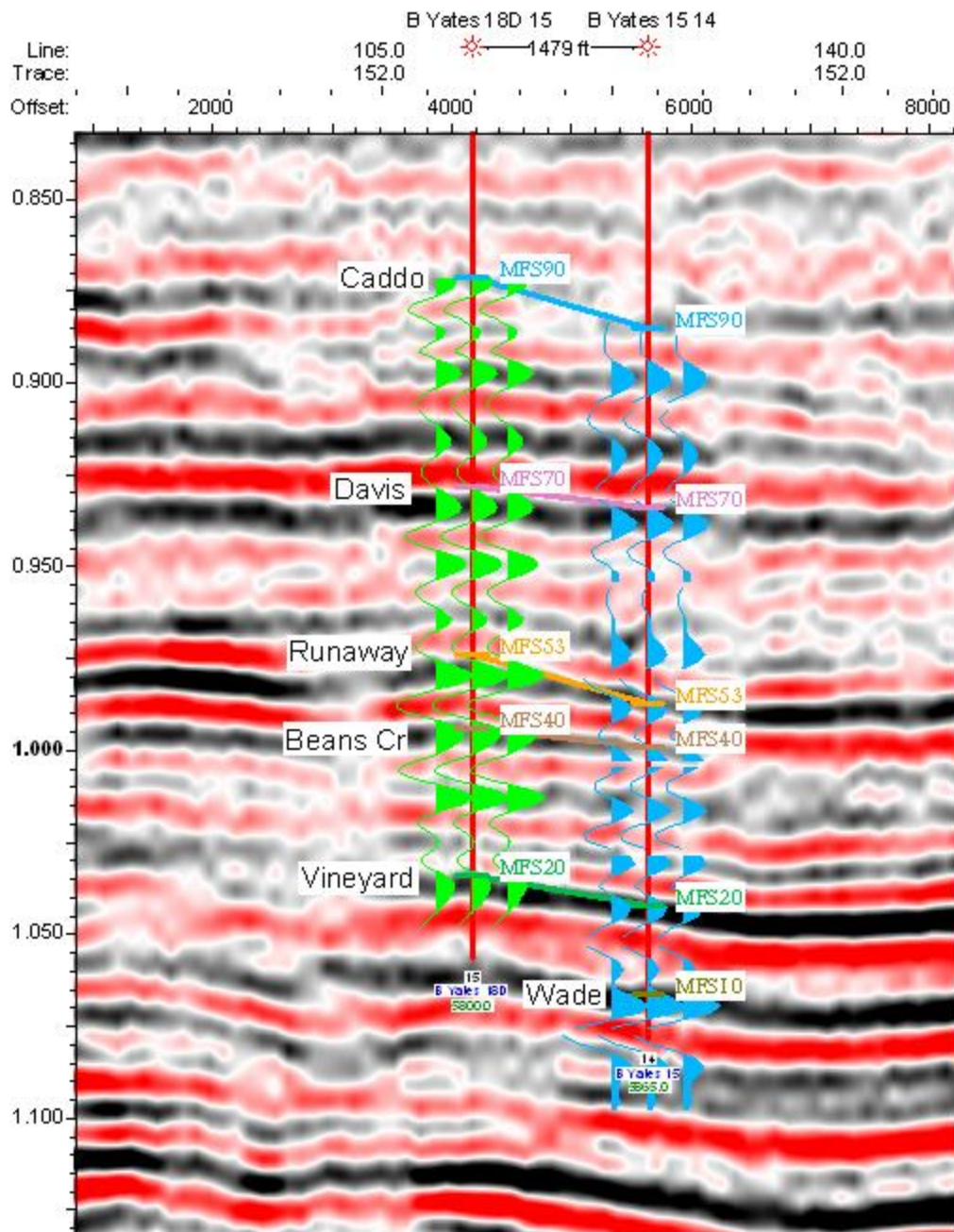


Figure 4.9. Seismic section of Crossline 152 with the generated synthetic seismograms from Well 15 (BY18D) (green), and Well 14 (BY15) (blue). Well 14 is deeper than Well 15. It has the Wade (MFS10) Formation top depth.

4.4. HORIZON INTERPRETATION

Horizon interpretation requires picking a reflection event across all the seismic survey inlines and crosslines. Interpreting specific event yields records of both time and amplitude values. Therefore, the interpreted horizon is a composite of different traces varying in time and amplitude values for a specific layer. The wavelet for the 3D data is a 90° phase. However, in order to conduct the horizon interpretation, the peak amplitudes are picked to identify the MFS for each formation.

4.4.1. Caddo and Davis. Caddo is the top formation of the Bend Conglomerate. Relatively, it can be easily identified since it is following a thick layer of shale that is followed by Caddo limestone Formation (Figure 2.8). Besides, all the 38 wells penetrate it and with the depth of the Caddo Formation top data. Consequently, interpreting Caddo helps to determine other formations in the Bend (Figure 4.10). Davis (MFS70) is also one of the main genetic sequences in the Bend. Both the Caddo and the Davis horizons are interpreted to support the objective of this study by giving a better geologic visualizing to the Bend Conglomerate features.

4.4.2. Runaway and Beans Cr. Both Runaway and Beans Cr represent, respectively, top and base of the Runaway Formation. The Runaway top horizon (MFS53) and the Beans Cr top horizon (MFS40) were targeted previously to perform many interpretations and applications of reservoir characterizations. The Runaway Formation is identified by picking its horizon top (MFS53) and base (MFS40). The targeted horizons are identified for many wells using the synthetic seismograms (Figure 4.10).

4.4.3. Vineyard and Wade. Vineyard Formation is located at the base of the Bend Conglomerate. Vineyard horizon (MFS20) was tracked as the Vineyard Formation top, and Wade horizon (MFS10) as base of the Vineyard Formation (Figure 4.10). The horizons are identified using the synthetic seismograms generated and tracked along the seismic data.

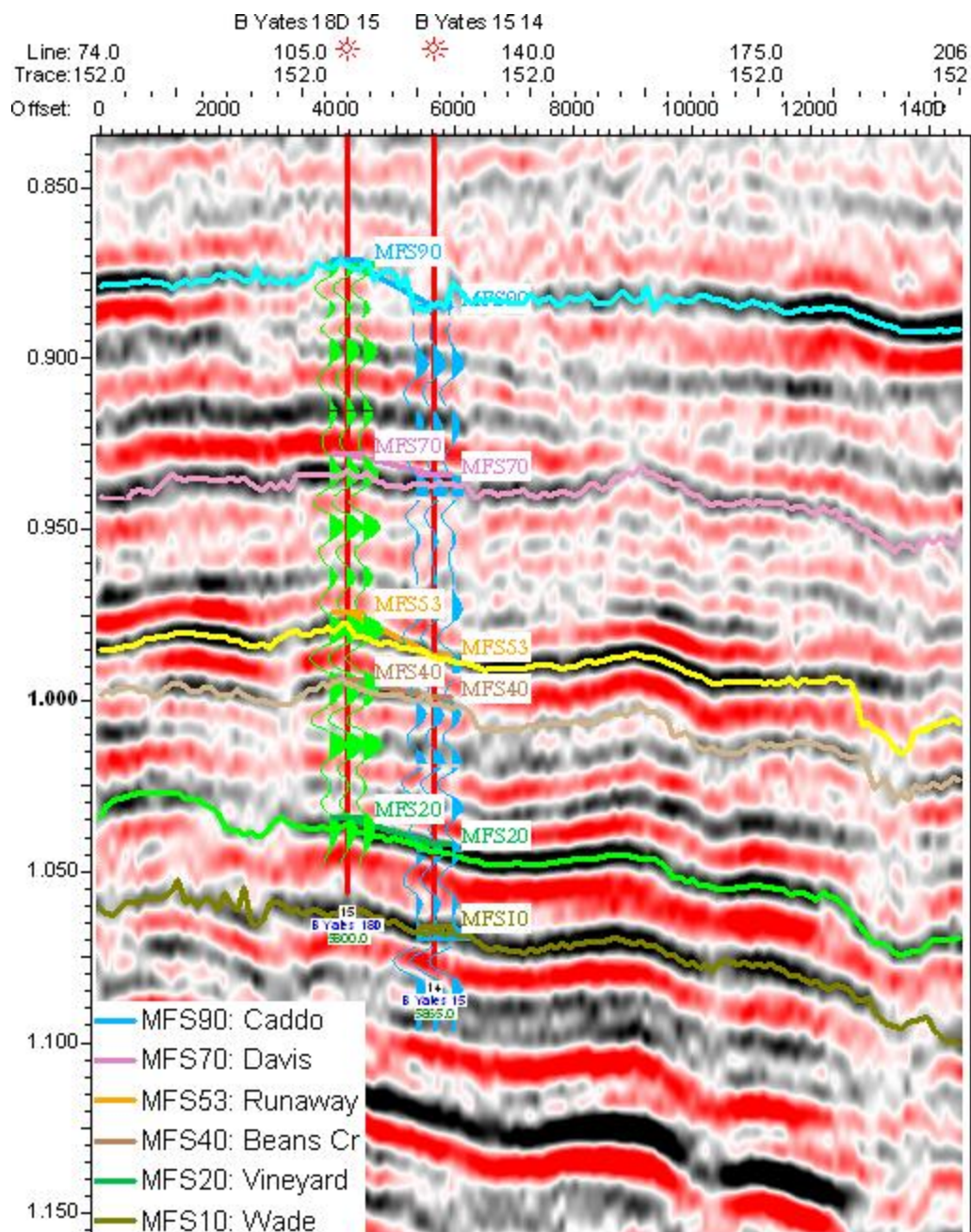


Figure 4.10. Seismic section of Inline 112 showing the horizon picking for: Caddo (MFS90) in blue, Davis (MFS70) in pink, Runaway (MFS53) in yellow, Beans Creek (MFS40) in light brown, Vineyard (MFS20) in green, and Wade (MFS10) in dark green. In addition, the seismic section shows the Wells 14 and 15 synthetic seismograms which helped identify the mentioned horizons.

4.4.4. Updating T-D Chart. The T-D chart was imported from the checkshots of Well 14 (BY18D) (Table 3.3). However, this T-D chart is near BY18D. Applying the chart to other wells will lead mislocated horizons. In order to better locate horizons, new T-D charts are generated for each well by correlating the formation top data (Table 3.4) with the horizon time (Figure 4.10). Table 4.1 below shows updated T-D charts for some wells.

Table 4.1. Updated T-D charts generated from the horizon picks and the formation tops. First column is the well number. The depth is in TVD from the seismic datum in ft. TWT is in second. Some wells such as Well 5 contains only one formation top

Well 1	TVD (ft)	0	4701	5027	5261	5327	5605	5742
	TWT (s)	0	0.897	0.951	0.997	1.025	1.051	1.078
Well 2	TVD (ft)	0	4680	5000	5240	5311	5595	5710
	TWT (s)	0	0.894	0.95	0.995	1.018	1.052	1.078
Well 3	TVD (ft)	0	4654	4980	5233	5294	5584	5715
	TWT (s)	0	0.891	0.944	0.992	1.012	1.051	1.076
Well 4	TVD (ft)	0	4621	4955	5227	5310	5609	5736
	TWT (s)	0	0.882	0.941	0.991	1.012	1.052	1.076
Well 5	TVD (ft)	0	4617					
	TWT (s)	0	0.886					
Well 6	TVD (ft)	0	4699	5040	5310	5656	5786	
	TWT (s)	0	0.902	0.963	1.015	1.073	1.098	
Well 7	TVD (ft)	0	4631	4977	5243	5309	5594	5715
	TWT (s)	0	0.89	0.952	1.001	1.018	1.057	1.089
Well 8	TVD (ft)	0	4665	4982	5235	5313	5613	5748.5
	TWT (s)	0	0.898	0.952	0.998	1.018	1.059	1.082
Well 9	TVD (ft)	0	4627	4940	5185	5252	5541	
	TWT (s)	0	0.881	0.943	0.983	1.005	1.037	
Well 10	TVD (ft)	0	4654	4960	5193	5252	5543	
	TWT (s)	0	0.895	0.948	0.987	1.007	1.045	

4.5. STRUCTURAL MAPPING

After the horizons are tracked, various structure maps can be constructed (Figure 4.4).

4.5.1. Time Structure Map. The Two Way travel Times (TWT) are stored after horizons are picked. To generate time structure maps, the Gradient Projection gridding algorithm is used. It computes X and Y derivatives at every data sample location. In addition, it allows projecting an interpolated value at a grid node using an inverse distance to a power weighting. The time structure maps are shown respectively for Caddo top (MFS90), Davis top (MFS70), Runaway top (MFS53), Beans Creek top (MFS40), Vineyard top (MFS20), and Wade top (MFS10) in Figures 4.11, 4.12, 4.13, 4.14, 4.15 and 4.16.

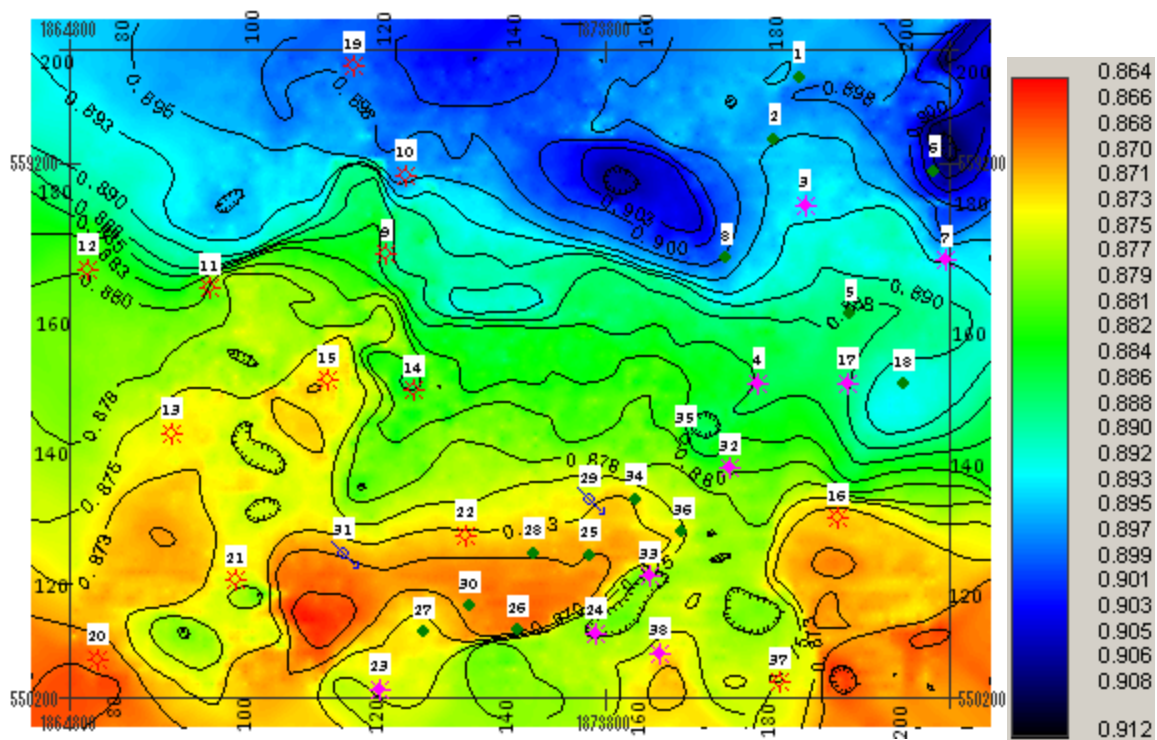


Figure 4.11. Time structure map of the Caddo top (MFS90) showing a dipping toward north.

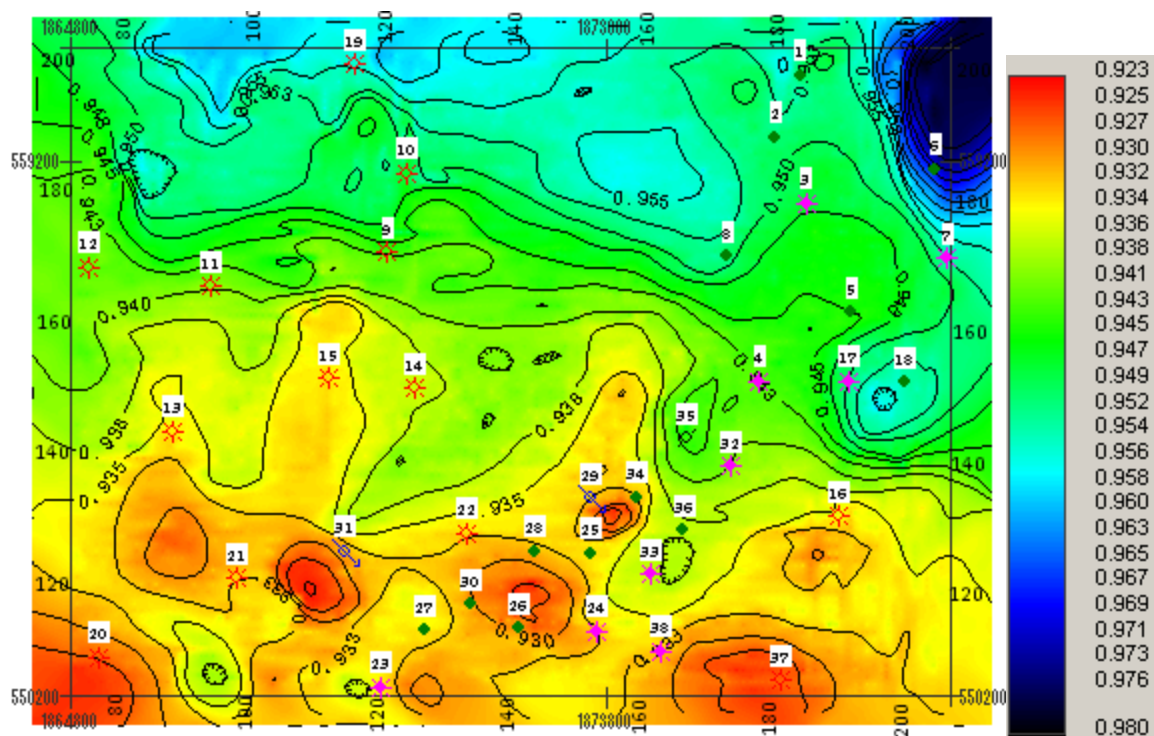


Figure 4.12. Time structure map of the Davis top (MFS70) showing a dipping toward north. TWT increases dramatically near the Well 6 which is interpreted as karst collapse features.

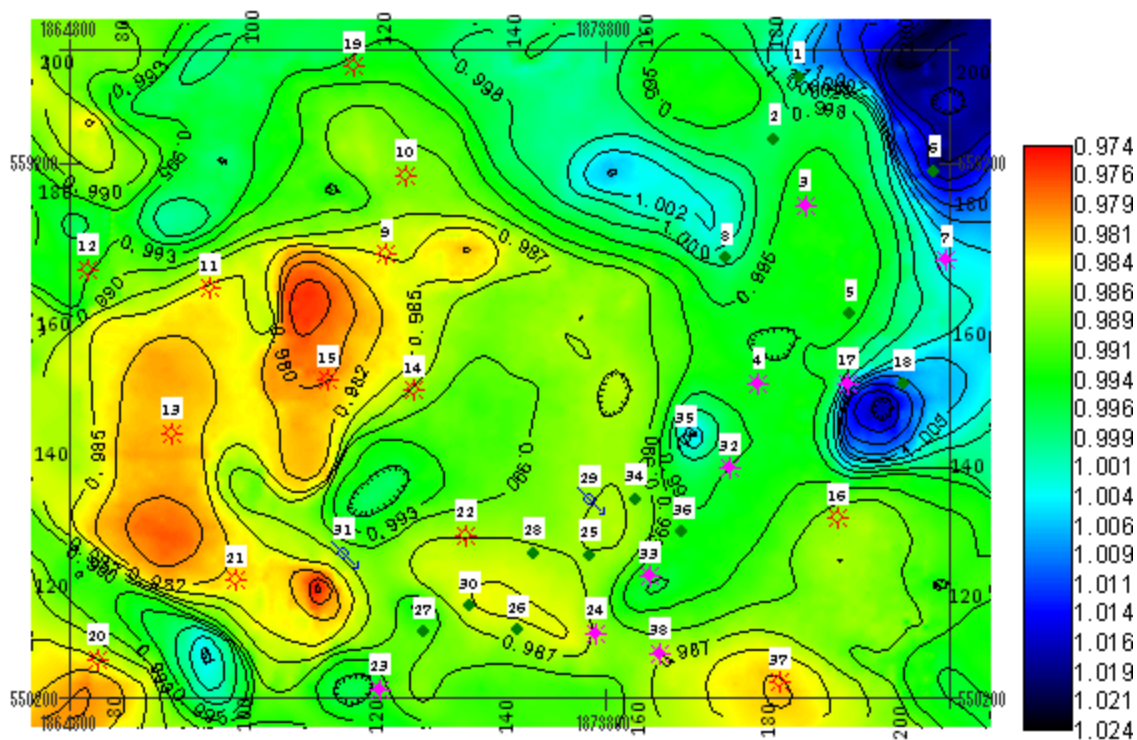


Figure 4.13. Time structure map of the Runaway top (MFS53) showing a dipping toward north-east. The two circles near the Wells 6 and 18 are interpreted as karst collapse features.

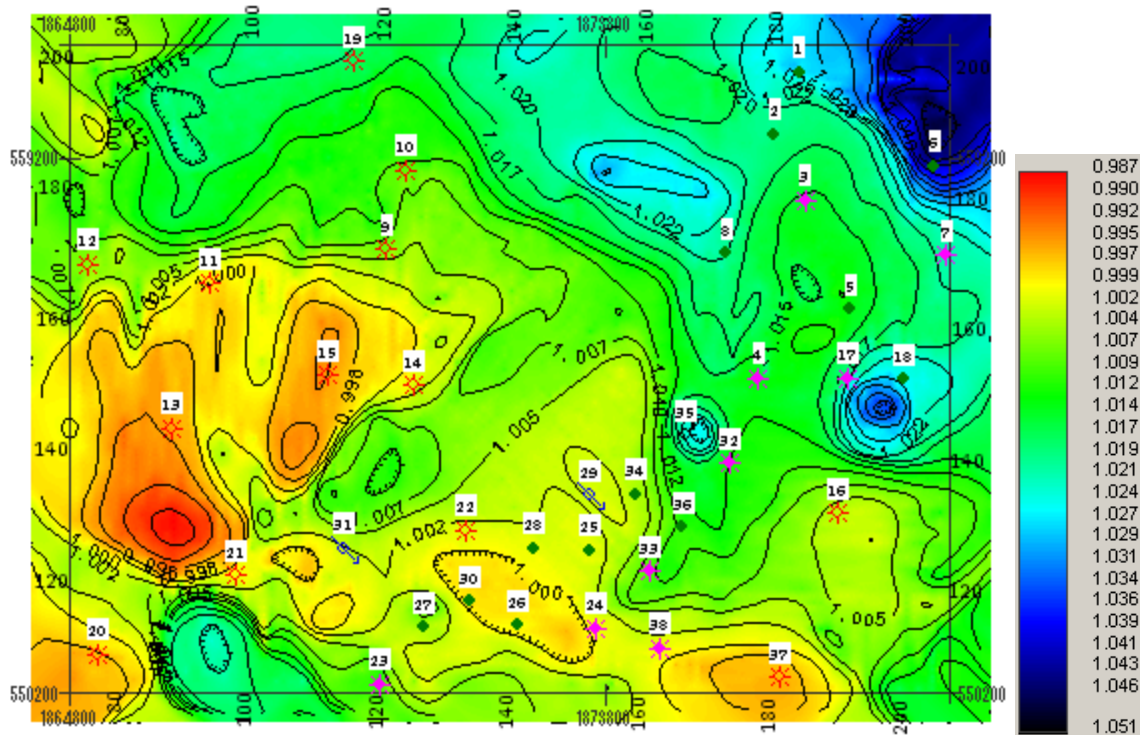


Figure 4.14. Time structure map of the Beans Creek top (Runaway bottom) (MFS40) showing a dipping toward north-east. Karst collapse features are observed near Wells 6, 8, and 18.

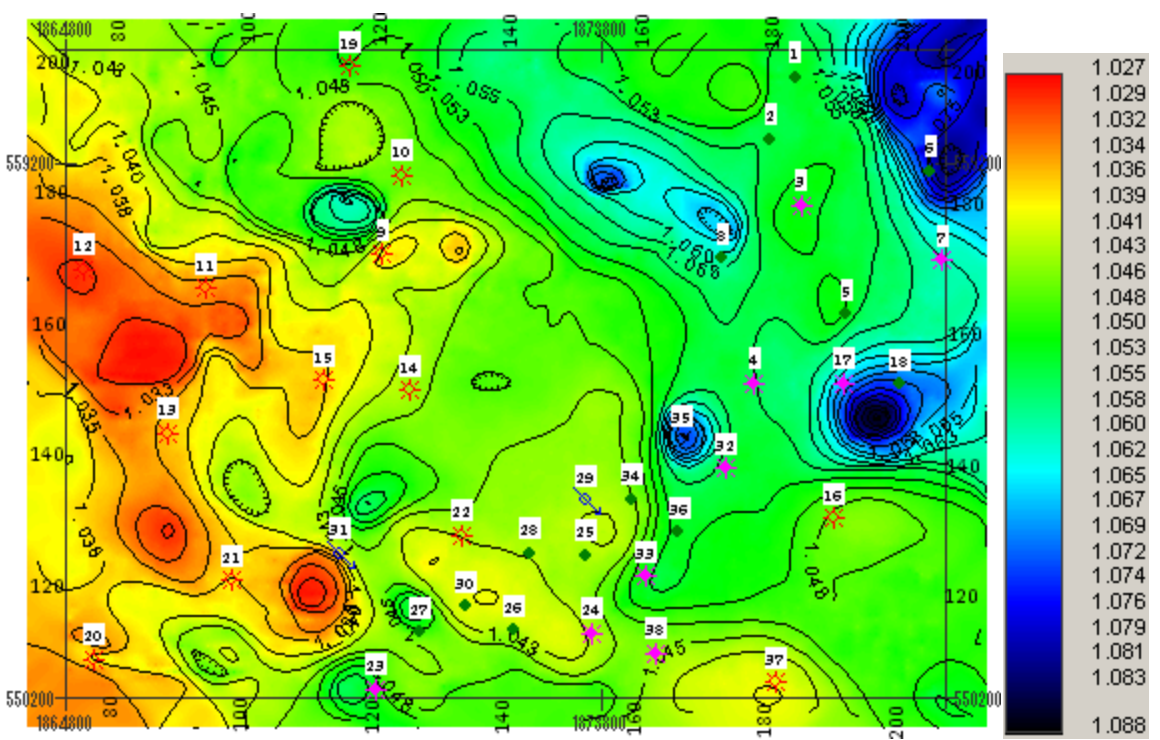


Figure 4.15. Time structure map of the Vineyard top (MFS20) showing a dipping toward east. Karst collapse features are observed as blue circles.

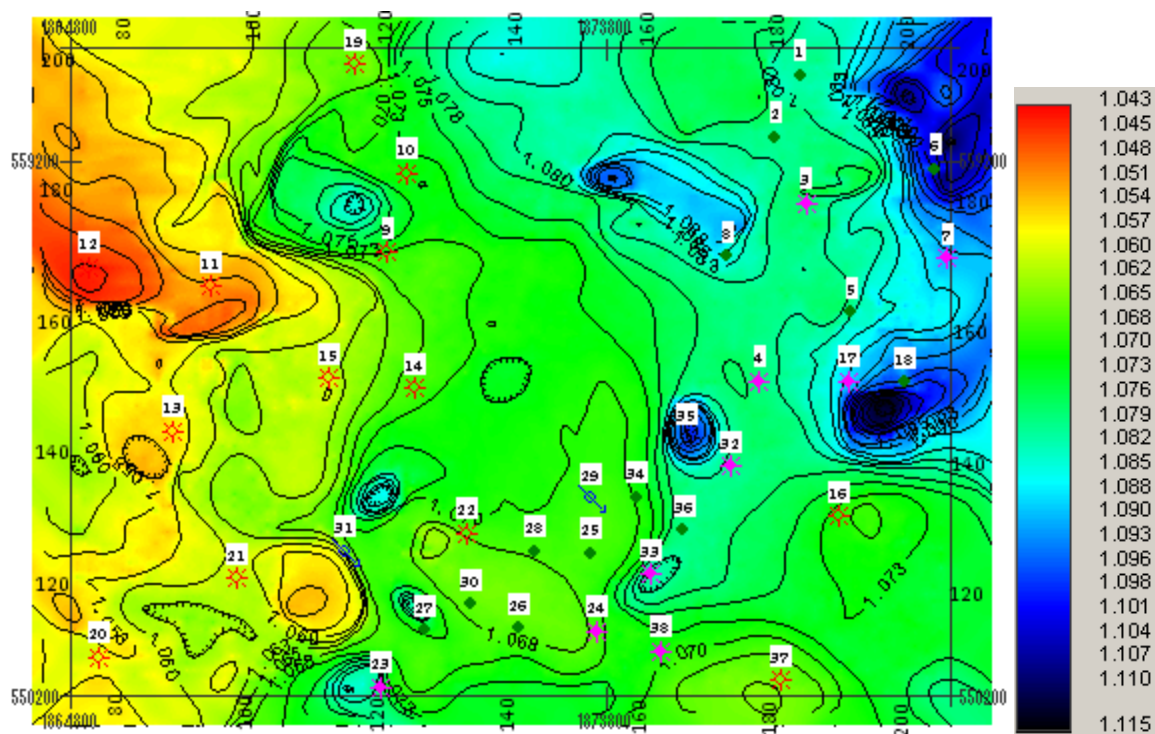
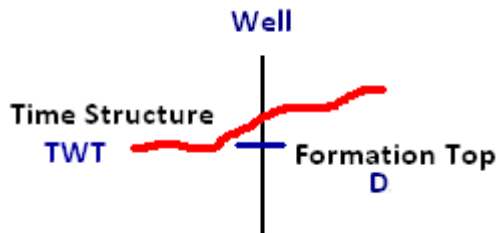


Figure 4.16. Time structure map of the Wade top (Vineyard bottom) (MFS10) showing a dipping toward east. Karst collapse features are observed near Wells 6, 8, 9, 18, 23, and 31.

4.5.2. Average Velocity Map. It is important to compute depth maps. After constructing the time structure maps, depth maps can be obtained with velocity information. The relationship between the average velocity (V_{avg}), the two way travel time to reflector (targeted horizon), and the depth of the horizon (D) is shown in equation (2) below.

$$V_{avg} = \frac{2D}{TWT} \quad (2)$$

The velocity used to convert the seismic data from time domain to depth domain is computed for each well. The TWT is obtained from the time structure of the targeted horizon. The formation top data are used for the depth value (D). The average velocity values calculated from the provided wells for specific horizon are gridded (Figure 4.17). As a result, the average velocity map computed is used for the depth map generation. The average velocity maps, respectively, for Caddo top (MFS90), Davis top (MFS70), Runaway top (MFS53), Beans Creek top (MFS40), Vineyard top (MFS20), and Wade top (MFS10) are shown in Figures 4.18, 4.19, 4.20, 4.21 4.22 and 4.23.



Figures 4.17. Illustration showing the method to compute the parameters from the well formation top and the seismic time structure in order to calculate the average velocity.

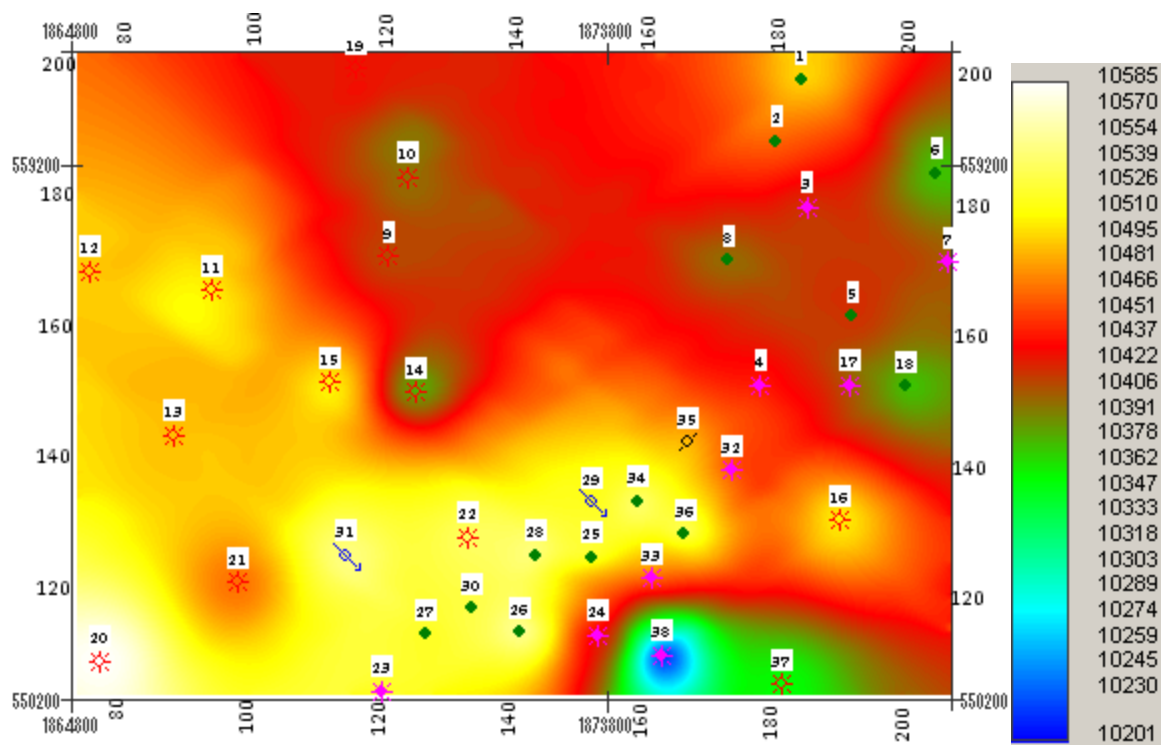


Figure 4.18. Average velocity map of the Caddo (MFS90). Velocity varies from 10200 ft/s to 10585 ft/s. The lowest velocity is observed near the Well 38, and the highest is near the Well 20.

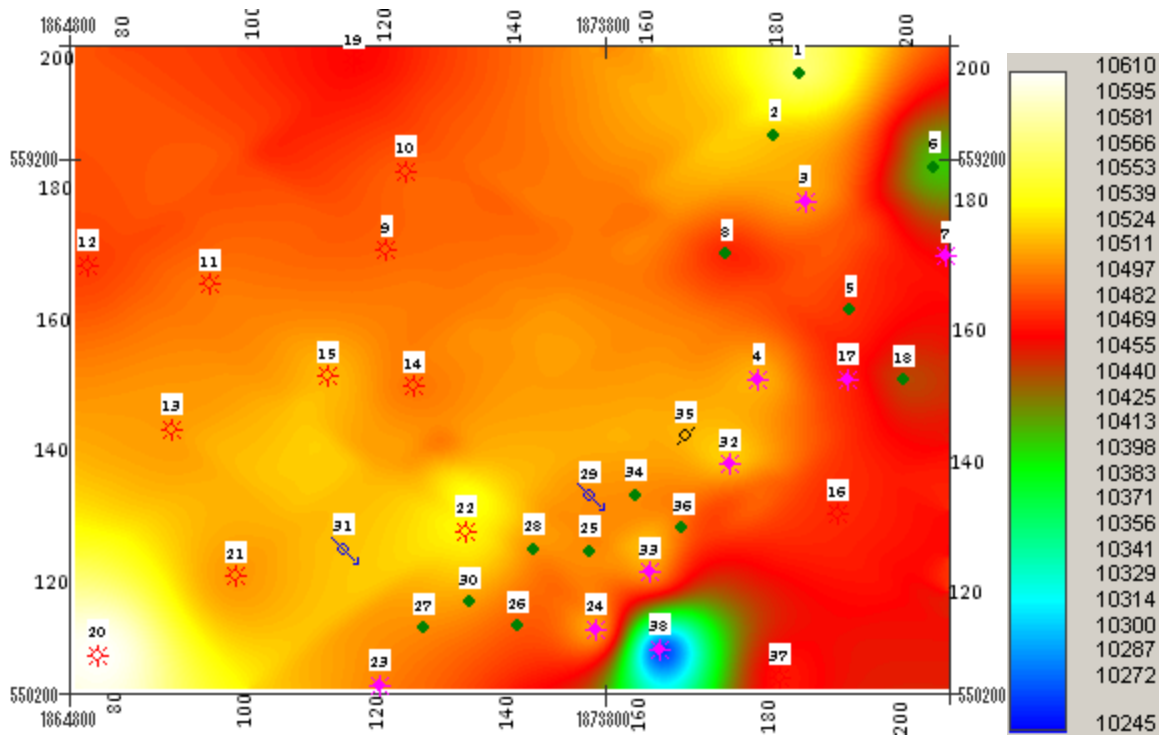


Figure 4.19. Average velocity map of the Davis (MFS70). Velocity varies from 10245 ft/s to 10610 ft/s. The lowest velocity is observed near the Well 38, and the highest is near the Well 20.

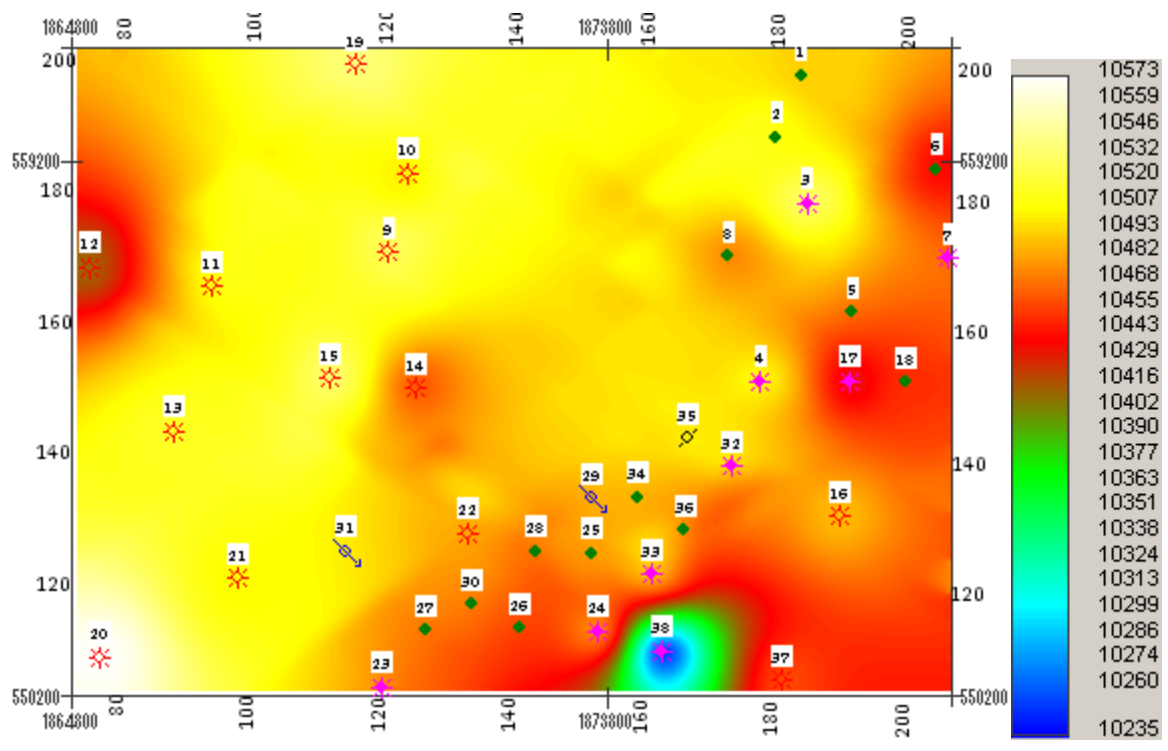


Figure 4.20. Average velocity map of the Runway (MFS53). Velocity varies from 10235 ft/s to 10573 ft/s. The lowest velocity is observed near the Well 38, and the highest is near the Well 20.

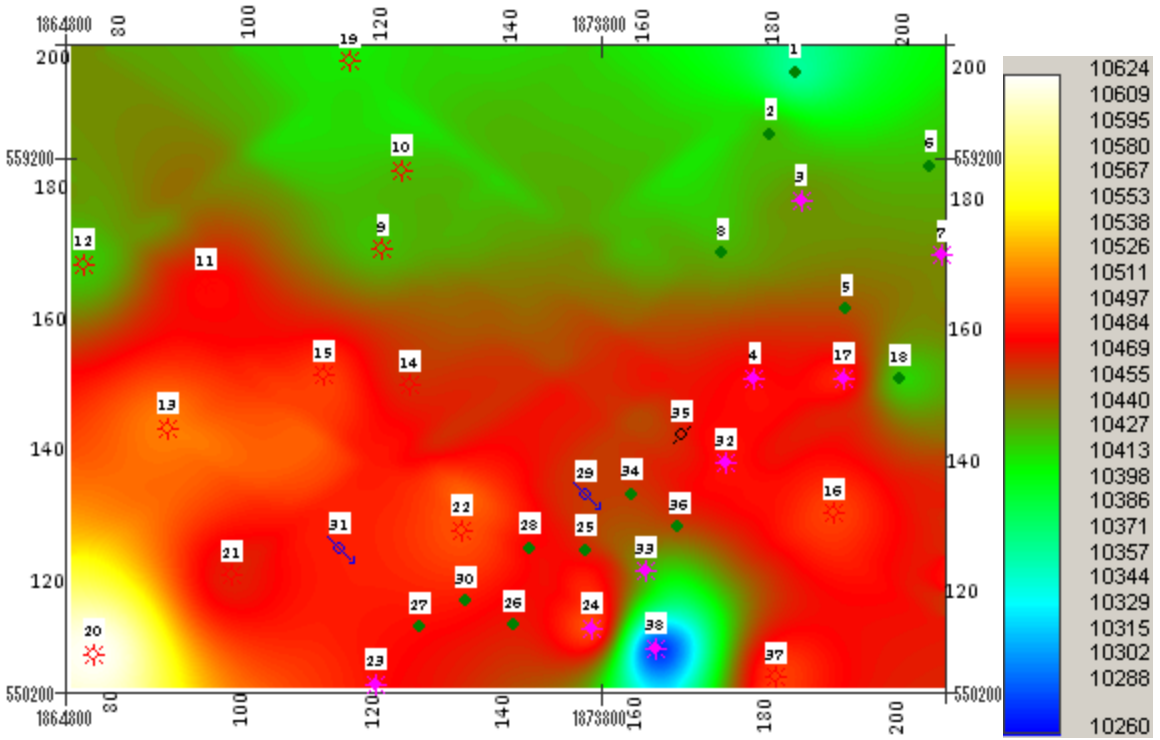


Figure 4.21. Average velocity map of the Beans Cr top (Runaway base) (MFS40). Velocity varies from 10260 ft/s to 10624 ft/s. The lowest velocity is observed near the Well 38, and the highest is near the Well 20.

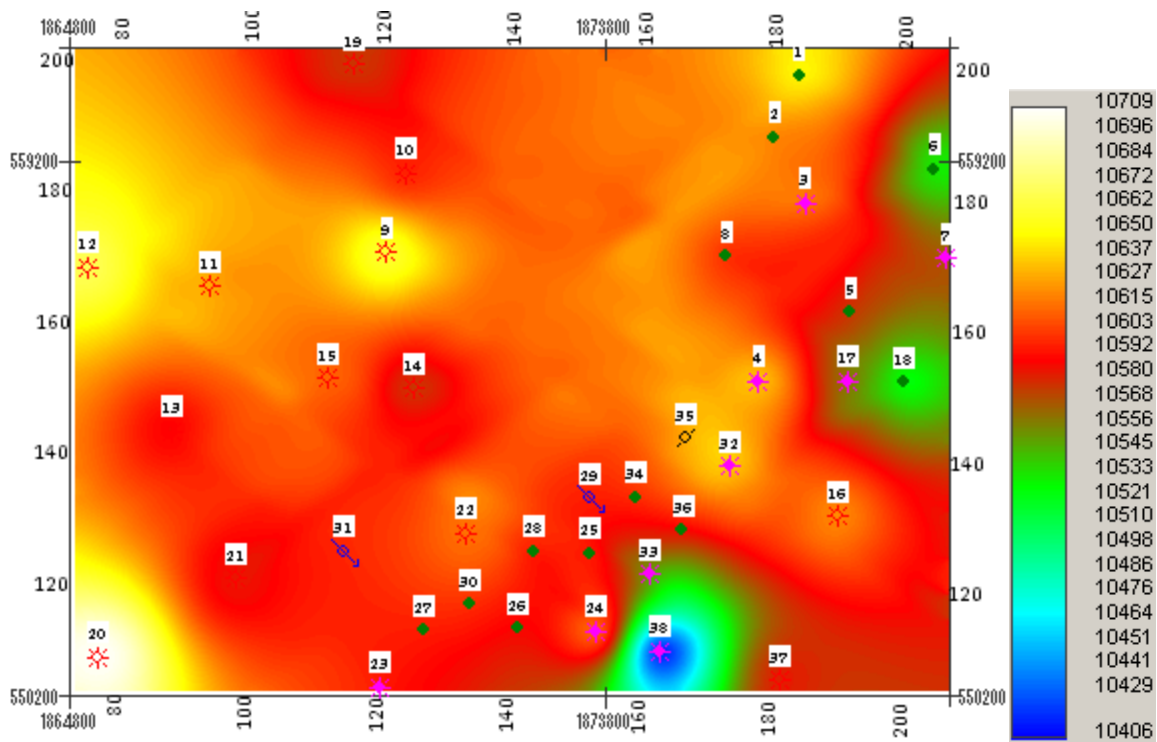


Figure 4.22. Average velocity map of the Vineyard (MFS20). Velocity varies from 10406 ft/s to 10709 ft/s. The lowest velocity is observed near the Well 38, and the highest is near the Well 20.

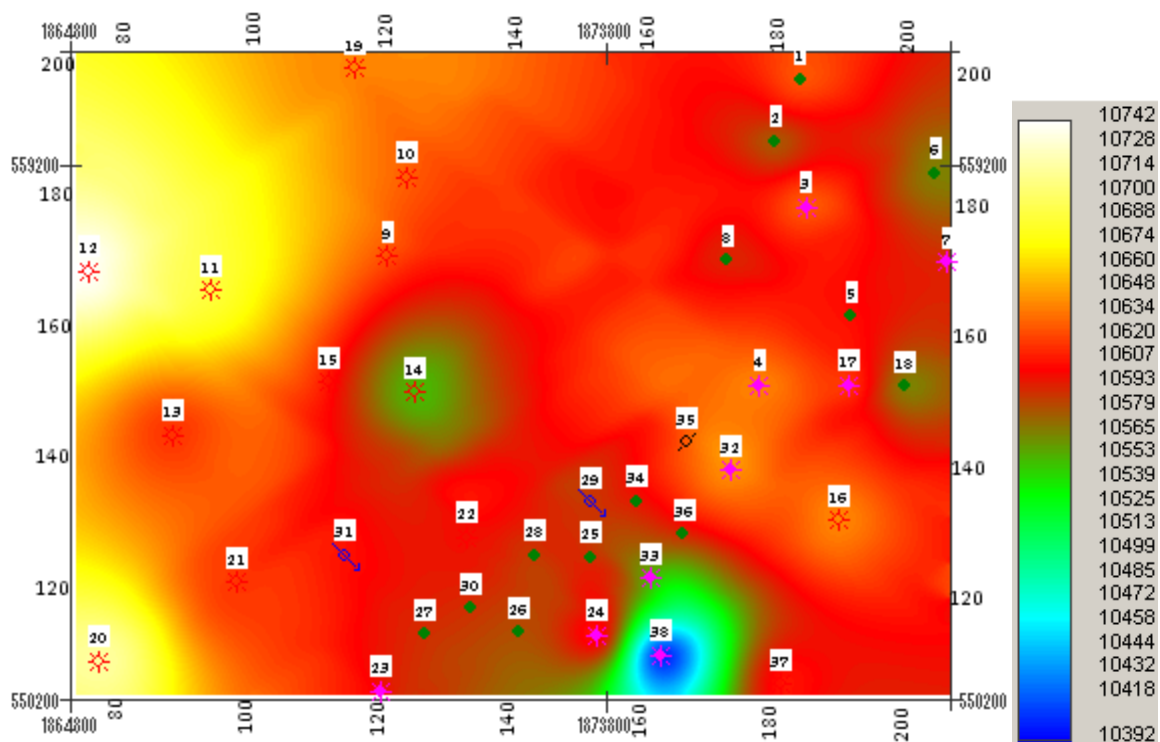


Figure 4.23. Average velocity map of the Wade top (Vineyard base) (MFS10). Velocity varies from 10392 ft/s to 10742 ft/s. The lowest velocity is observed near the Well 38, and the highest is near the Well 12.

4.5.3. Depth Map. The structure maps obtained from the seismic data are in time. In order to provide a good visualization to the structural features of horizons and wells, time-depth conversion processing is needed. Using the average velocities, the depth map for the targeted horizons are shown in Figures 4.24, 4.25, 4.26, 4.27, 4.28 and 4.29, respectively, for the Caddo top (MFS90), Davis top (MFS70), Runaway top (MFS53), Beans Creek top (MFS40), Vineyard top (MFS20), and Wade top (MFS10). In addition, a 3D view of all the generated depth maps for the targeted formations in Atoka is shown in Figure 4.30. In Figure 4.31, the Runaway Formation, bounded by MFS53 and MFS40, is visualized by the 3D depth view. The 3D depth view of the Vineyard Formation, bounded by MFS20 and MFS10, is visualized in Figure 4.32. These 3D views show the effect of the karst collapse features on the structure of the formations. The anticlines traps can be identified.

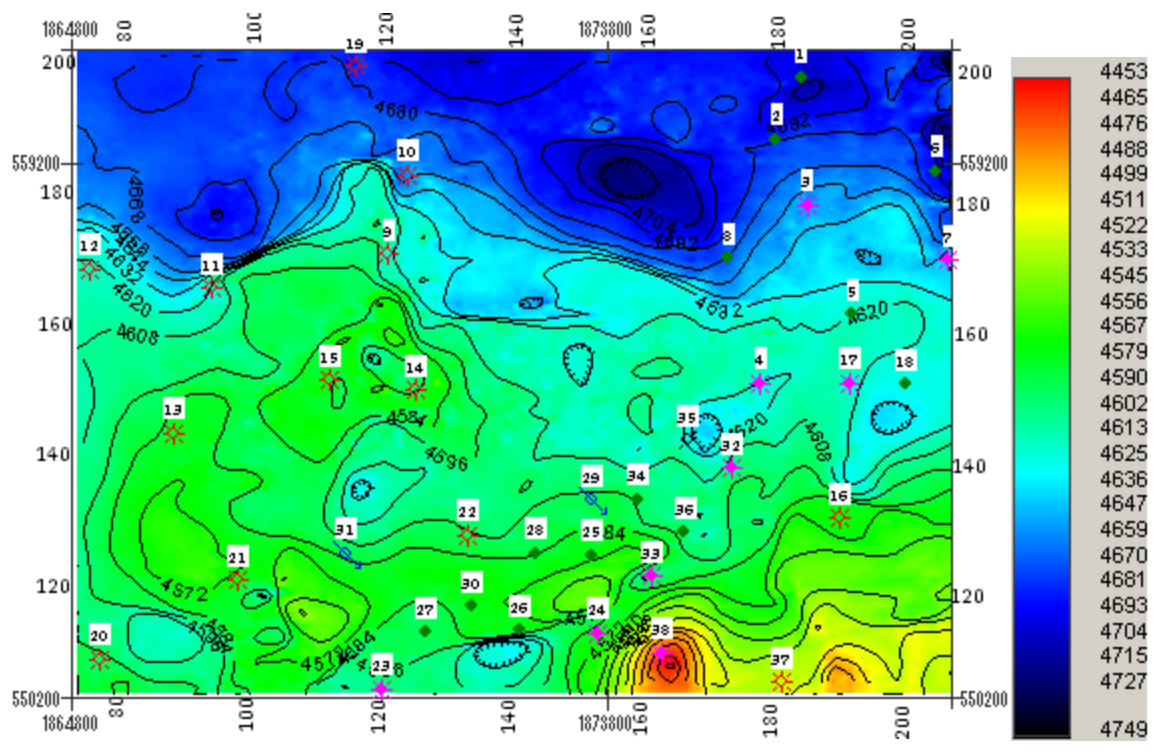


Figure 4.24. The Caddo (MFS90) depth map in TVD from the seismic datum (ft) showing that the layer is dipping toward north. Depth varies from 4453 ft to 4749 ft. Anticline is observable near the Well 38.

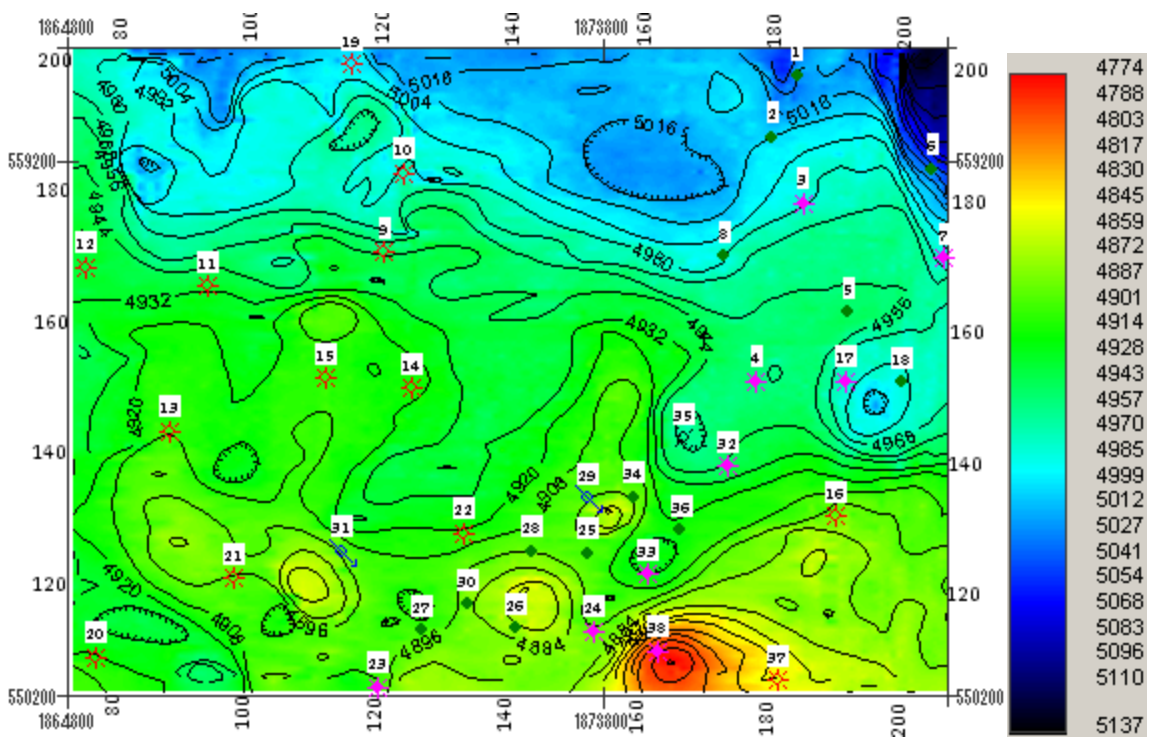


Figure 4.25. The Davis (MFS70) depth map in TVD from the seismic datum (ft) showing that the layer is dipping toward north. Depth varies from 4774 ft to 5137 ft. Anticline are visible near the Wells 26, 31, and 38. Karst collapse features are observed near the Wells 6 and 18.

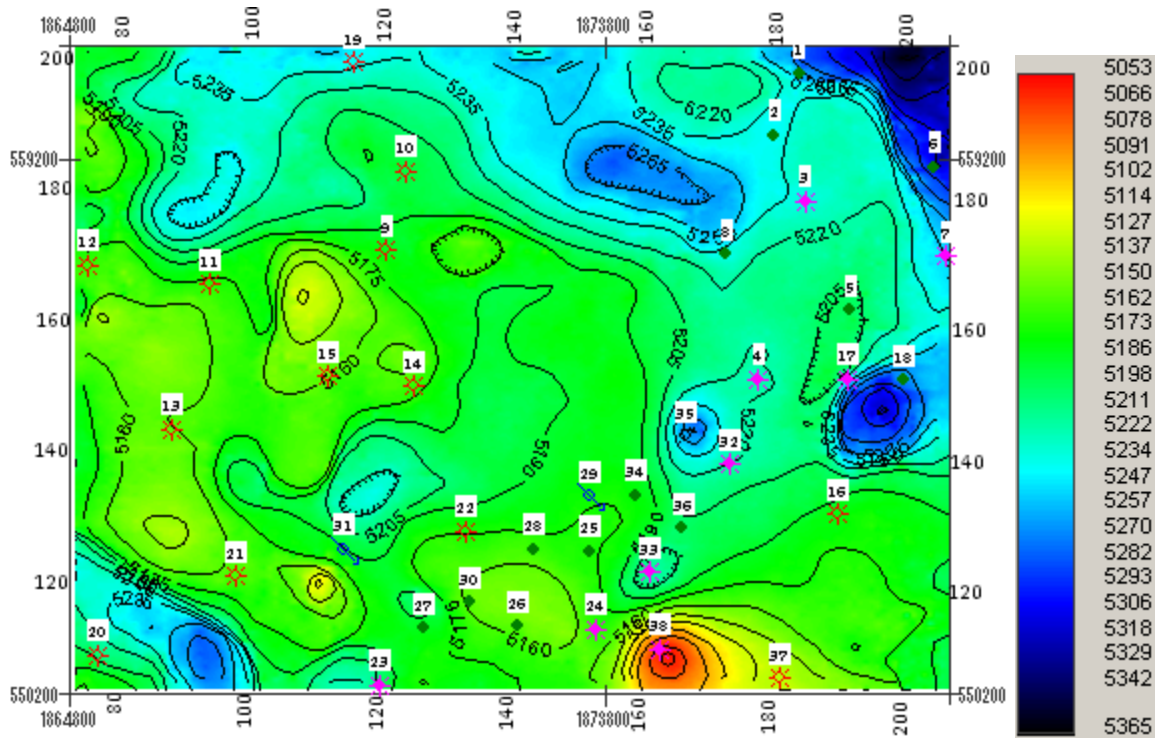


Figure 4.26. The Runaway (MFS53) depth map in TVD from the seismic datum (ft) showing that the layer is dipping toward north-east. Depth varies from 5053 ft to 5365 ft. Anticline are observable near the Wells 2, 15 and 38. Karst collapse features are observed near the Wells 6, 8, 18, and 35.

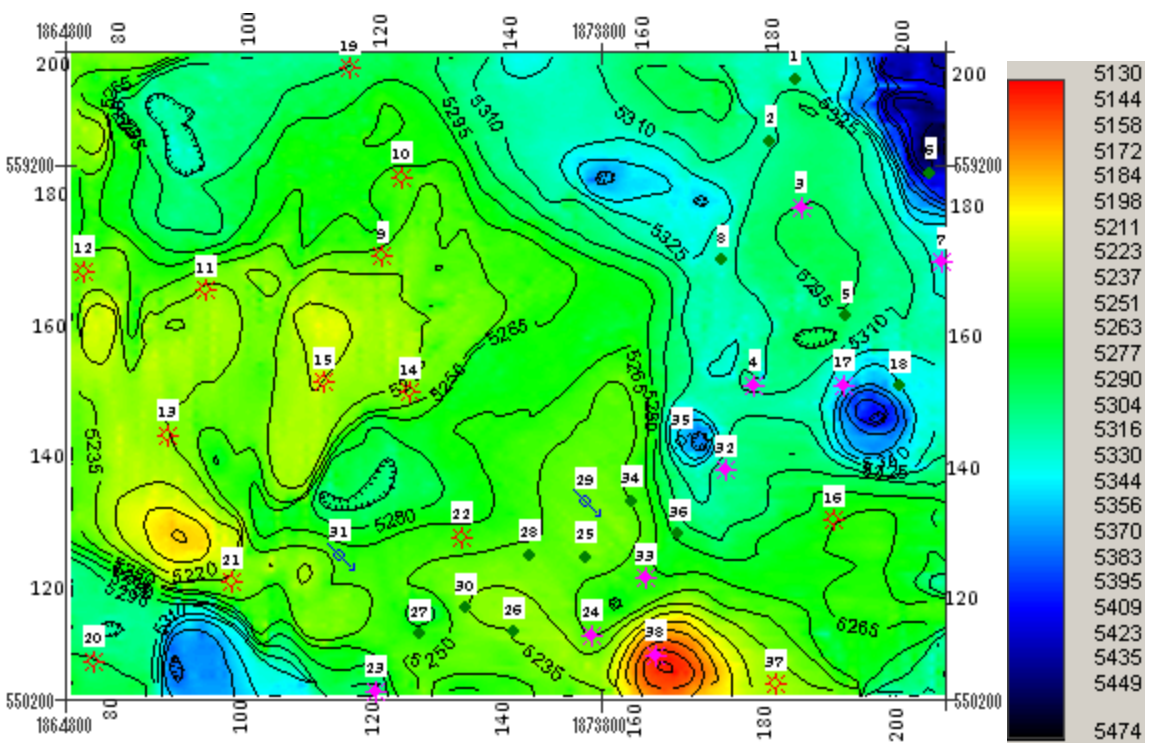


Figure 4.27. The Bean Cr (MFS40) depth map in TVD from the seismic datum (ft) showing that the layer is dipping toward north-east. Depth varies from 5130 ft to 5474 ft. Anticlines are observable near the Wells 15, 21 and 38. Karst collapse features are observed near the Wells 6, 8, 18, and 35.

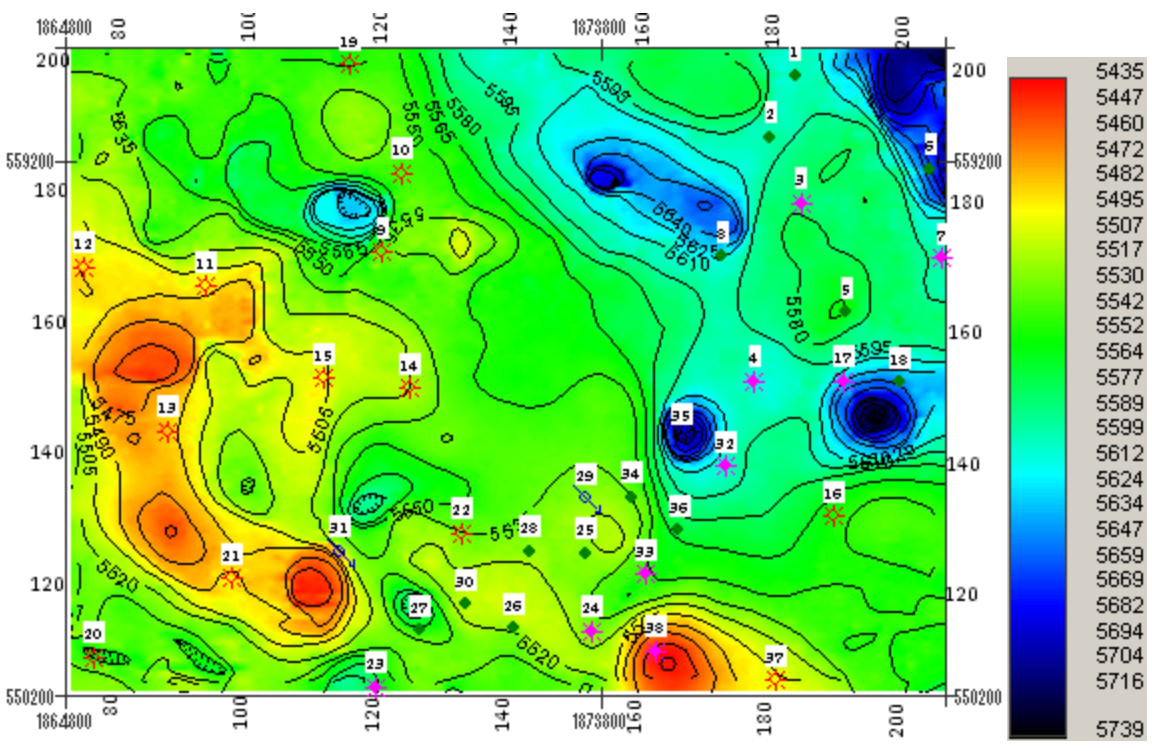


Figure 4.28. The Vineyard (MFS20) depth map in TVD from the seismic datum (ft) showing that the layer is dipping toward north-east. Depth varies from 5435 ft up to 5739 ft. Anticline are observable near the Wells 5, 13, 21, 31 and 38. Karst collapse features are observed near the Wells 6, 8, 9, 18, and 35.

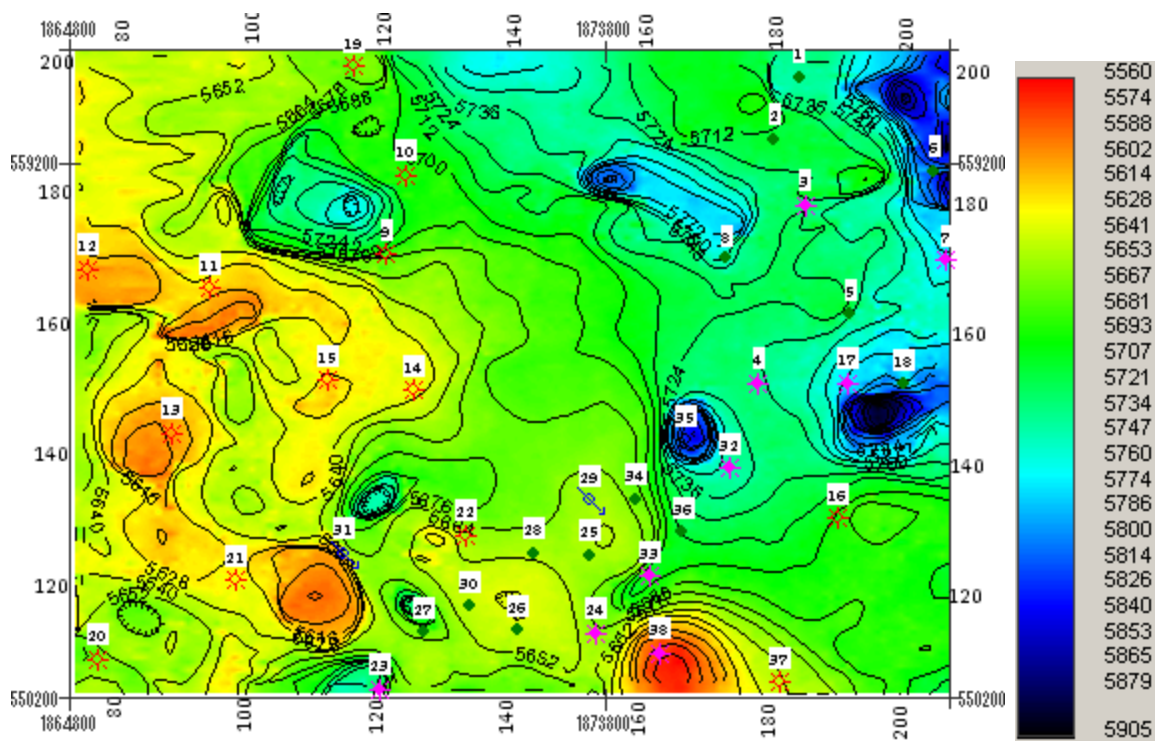


Figure 4.29. The Wade (MFS10) depth map in TVD from the seismic datum (ft) showing that the layer is dipping toward east. Depth varies from 5560 ft up to 5905 ft. Anticline are observable near the Wells 2, 5, 11, 12, 13, 31 and 38. Karst collapse features are observed near the Wells 6, 8, 9, 18, and 35.

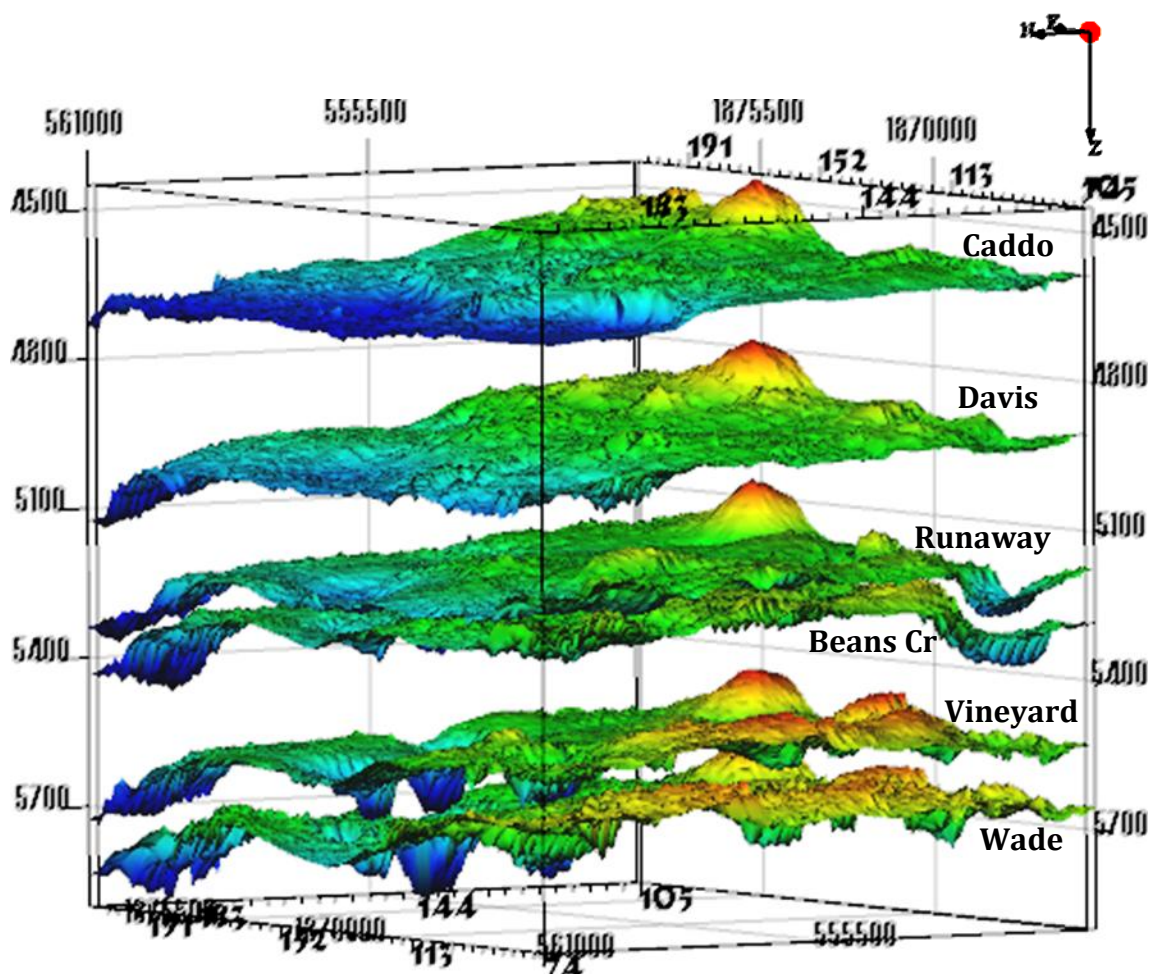


Figure 4.30. 3D structure depth view for all the targeted formations. Depth is in TVD from the seismic datum (ft). From the top: the Caddo top (MFS90), Davis top (MFS70), Runaway top (MFS53), Beans Creek top (MFS40), Vineyard top (MFS20), and Wade top (MFS10). The Bend Conglomerate interval can be represented by the thickness of 1200 ft from the top of the Caddo to the bottom of the Wade. Some karst collapse features are found in the north-east. The dipping directions of the structure change from the northeast dipping at the top to the east dipping at the bottom.

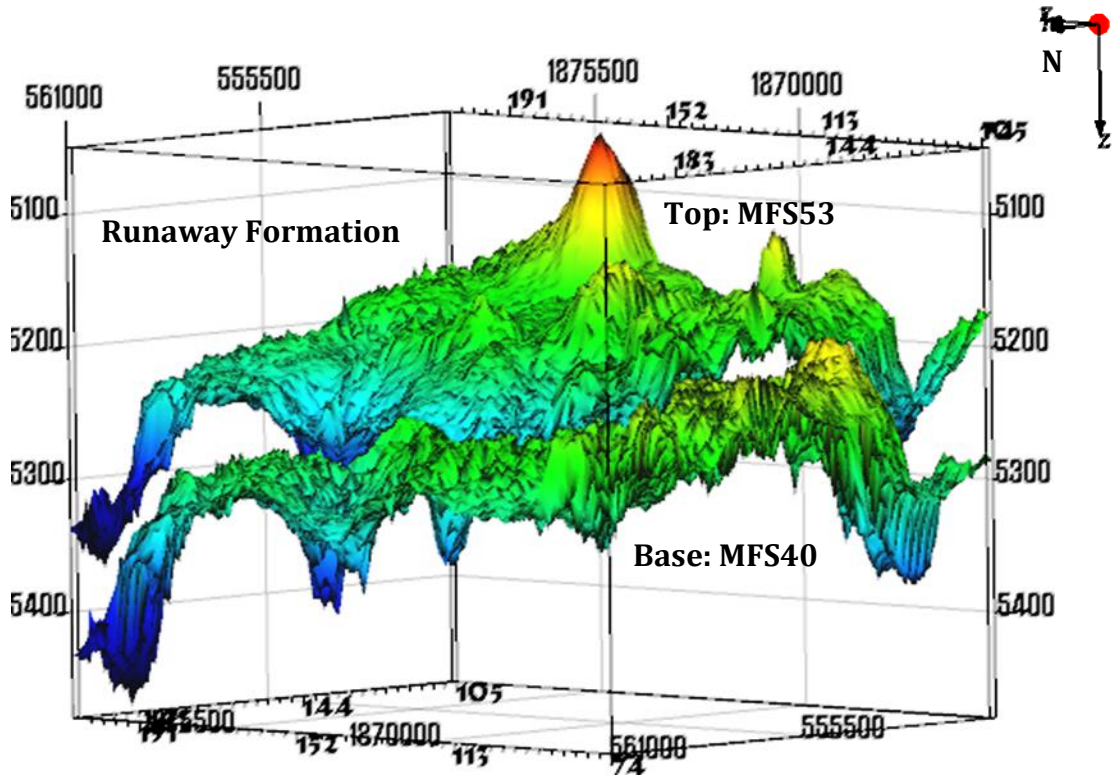


Figure 4.31. 3D depth structure view of the Runaway Formation top (MFS53) and base (MFS40). Some karst collapse features are in the northern-east part. Anticline is at south. Depth is in TVD from the seismic datum (ft).

4.5.4. Time to Depth Conversion. Seismic data are provided in time domain. However, it is more realistic to view the seismic data in depth, which gives better understanding of the geological features.

By correlating depth grids with the time structure grids, the conversions for the seismic data from time to depth are conducted using the SMT Kingdom Suite Software. Figure 4.33 shows a vertical seismic section in depth after conversion.

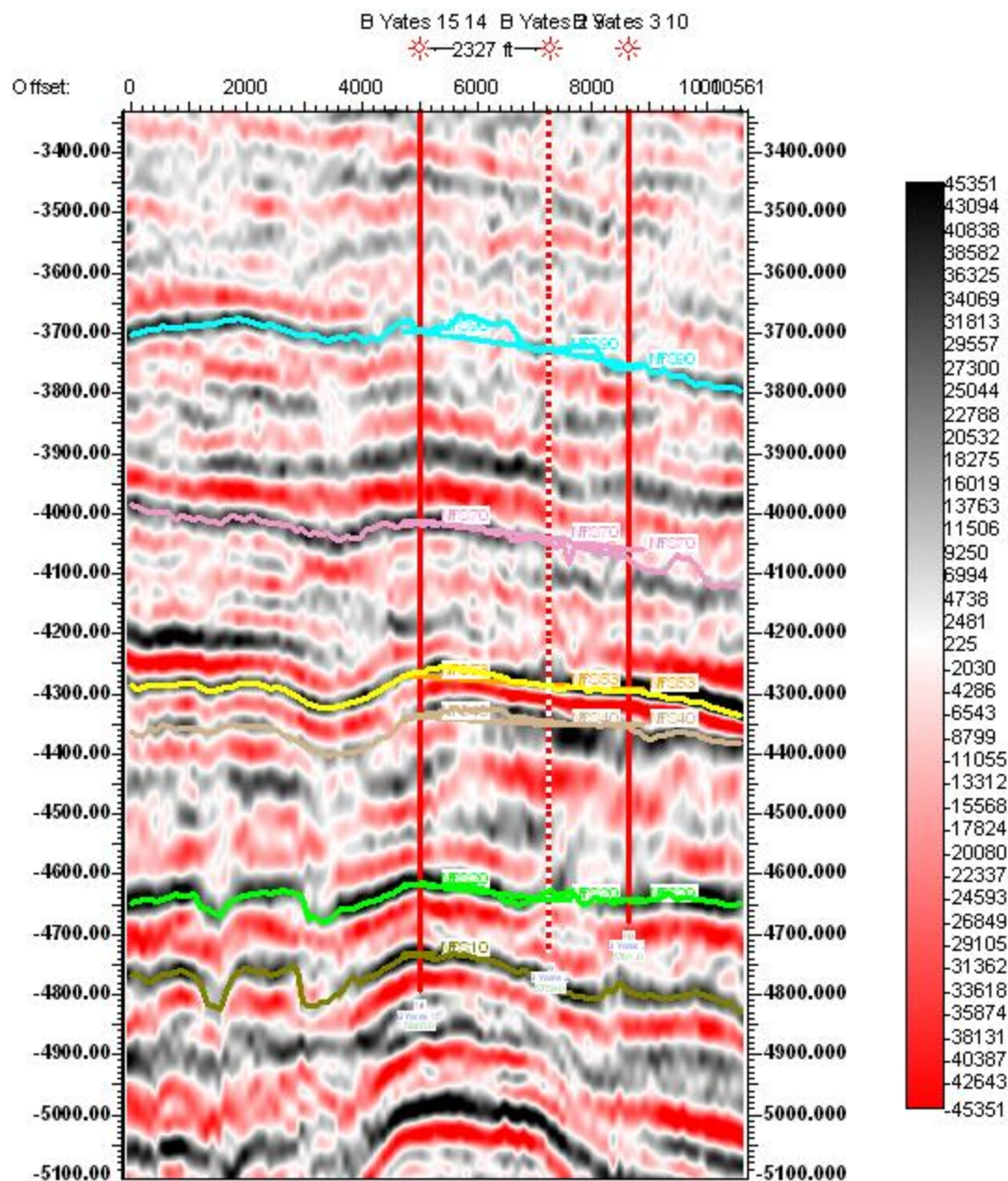


Figure 4.33. Vertical seismic section in depth. The horizons of the targeted formations are shown as follows: Caddo (blue), Davis (Pink) Runaway (yellow) Beans Cr (light brown) Vineyard (green), and Wade (dark green). Depth is subsea in ft. Color bar shows the amplitude variation values.

5. STRATIGRAPHIC INTERPRETATION

Stratigraphic interpretation of the Boonsville field is challenging, because there are many karst collapse features, which randomly cut the targeted formations. This affects the continuity of the targeted formations. The fluvial to deltaic depositional environment is characterized by deltas, sand bodies, channel, and point bars, which are shown as discontinuous thin sequences formed as described in Figure 2.9. In order to better understanding the stratigraphic features in the area, the following interpretations are conducted.

5.1. HORIZON SLICE

Horizon slice is useful in stratigraphic interpretations. It can help identifying the features over the mapped formation. Horizon slices computed from the tracked horizons are illustrated in Figures 5.1, 5.2, 5.3, and 5.4.

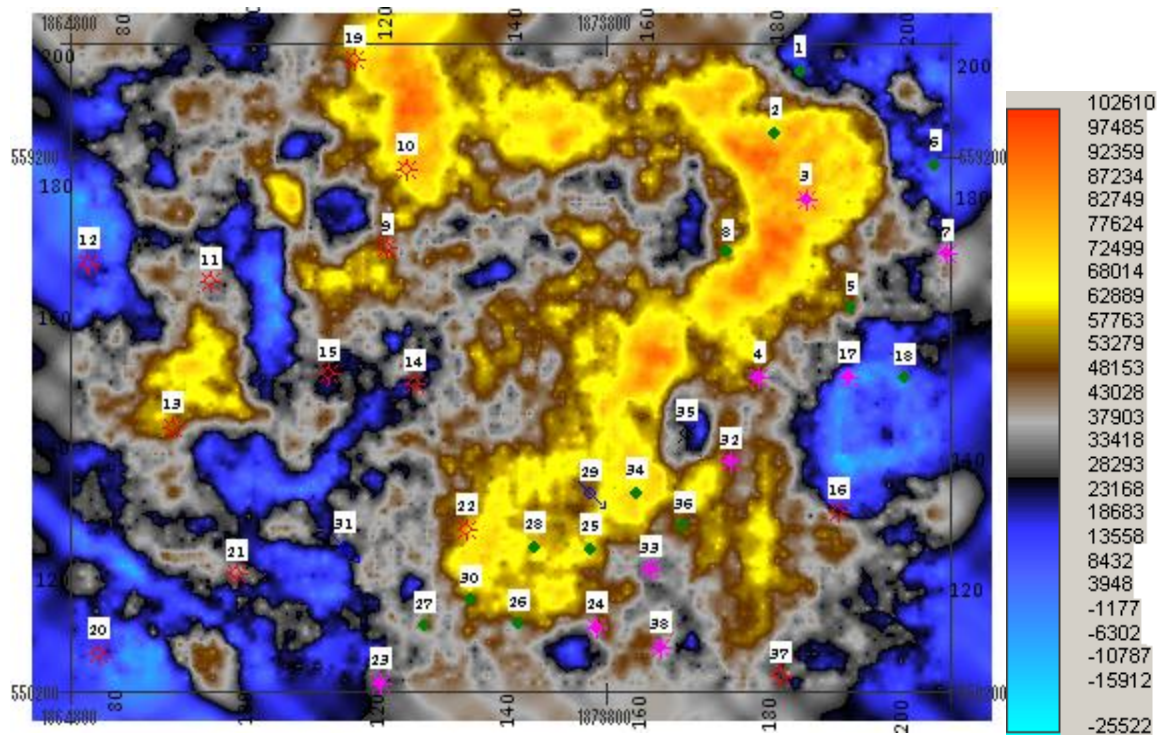
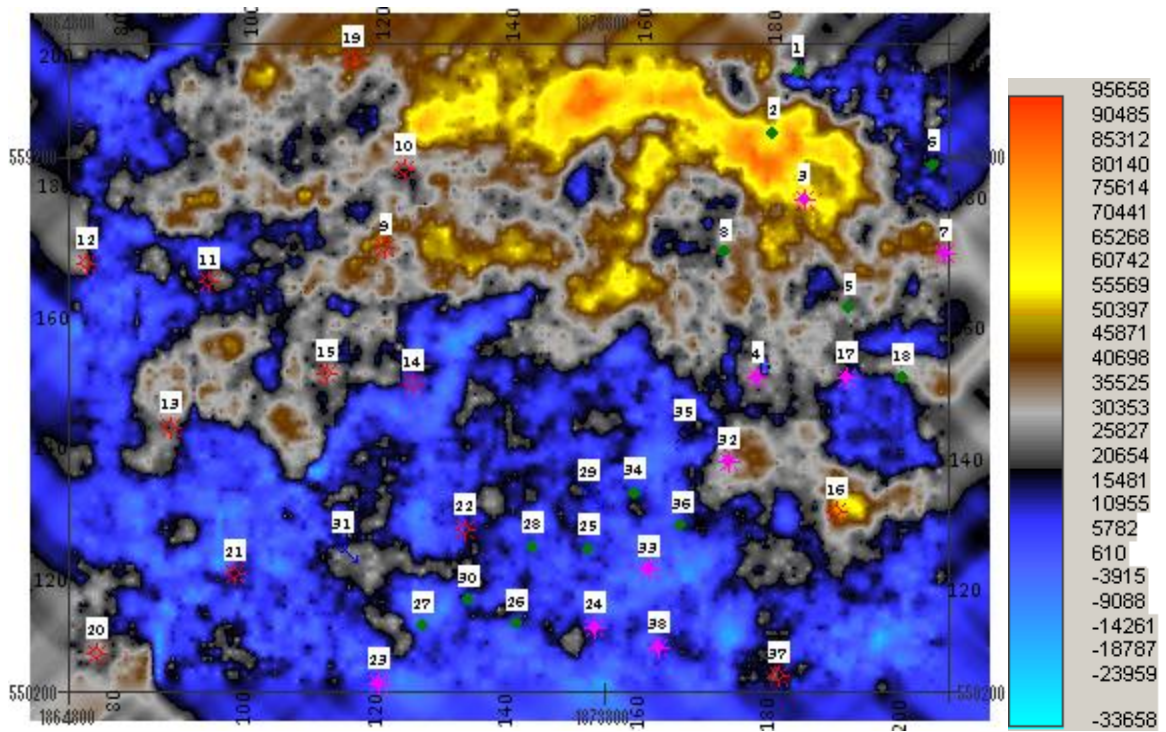


Figure 5.1. The Runaway top (MFS53) horizon slice indicating a channel by the high amplitudes.



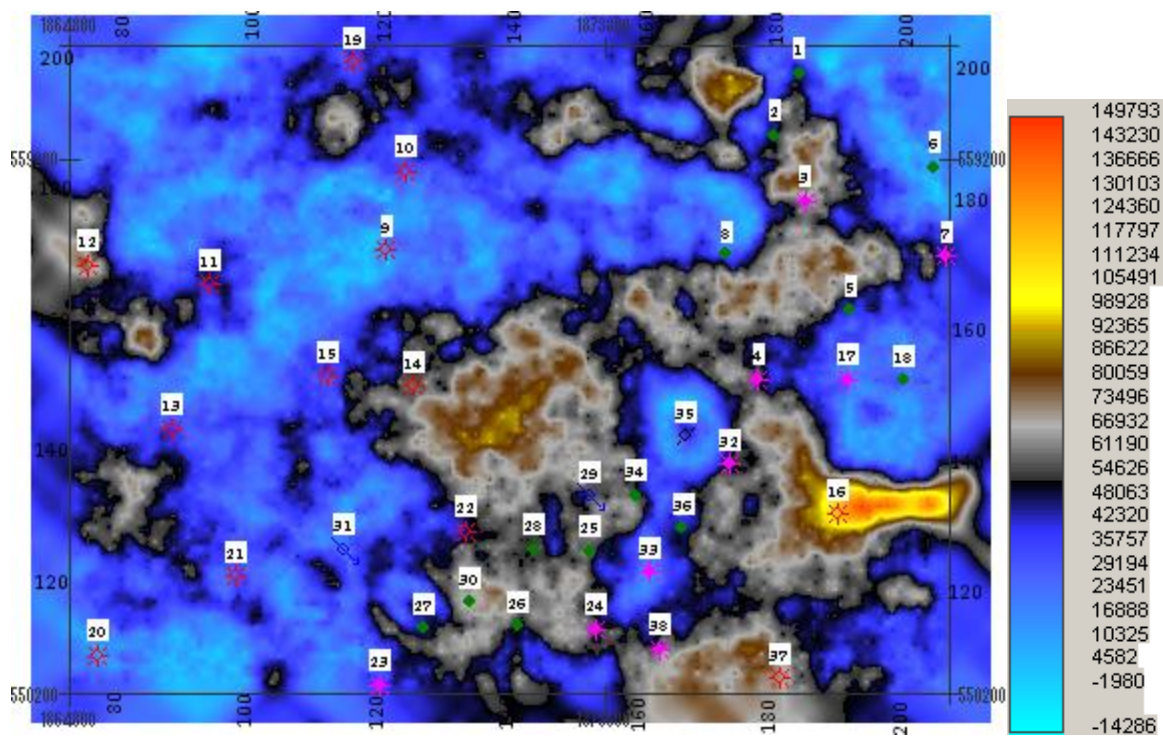


Figure 5.3. Top Vineyard (MFS20) horizon slice showing a channel indicated by the high amplitudes from the south to north. The Karst collapse features are observed around the Well 25. Very high amplitudes near the Well 16 suggest a Direct Hydrocarbon Indicator (DHI) bright spot.

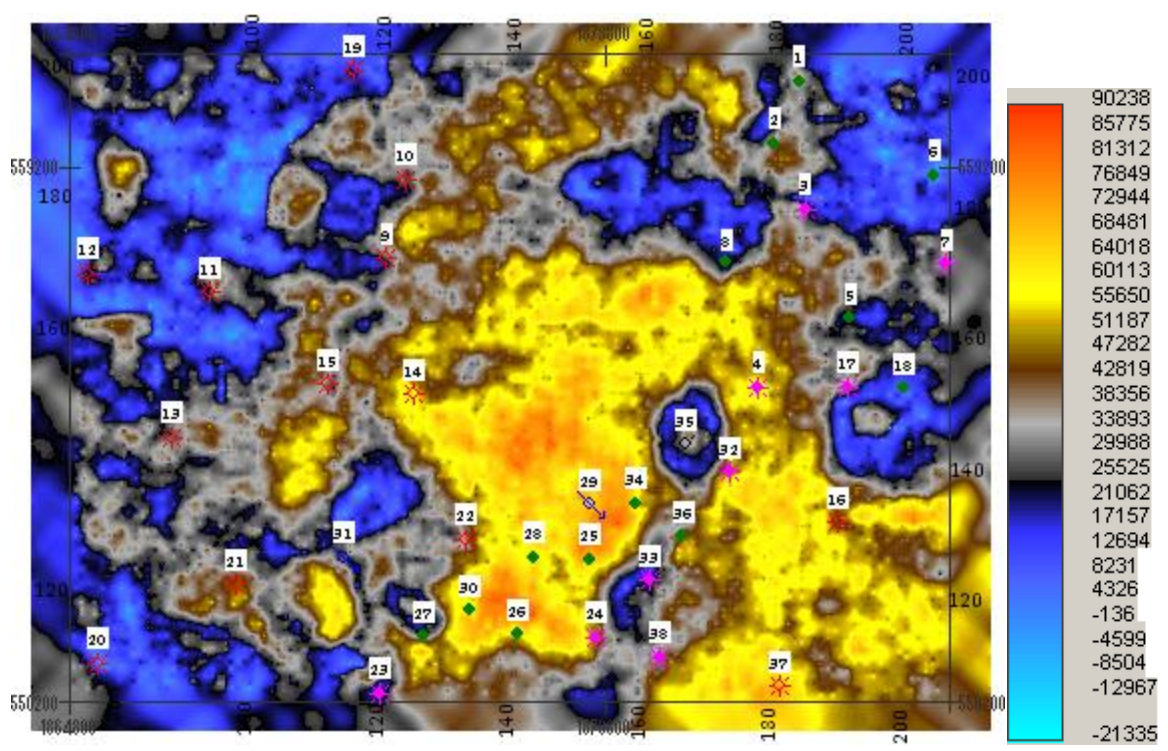


Figure 5.4. Horizon slice of the Wade (MFS10), the Vineyard Base showing the effect of karst collapse features at the base of the Bend Conglomerate near the Wells 6, 8, 18, 27, 33, and 35. The high amplitude feature that elongates north-south is suggested to be a fluvial dominated mouth bar.

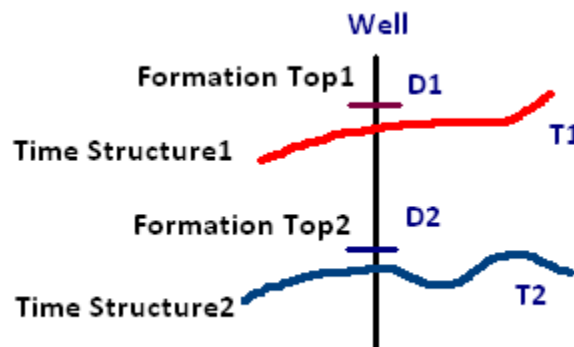
5.2. ISOPACH MAP

Once the horizons are tracked, the isopach maps can be constructed if the interval velocity information is available. Isopach maps show the thickness variations of the targeted formations in the study area.

5.2.1. Interval Velocity Map. Interval velocity is the seismic velocity over a specific interval of rock or strata. It can be expressed mathematically by the following equation:

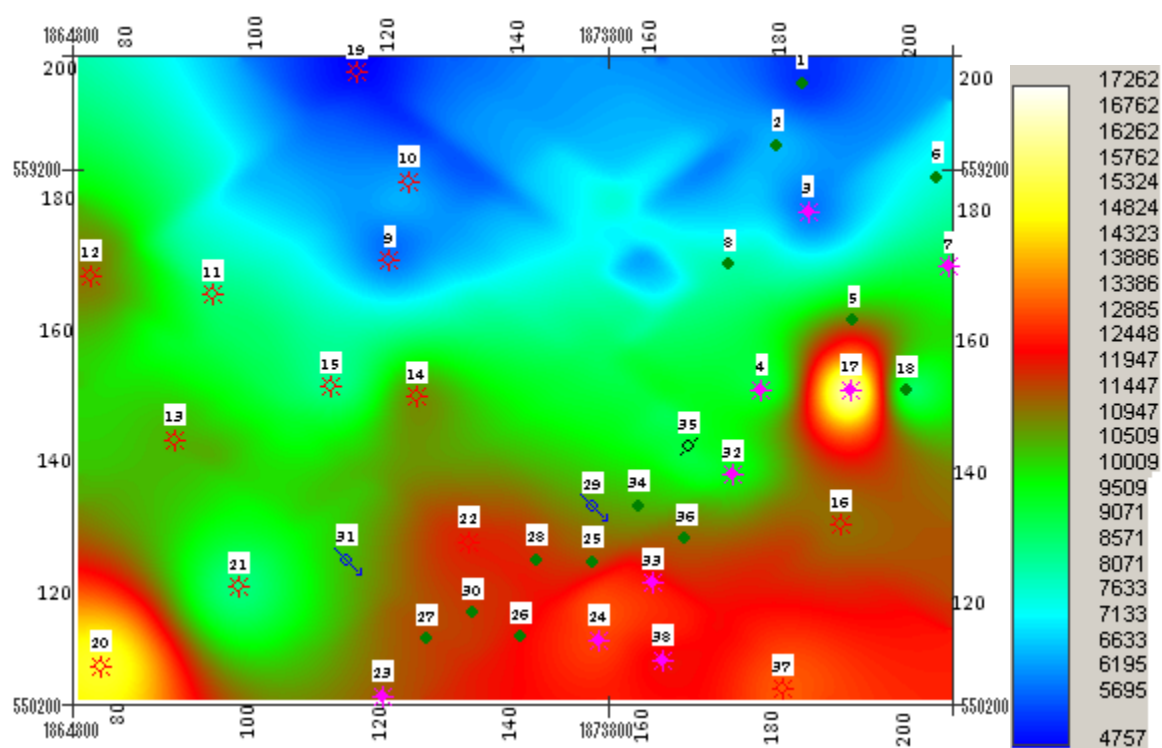
$$V_{int} = \frac{2(D_1 - D_2)}{(T_1 - T_2)} \quad (3)$$

Where V_{int} is the interval velocity, D_1 is the depth to the upper reflector, D_2 is the depth to the lower reflector, T_1 is the two way travel time to the upper reflector, and T_2 is the two way travel time to the lower reflector (Figure 5.5)

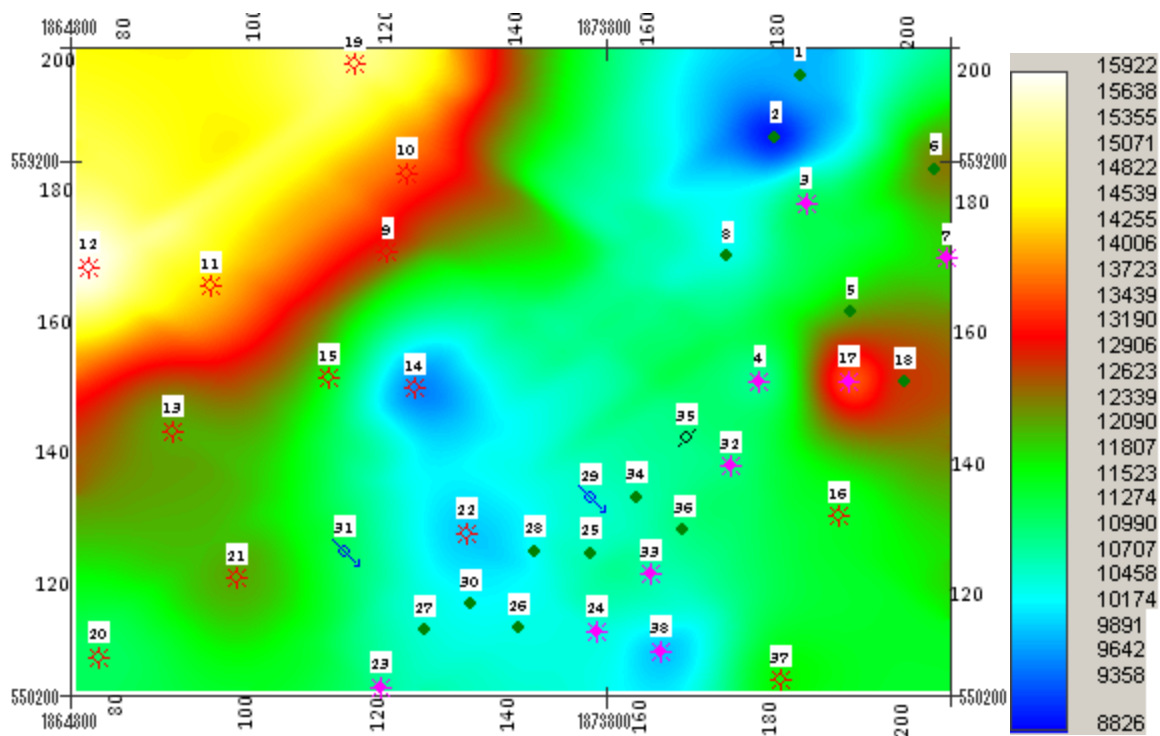


Figures 5.5. Illustration showing the method to compute the parameters from the well formation tops and the seismic time structure in order to calculate the interval velocity.

Using the Kingdom Suite Software, the interval velocity map is generated once the time structure is obtained for both the upper horizon and the lower horizon of the targeted formation. For each well, the formation tops are needed to calculate the velocity interval. The interval velocity values from each well can be gridded to generate an interval velocity map for a specific formation. The gridding method used is the gradient projection, which is similar to the method used in the structural interpretation maps. Figures 5.6 and 5.7 show the interval velocity maps generated for the Runaway and Vineyard Formations, respectively.



Figures 5.6. The Runaway Formation interval velocity map. The lowest interval velocity is observed near the Wells 1 and 19, and the highest is near the Wells 17 and 20. The interval velocity is decreasing toward north.



Figures 5.7. The Vineyard Formation interval velocity map. The lowest interval velocity is observed near the Well 2, and the highest is near the Wells 12 and 19.

5.2.2. Isopach Map. Isopach map shows the variation in thickness of the targeted formation, which can be used for many geological and petrophysical interpretations, especially for studying the stratigraphic thickness and the depositional environment of formation. In addition, it is used for the reservoir estimation and obtaining petrophysical parameters such as the Net to Gross Ratio (NGR). In this study, isopach maps are generated for the Runaway and Vineyard Formations (Figures 5.8 and 5.9).

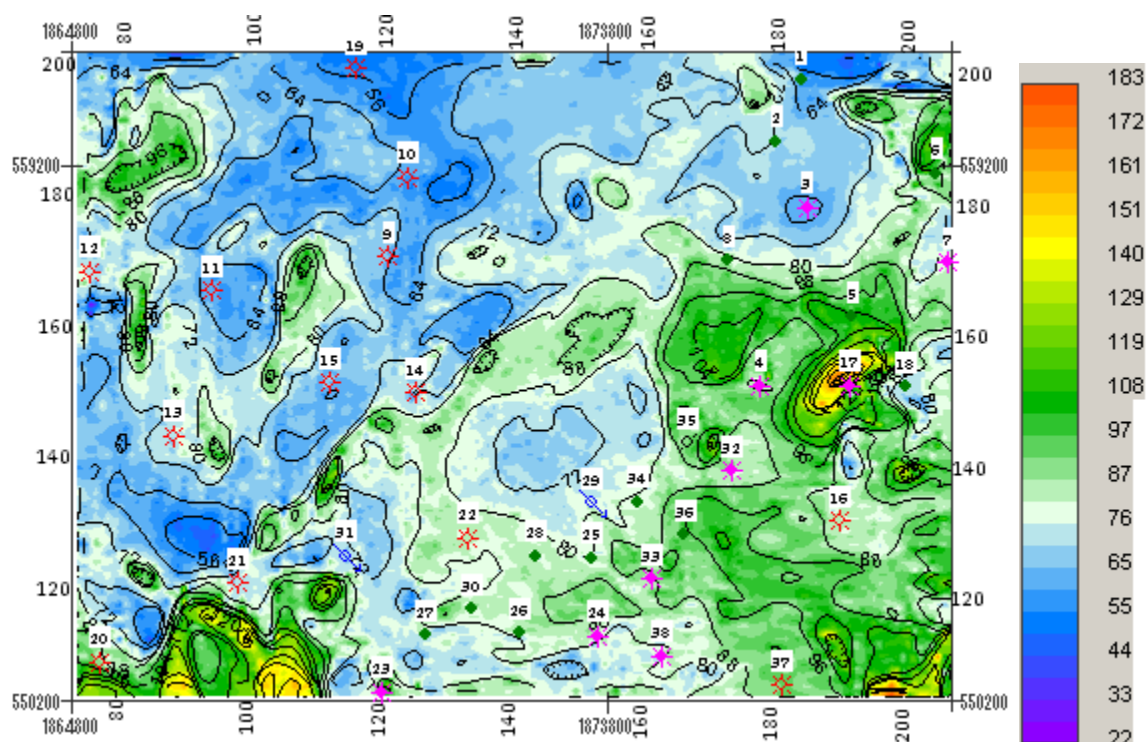


Figure 5.8. The Runaway Formation isopach map showing the formation thickness varying from 22 ft to 183 ft. The formation becomes thinner toward northwest.

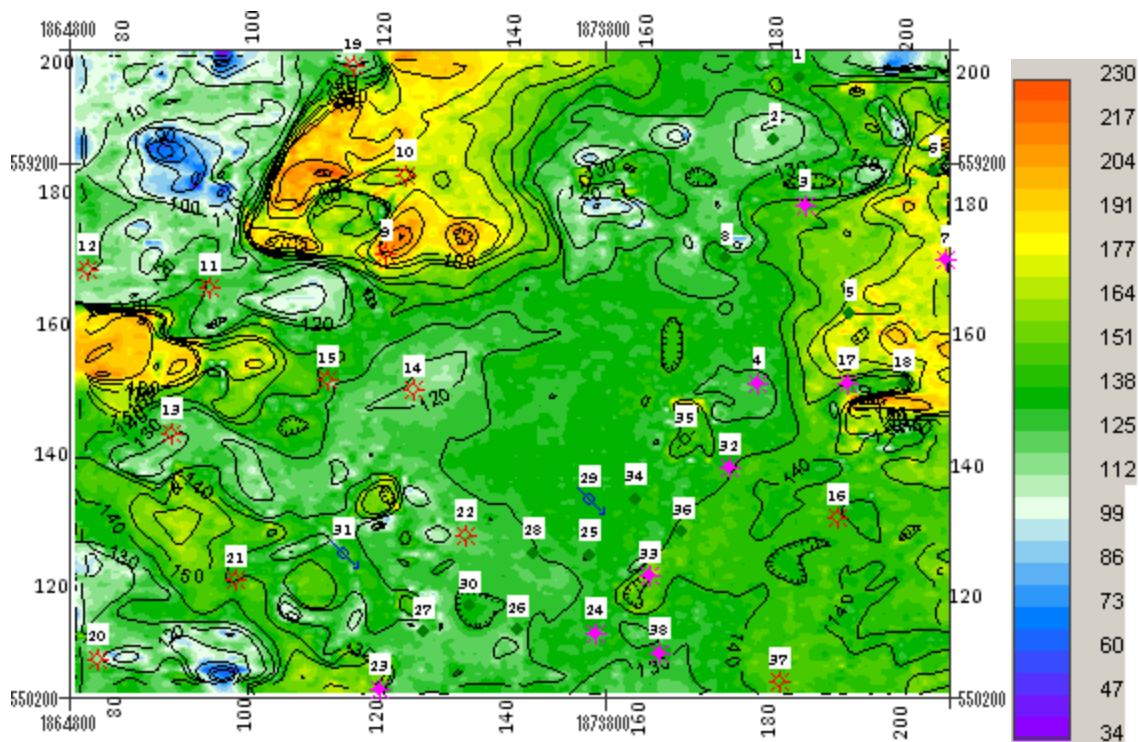


Figure 5.9. The Vineyard Formation isopach map showing the formation thickness varying from 34 ft to 230 ft.

5.3. WELL LOG CORRELATION

Well logs are used to interpret the stratigraphic features in the study area. Gamma Ray (GR) and Spontaneous Potential (SP) are utilized to identify the lithology (Asquith and Kryqowski, 2004). Resistivity logs (Rt) helps identify the type of fluids in the rock voids (Asquith and Kryqowski, 2004). GR and Rt logs provided are shown in the base map for the Runaway and Vineyard Formations, respectively (Figures 5.10 and 5.11).

Figure 5.12 shows correlations between logs of the Wells 1, 2, 3, 10, and 19 for the Runaway Formation. Thick sand is presented in the Well 2. It represents a channel. Figure 5.13 shows correlations between logs of the Wells 1, 2, 3, and 7 for the Runaway Formation. In Figure 5.14, GR and Rt logs of the Well 2 are shown on the seismic section for the Runaway Formation. In Figure 5.15, Gr and Rt logs of the Well 19 are shown on a seismic section. A point bar truncation is observed in the Runaway Formation. A channel near the Well 2 can be identified in Figure 5.16.

A cross correlation between logs of the Wells 16, 17, 27 and 37 for the Vineyard Formation is shown in Figure 5.17. The logs from the Wells 16 and 37 indicate channel fills in the upper of the Vineyard Formation. In Figure 5.18, logs of the Wells 16 and 24 are shown on a seismic section. A point bar truncation is identified in the Vineyard Formation near the Well 24.

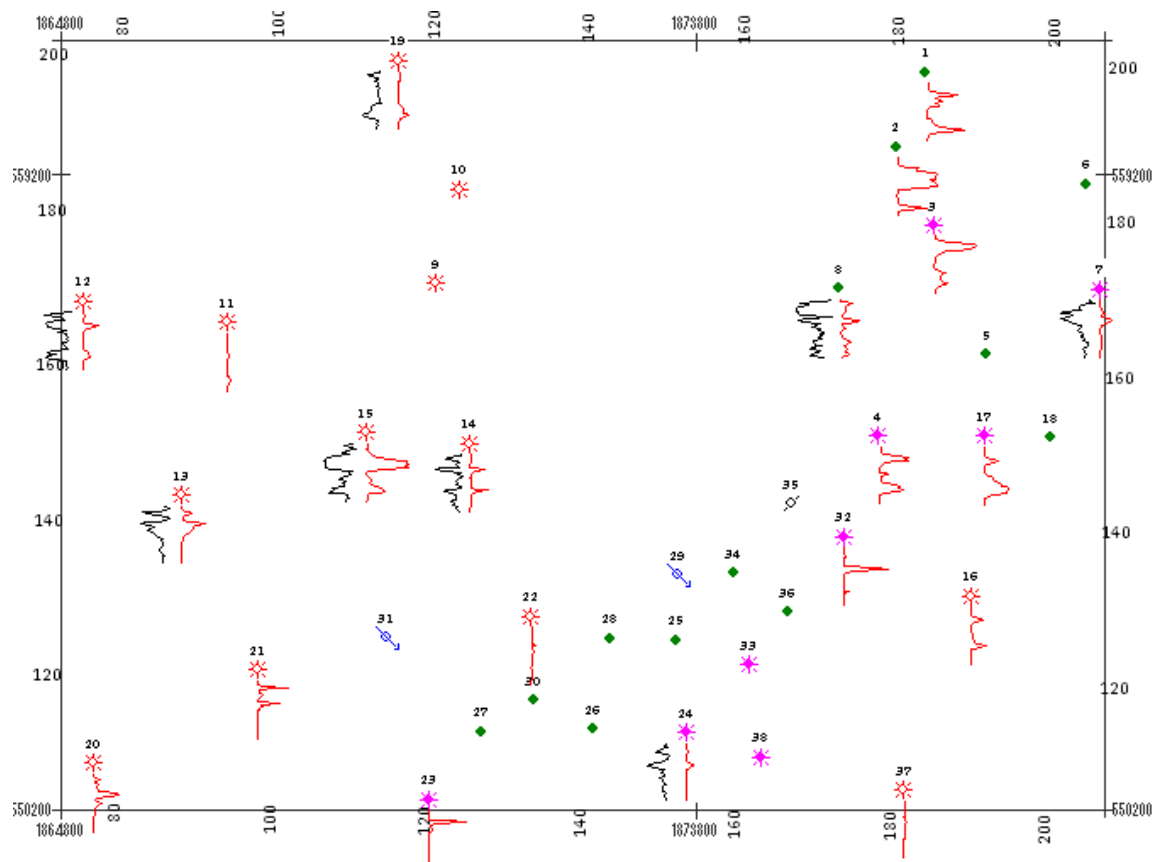


Figure 5.10. GR and Rt logs showing in the basemap for the Runaway Formation.

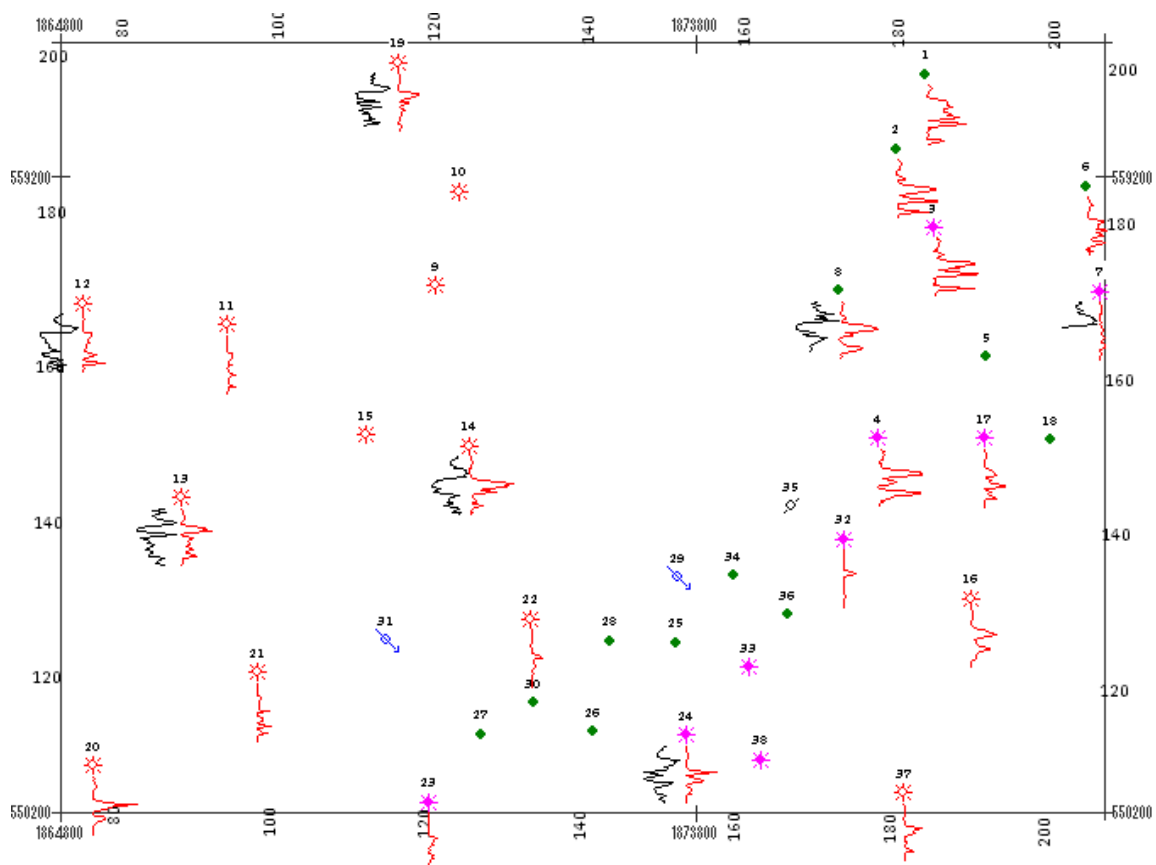


Figure 5.11. GR and Rt logs showing in the basemap for the Vineyard Formation.

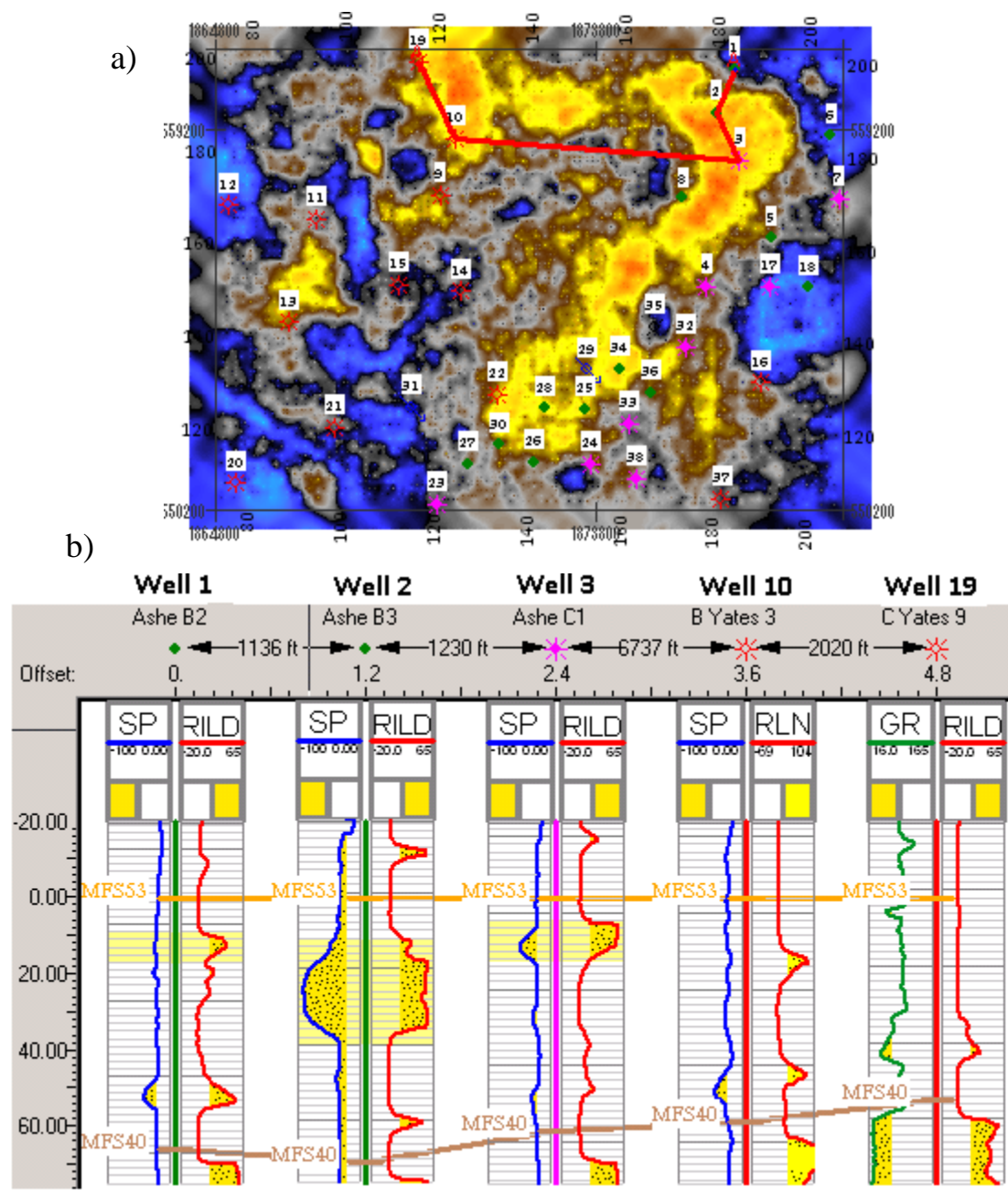


Figure 5.12. Well log correlation for the Runaway Formation. **a)** Horizon slice of the Runaway top showing a channel and the arbitrary line location from the Well 1 to the Well 19. **b)** The Runaway Formation bounded between MFS53 and MFS40 along the cross section for well log correlation. Channel sand body is noticed in the Well 2. The logs in the Wells 10 and 19 indicate shale dominating.

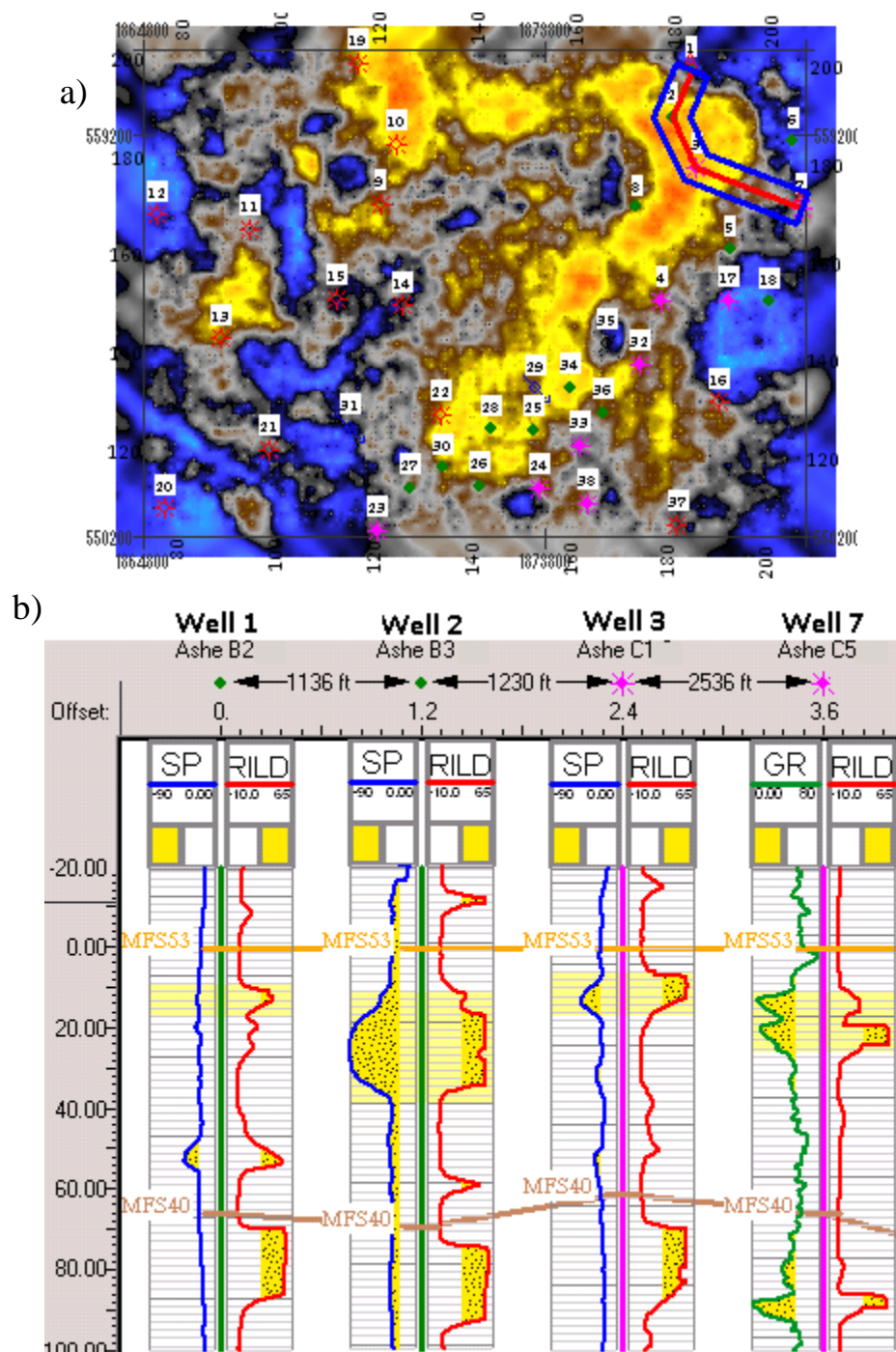


Figure 5.13. Well log correlation for the Runaway Formation **a)** Horizon slice of the Runaway top showing the arbitrary line location from the Wells 1 to the Well 7. **b)** The Runaway Formation bounded between MFS53 and MFS40 along the cross section for well log correlation. Channel sand body is noticed in the Well 2. The logs in the Well 7 show dominate point bar.

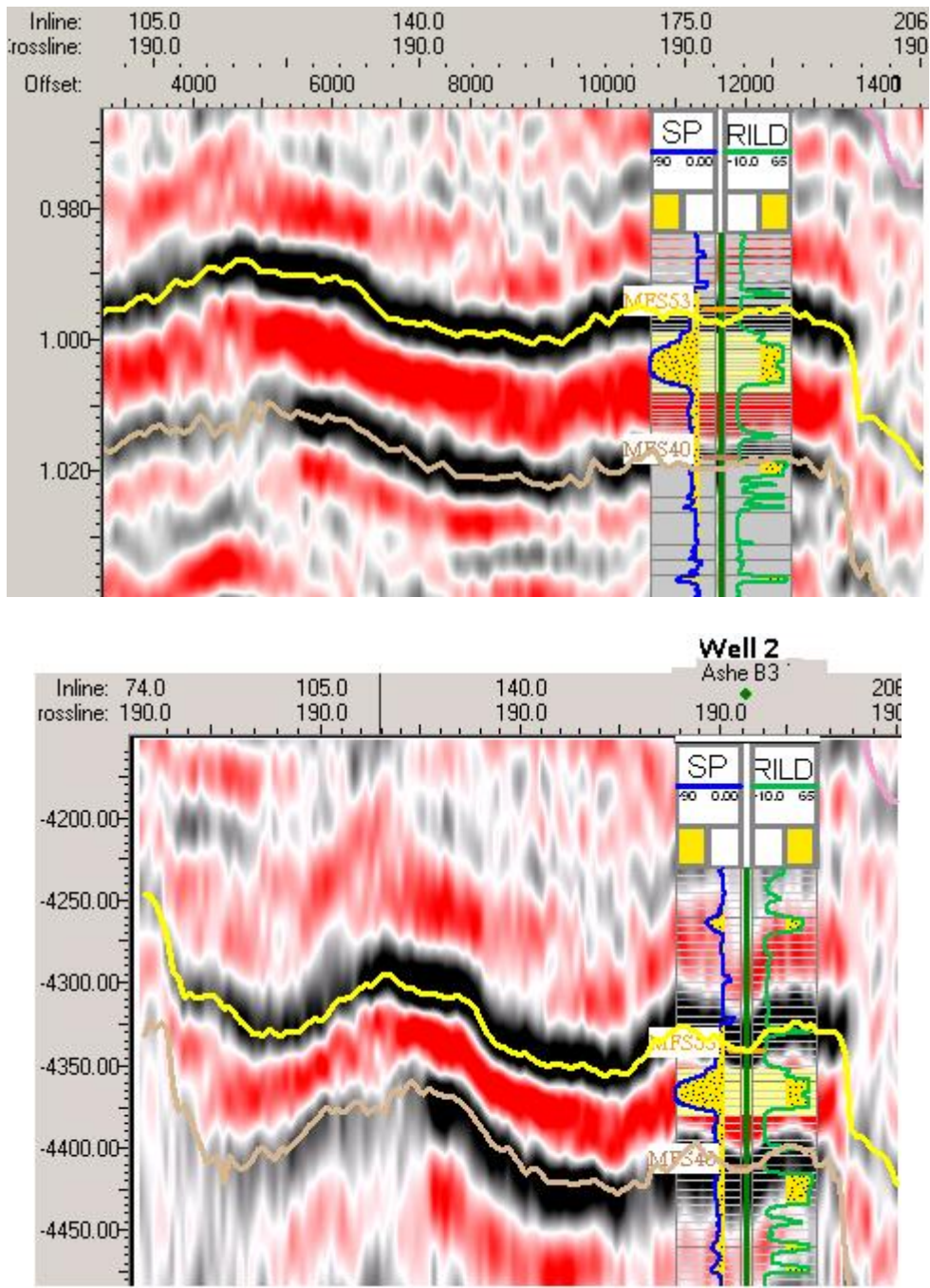


Figure 5.14. SP-Rt log from the Well 2 showing in the seismic section for the Runaway Formation. A channel is identified in both seismic sections in time (top) and in depth (bottom). Depth is subsea (ft).

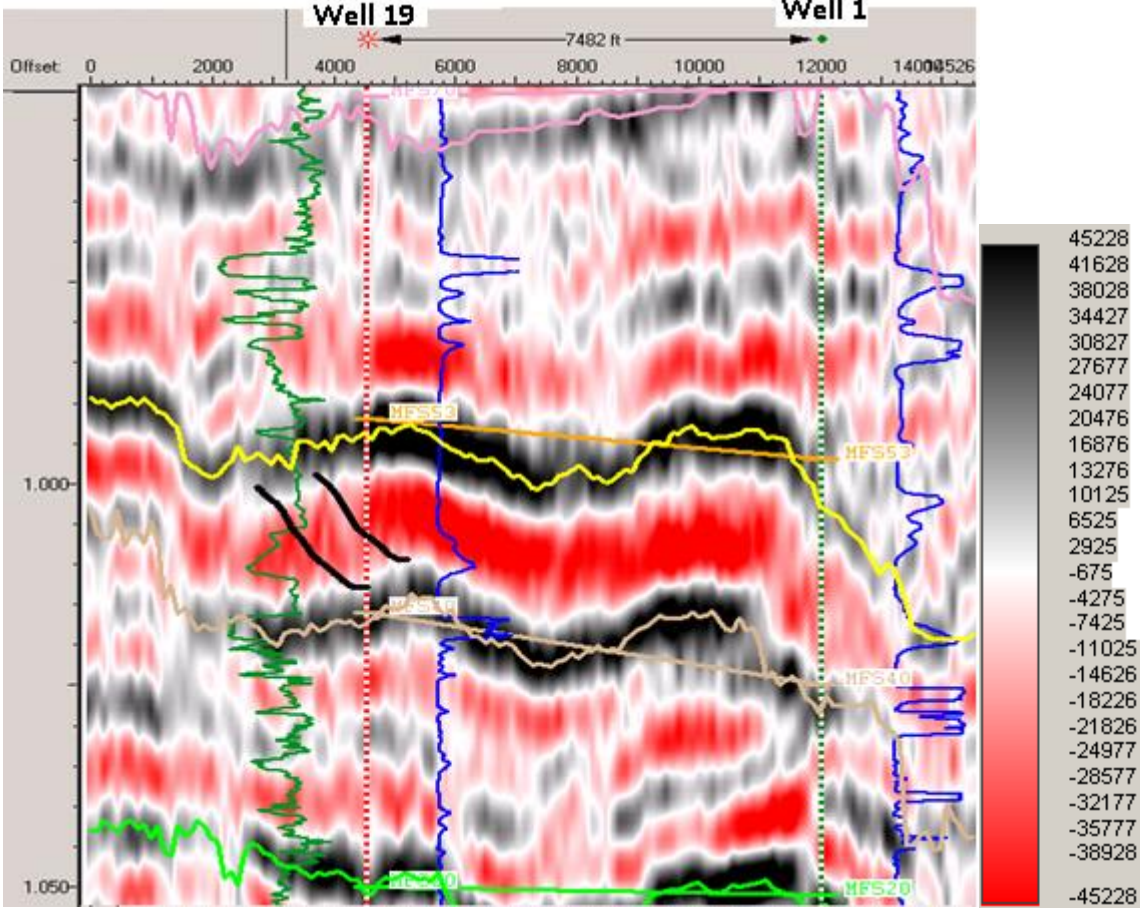


Figure 5.15. GR (green) and Rt (blue) logs from the Well 19 showing in the seismic section of crossline 199. A point bar truncation is observed in the Runaway Formation.

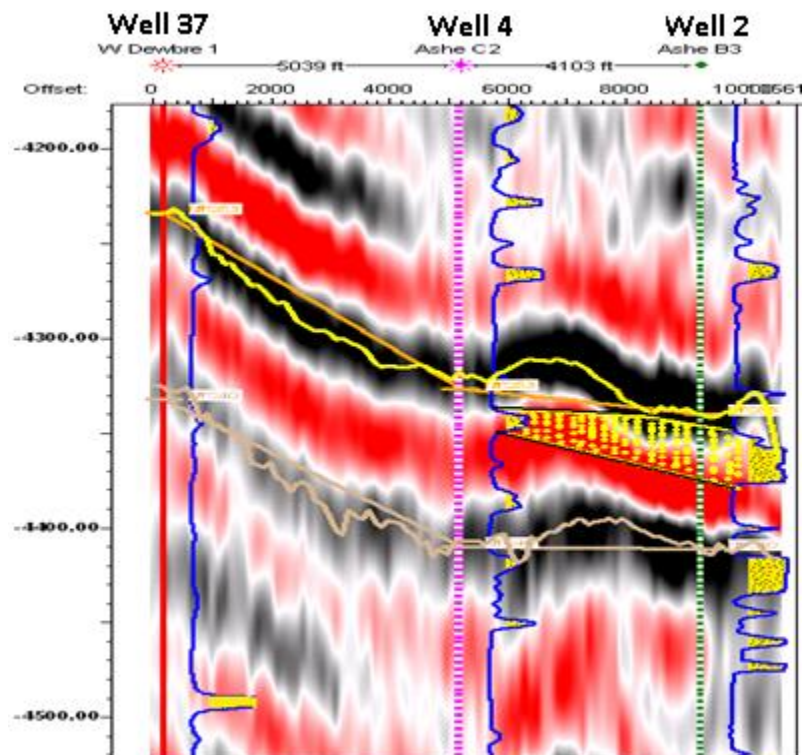


Figure 5.16. Rt logs for the Wells 2, 4 and 37 plotted in the seismic section. A channel fill is located near the Well 2 in the Runaway Formation.

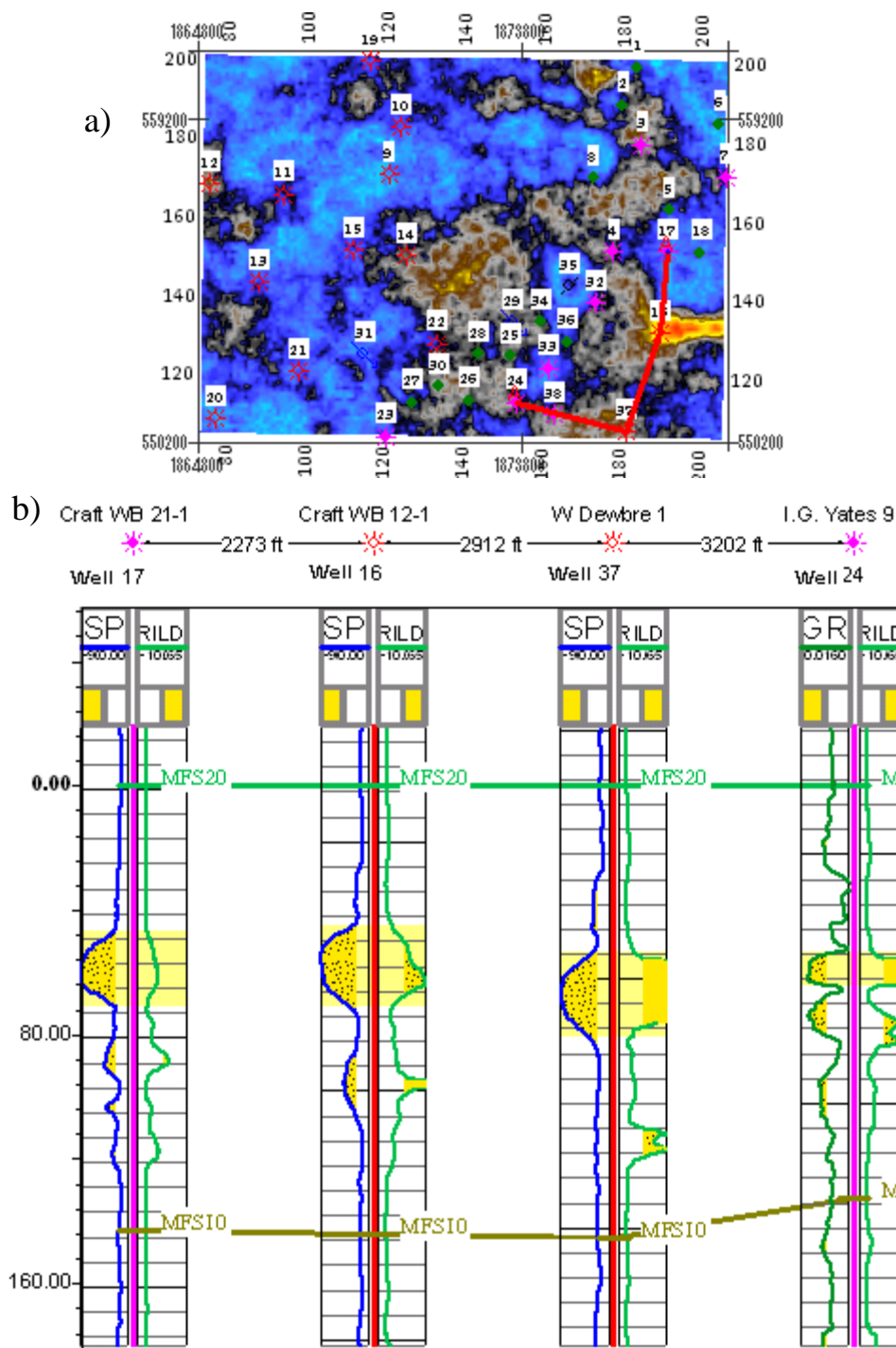


Figure 5.17. Well log correlation for the Vineyard Formation. **a)** Horizon slice of the Vineyard top showing the arbitrary line location from the Well 17 to the Well 24. **b)** The Vineyard Formation bounded between MFS20 and MFS10 along the cross section for the well log correlation. Channel sand body is noticed in the Wells 16 and 37. The logs in the Well 9 show dominate point bar.

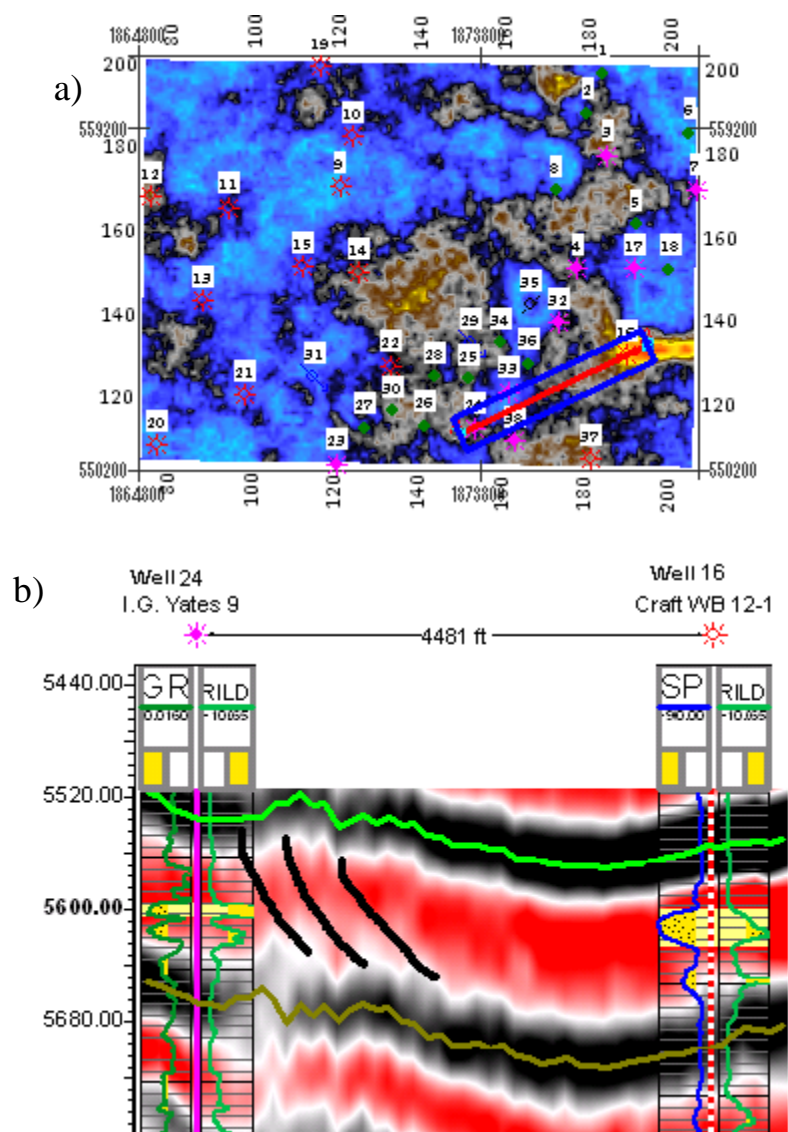


Figure 5.18. Well logs placed in the vertical seismic section for the Vineyard Formation. **a)** Horizon slice of the Vineyard top showing the arbitrary line location. **b)** The seismic section showing SP-Rt logs for the Well 16 indicates a channel fill, and the GR-Rt logs for the Well 24 indicates a point bar truncation in the Vineyard Formation bounded by MFS20 (top) and MFS10 (base).

6. RESERVOIR ESTIMATION

6.1. INTRODUCTION

Reservoir estimation is important for many aspects. The information obtained is used to identify prospects. It is also valuable for production and development for the hydrocarbon reservoir fields. Various data such as well data, logs, cuttings, core data, core plugs, production tests, and petrophysical data can be processed, analyzed and interpreted to improve the well production, or help identifying prospects.

The reservoir properties are extracted from the seismic data in the target zones. They are used for attribute measurements of the geophysical and geological data, which are used in many different interpretation aspects such as stratigraphic interpretation, structural interpretation, and reservoir evaluation.

6.2. ROOT-MEAN SQUARE AMPLITUDE

The depth difference between a top layer and a bottom layer of a reservoir is the isopach. The isopach can provide the volume of the reservoir zone of the targeted formations. The formation zones of the Runaway and Vineyard Formations have been identified in this study using the depth maps and the isopach maps illustrated in Chapters 5. A top plane indicates the starting point of the volumetric calculation. A bottom plane defines the volumetric polygon areas that describe the xy extent of the volumetric calculation.

The Root-Mean-Square (RMS) amplitude is a post stack amplitude attribute. Mathematically, it is calculated by using the square root of the sum of squared amplitudes divided by the number of samples within the specified window. It is an effective attribute

that helps determining hydrocarbon prospects. In fact, it enhances hydrocarbon bright spots and can be used as a Direct Hydrocarbon Indicator (DHI). The RMS amplitude map for the Runaway Formation bounded by MFS53 and MFS40 is illustrated in Figure 6.1.

In Figure 6.2, the RMS amplitude map is illustrated for the Vineyard Formation bounded by MFS20 and MFS10.

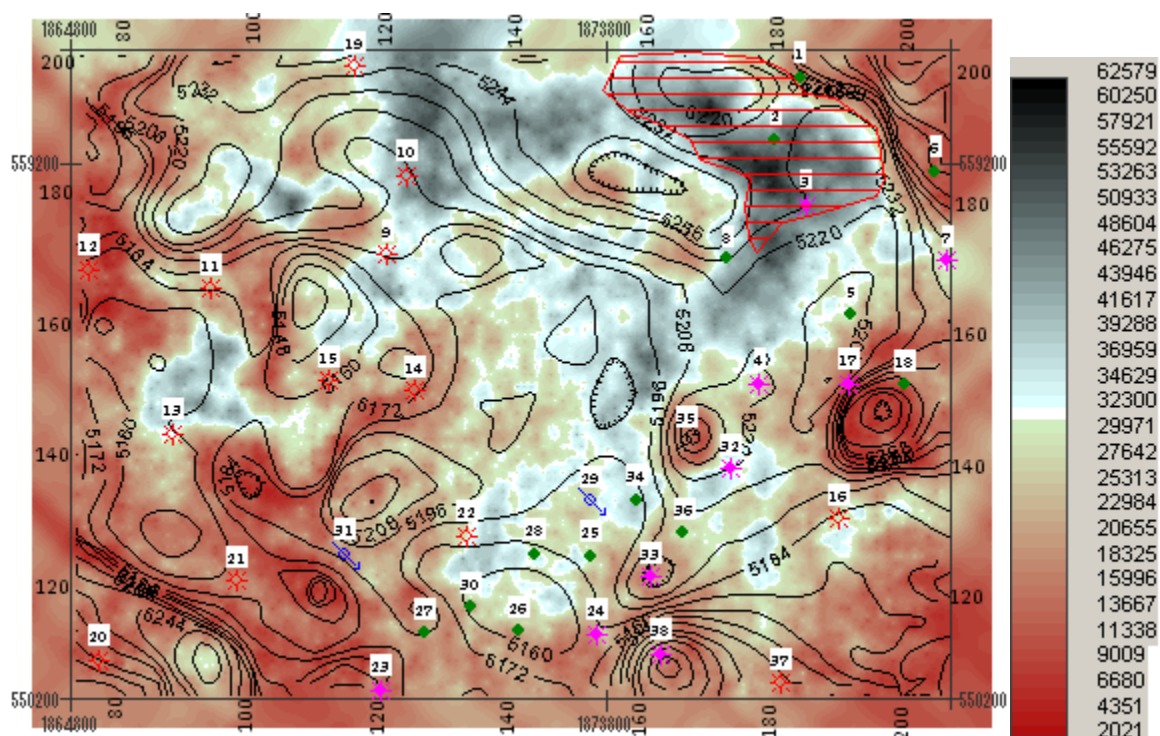


Figure 6.1. RMS amplitude map of the Runaway Formation with the depth structural contour of the Runaway top. Black shows bright spots near the Well 2. The suggested prospect area is shaded by the red lines.

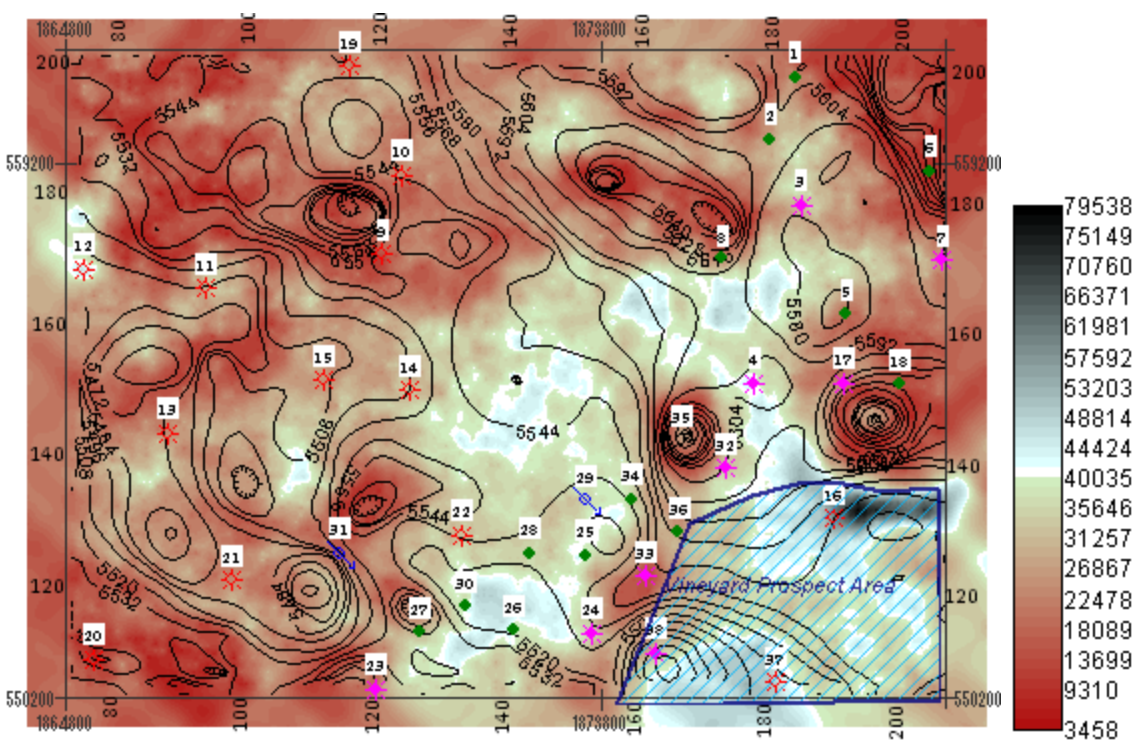


Figure 6.2. RMS amplitude map of the Vineyard Formation with the depth structural contour of the Vineyard top. Black shows bright spots near the Wells 16, 37, and 38. The suggested prospect area is shaded by the blue lines.

6.3. PETROPHYSICAL ANALYSIS

Petrophysical analyses are conducted by integrating the previous interpretations and well log analysis to obtain the reservoir properties. Figure 6.3 shows the logs computed from the Rt log of the Well 2. Figure 3.1 shows a list of wells with resistivity logs while many do not have the bulk density logs (RHOB), and velocity or sonic logs (DLT). In this study, some petrophysical parameters are obtained from analyzing the well logs. The reservoir properties calculated are shown below in Table 6.1 for the Runway Formation and in Table 6.2 for the Vineyard Formation.

Table 6.1. Calculated reservoir properties from the Runaway Formation

Well#	Well	Gross (ft)	Net (ft)	NGR	Porosity	Sw	K (md)	HPV (ft)
2	ASHEB3	69.54	67.00	0.96	0.08	0.46	0.05	2.92
8	ASHEC6	78	67.5	0.870	0.17	0.32	0.01	7.7
12	BY11	75	7	0.090	0.09	0.4	0.12	0.37
13	BY13	72	43.5	0.600	0.18	0.4	0.36	4.96
14	BY15	70	32	0.460	0.19	0.36	0.5	4.27
15	BY18D	73	35	0.480	0.12	0.32	0.1	3.05
19	CY9	53	25.5	0.480	0.15	0.44	0.11	2.12

Table 6.2. Calculated reservoir properties from the Vineyard Formation

Well#	Well	Gross (ft)	Net (ft)	NGR	Porosity	Sw	K (md)	HPV (ft)
8	ASHEC6	135.5	108.5	0.8	0.15	0.35	0.01	10.66
12	BY11	117	16.5	0.14	0.08	0.34	0.23	0.99
13	BY13	120	24	0.2	0.11	0.33	0.22	1.83
14	BY15	116	25	0.22	0.12	0.24	0.17	2.4
19	CY9	112.1	39	0.35	0.13	0.29	2.2	3.61
24	IGY9A	132.6	94	0.71	0.16	0.34	0.02	9.82

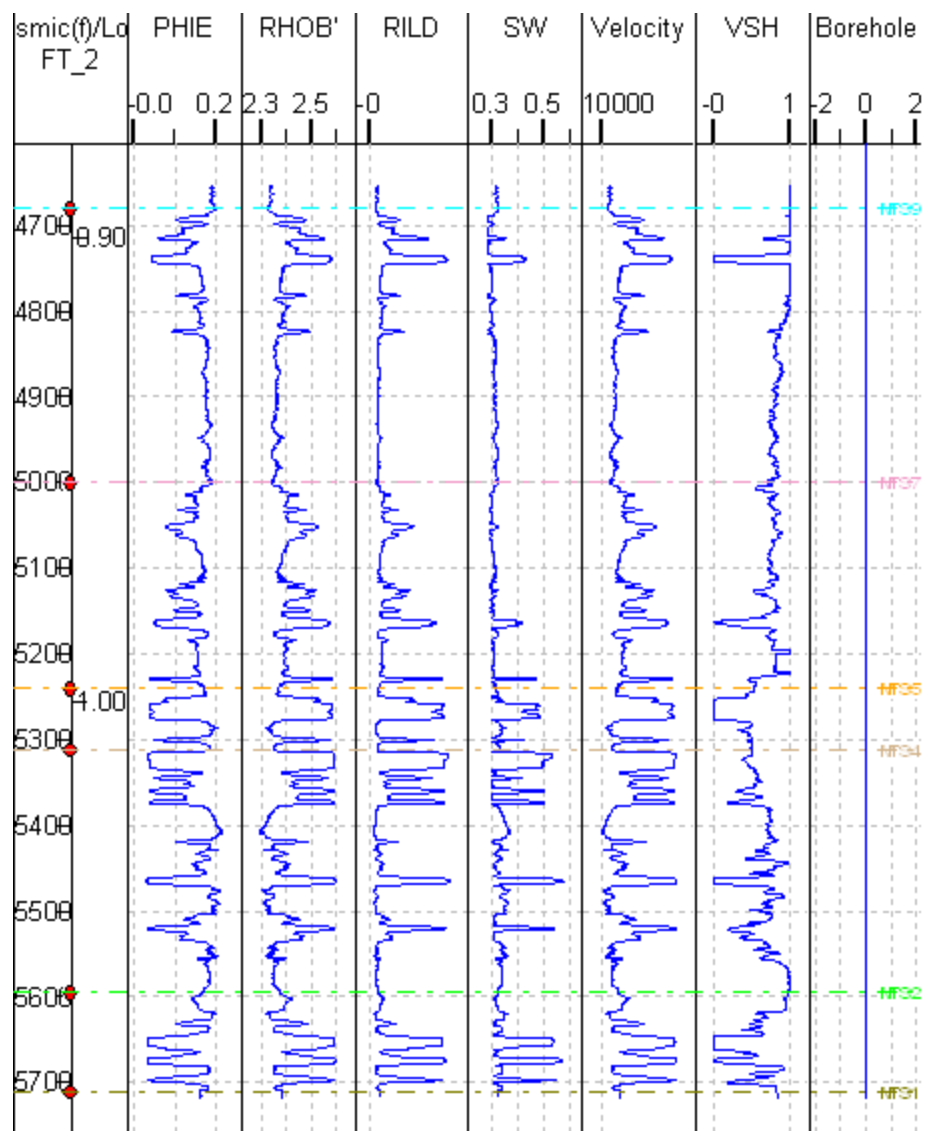


Figure 6.3. Logs generated from the Rt (RILD) log of the Well 2.

The petrophysical parameters describe the reservoir properties and can be used for the volumetric calculation. They are either collected from the Boonsville field data set, or calculated using the SMT Kingdom suite. Following are a list of these reservoir properties:

6.3.1. Volume of Shale (Vsh). The Vsh is an important parameter in petrophysical analysis. It indicates the lithology of the rock. SP log was used to calculate Vsh. Equation (4) below expresses the relationship between Vsh and the SP log (Asquith and Kryqowski, 2004).

$$V_{sh} = (SP - SP_{cln}) / (SP_{sh} - SP_{cln}) \quad (4)$$

Where SP is the spontaneous potential (in millivolts), SP_{cln} is the spontaneous potential within clean interval which is estimated 7% cut off (in millivolts), and SP_{sh} is the spontaneous potential within shale interval estimated 10% cut off (in millivolts) (Figure 6.4). Vsh logs generated are shown in Figures 6.3, 6.5 and 6.6.

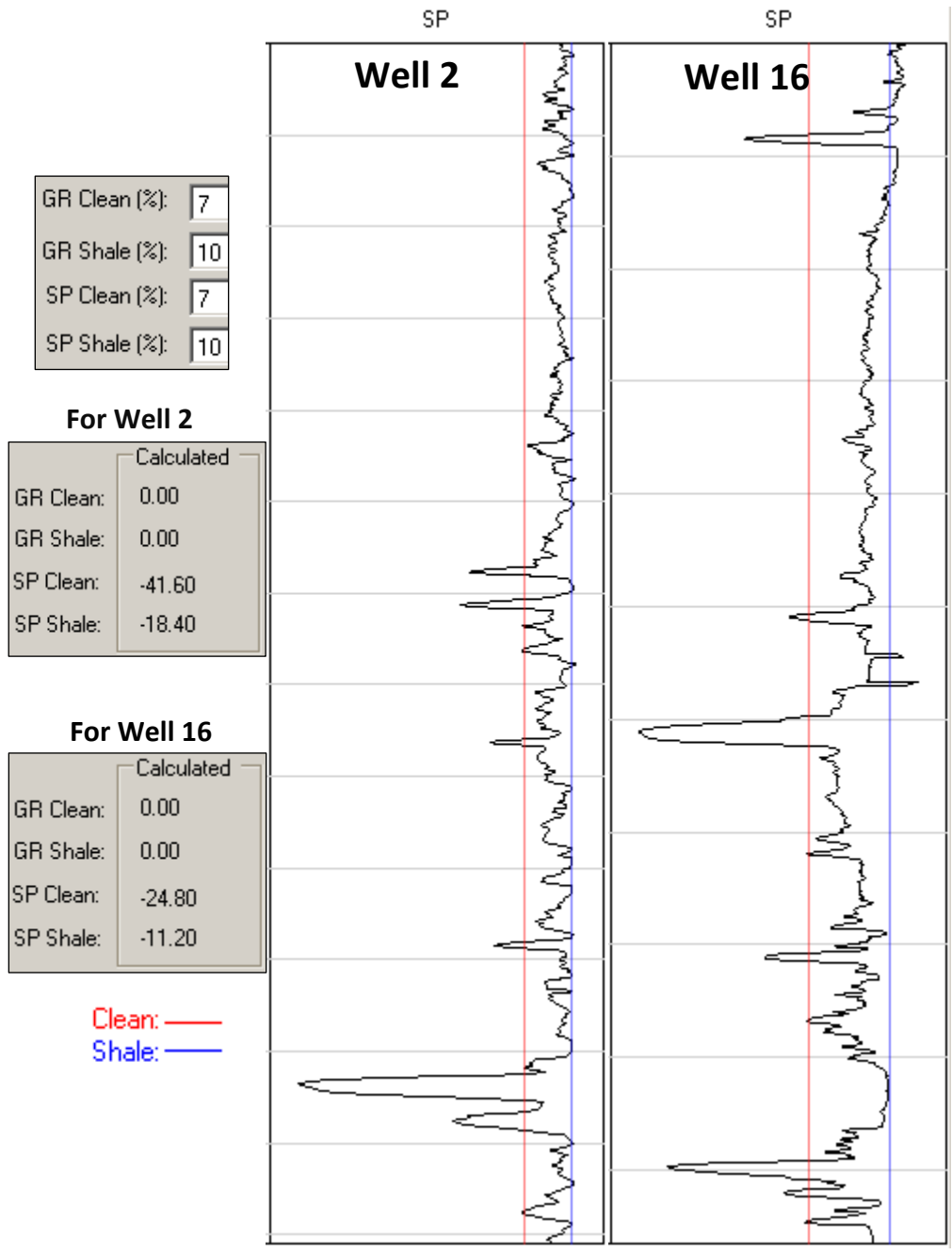


Figure 6.4. SP logs for the Wells 2 and 16 showing examples for calculating the SP_{cln} by 7% cut off and calculating SP_{sh} by 10% cut off.

6.3.2. Net to Gross Ratio (NGR). NGR is the ratio between Gross and Net pays.

Gross pay is the thickness between the upper and lower layers. Net pay is the total thickness of zones satisfying conditions of productive formations. NGR is useful to calculate the pore volume or the net volume (PV). PV is the total volume of the effective pores in the reservoir (Djebbar and Erle, 2004).

6.3.3. Porosity (Φ). Porosity expresses the fraction of the rock pore volume (PV) over the bulk volume (BV). The most important type of porosity is the effective porosity (Φ_e) which measures the connectivity of voids of the rock (Figures 6.5 and 6.6). The density logs are useful for porosity calculation. First, velocity logs were estimated using the Faust relationship (Faust, 1953):

$$\text{Velocity} = C (D R_t)^{1/6} \quad (4)$$

Where $C = 1948$, a constant for English unite. R_t is the resistivity, and D is the corresponding depth. Then, density logs (RHOB) are generated using the velocity logs (Gardner, 1974):

$$\text{RHOB} = C_1 \text{Velocity}^{0.25} \quad (5)$$

Where $C_1 = 0.2295$, a constant depending on the rock type. Density porosity (PHID) can be calculated (Asquith and Kryqowski, 2004):

$$PHID = (RHOMA - RHOB) / (RHOMA - RHOF) \quad (6)$$

Where fluid density (RHOF) can be assumed as 1.0, and the matrix density (RHOMA) is 2.65 for sand. If density and neutron logs are available, the effective porosity log (PHIE) can be calculated (Asquith and Kryqowski, 2004). The relation is expressed as following:

$$PHIE = [(PHID + PHIN) / 2.0] \times (1 - Vsh) \quad (7)$$

Where PHID is the density porosity (in decimals), PHIN is the neutron porosity (in decimals), and Vsh is the shale volume (in decimals). In addition, porosity can be calculated from the sonic log (DLT) (Asquith and Kryqowski, 2004). It is called sonic porosity (PHIS) and is calculated in equation (8) below:

$$PHIS = [(DLT - DLTM) / (DLTF - DLTM)] \times C \quad (8)$$

Where DLT is the sonic travel time (in $\mu\text{s}/\text{ft}$), DLTM is the sonic travel time of the matrix which is $52.6 \mu\text{s}/\text{ft}$ for consolidated sandstone, DLTF is the sonic travel time of the fluid $190 \mu\text{s}/\text{ft}$, and C is a constant, which is 0.7 for gas and 0.9 for oil. PHIE logs generated are shown in Figures 6.3, 6.5 and 6.6.

6.3.4. Water Saturation (Sw). Sw is a ratio of the pore volume filled with water over the bulk volume. It can be obtained from the resistivity logs (Asquith and Kryqowski, 2004). Sw is expressed mathematically by the Archie equation:

$$S_w = \frac{A R_w}{\Phi^m R_t} \quad (9)$$

Where R_w is the resistivity of the formation water assumed to be 0.02 ohm-meter, R_t is the value from the resistivity log in ohm. A is the tortuosity factor which is 1, m is the cementation exponent which is 2, n is a constant varying from 1.8 – 2.5, commonly, it is 2.0. Sw generated is shown in Figures 6.3, 6.5 and 6.6.

6.3.5. Permeability (K). Permeability is the movement ability of fluids within the formation. The permeability log can be derived from the water saturation and the porosity using the Wyllie and Rose (1950) method (Asquith and Kryqowski, 2004):

$$K = C \frac{\Phi^3}{S_{w-irr}} \quad (10)$$

Where K is the permeability in millidarcies (md), C is 250 for medium gravity oils or 79 for dry gas, Φ is the porosity, and S_{w-irr} is the water saturation of a zone at irreducible water saturation.

6.3.6. Gas Formation Factor (Bg). Gas formation factor is the volume of gas in the reservoir occupied by a standard cubic foot of gas at the surface, which equals the volume at reservoir conditions per volume at standard conditions in SCF/ft³ (Djebbar and Erle, 2004).

$$B_g = \frac{35.5p}{zT} \quad (11)$$

Where p is the reservoir pressure in psi which can be estimated to be 1200 psi for the Boonsville field, Z is the Z factor or gas deviation factor (also known as compressibility factor estimated to be 0.78), T is the absolute temperature which is 460 + reservoir temperature in °F (150+460) = 610°. The calculated gas formation factor (Bg) is 89.2 SCF/ft³ for the Boonsville field.

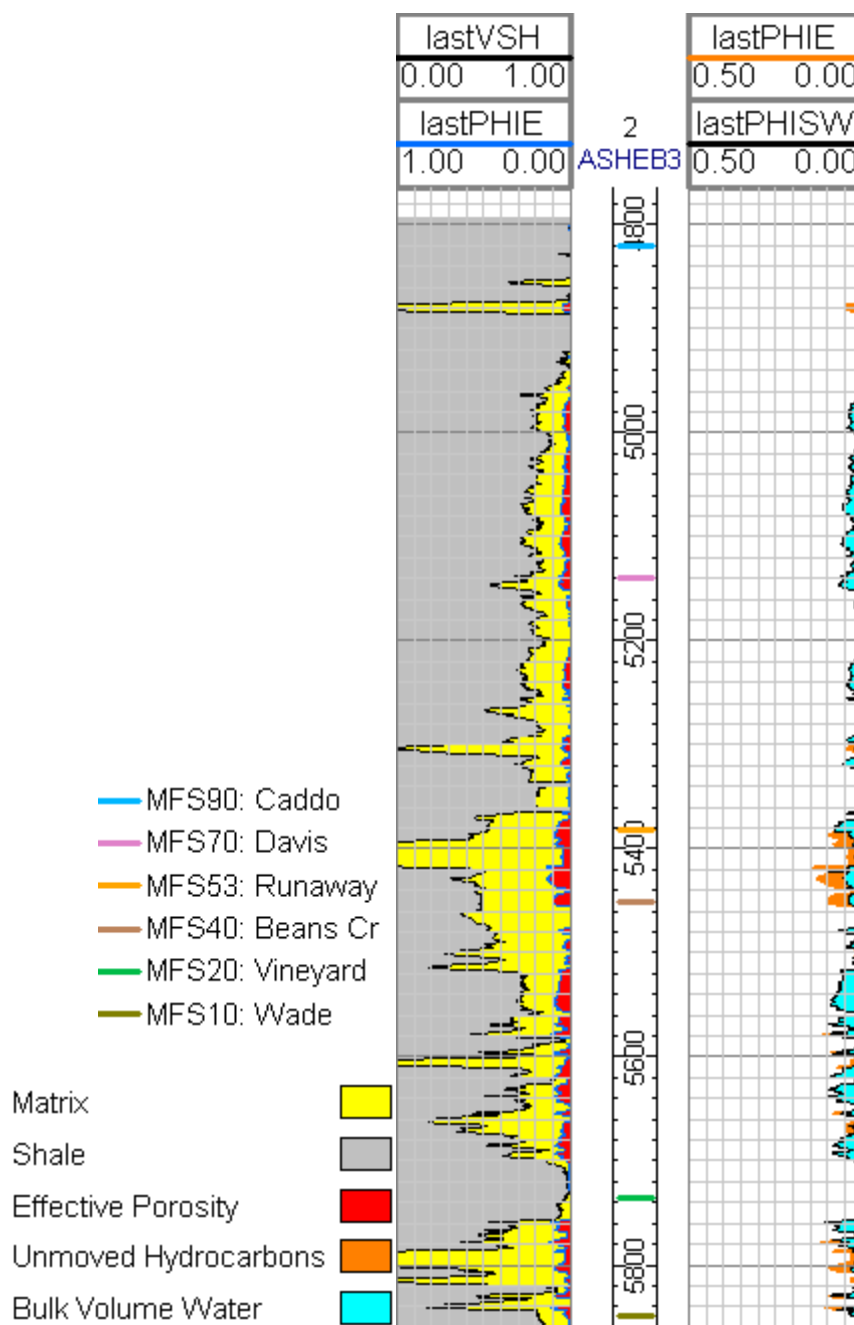


Figure 6.5. Well 2 logs generated from the petrophysical analysis showing the shale volume (Vsh) and effective porosity (PHIE). For the Runway Formation (between MFS53 and MFS40), the logs show good PHIE and unmoved hydrocarbons indicating a potential reserve near the Well 2.

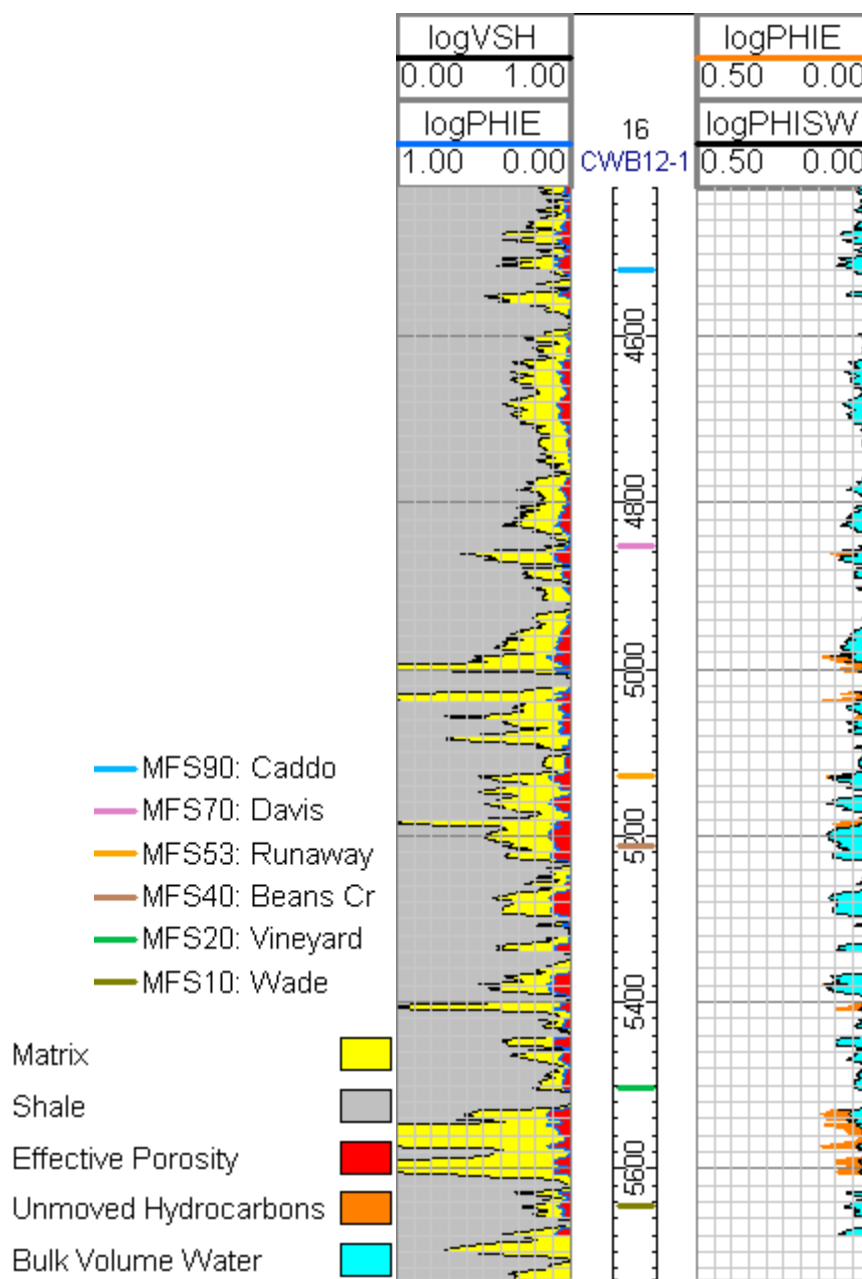


Figure 6.6. Well 16 logs generated from the petrophysical analysis showing the shale volume (Vsh) and effective porosity (PHIE). For the Vineyard Formation (between MFS20 and MFS10), the logs show good PHIE and unmoved hydrocarbons indicating a potential reserve near the Well 16.

6.4. VOLUMATRIC CALCULATION

The volumetric analysis provides an estimation of the hydrocarbon reserve in the targeted formation. To get a good understanding of the hydrocarbon potential of the Bend Conglomerate, volumetric prospect are calculated by obtaining the Recoverable Original Gas in-Place (ROGIP) in million cubic feet (MMCF) in the following equation (Djebbar and Erle, 2004):

$$\text{ROGIP} = 43,560 \text{ NV } \Phi_e (1-S_w) B_g \times \text{RF} \quad (11)$$

Where NV is the net volume, Φ_e is the effective porosity represented by PHIE, S_w is the water saturation, B_g is the gas formation factor, and RF is the recovery factor which is estimated to be 70% of the OGIP.

Both targeted formations, the Runaway and Vineyard, are potential reservoirs in the Bend Conglomerate. RMS amplitude maps are generated for both formations to get the best DHI bright spots and helps to identify the prospect area for both formations by correlating with the seismic interpretation and petrophysical analysis. The prospect for the Runaway and Vineyard Formations are indicated in Figures 6.2 and 6.3, respectively. The isopach grid Lower Cut Off (LCO) assumed to be 35 ft for the Runaway Formation and 40 ft for the Vineyard Formation. LOC is used to optimize the Gross Volume (GV) of the areas identified in the polygons in Figures 6.2 and 6.3, to the estimated lower cut off. Table 6.3 shows the calculated average reservoir properties and petrophysical parameters used for the volumetric calculation.

Table 6.3. Petrophysical parameters calculated for both Runaway and Vineyard Formations

Formation	Area (Acre)	LCO (ft)	$\overline{\text{NGR}}$	$\overline{\text{PHIE}}$	$\overline{\text{Sw}}$	Bg
Runaway	184.269	35	0.497	0.157	0.259	89.20
Vineyard	382.697	40	0.40	0.12	0.32	89.20

In order to conduct the reservoir volumetric calculation, the estimated values for the Gross Volume (GV), Net Volume (NV), Pore Volume (PV), Hydrocarbon Pore Volume (HPV), OGIP, and ROGIP are needed. The volumetric calculation results are shown in Table 6.4.

Table 6.4. The results of the volumetric calculations for both Runaway and Vineyard Formations. mega (M) = 10^3 , million (MM) = 10^6 , billion (B) = 10^9

Formation	Grid Area (Acre)	GV (Acre ft)	NV (Acre ft)	PV (Acre Ft)	HPV (Acre ft)	OGIP (SCF)	ROGIP (SCF)
Runaway	183	6.69 M	3.28 M	491.60	363.78	1.41 B	989.44 MM
Vineyard	364	36.92 M	14.88 M	1.78 M	1.22 M	4.75 B	3.32 B

7. CONCLUSION

This study is an integrated interpretation of the Boonsville field data set. The results are summarized as following:

1. Structural interpretation yields valuable depth maps of the Caddo, Runaway, and Vineyard. These structural depth maps help to identify traps and anticlines over both Runaway and Vineyard Formations. The study supported previous studies by suggesting that the Ellenberger karst collapse features have critical role in hydrocarbon migration from the Barnett Shale (source rock). The depth maps visualize the distribution of these collapses in the Runaway and the Vineyard Formations. The anticlines, that are close to the karst collapse features, are most likely high potential reserve areas. In addition, the depth maps show that the structures of the Bend are altering the dipping direction from dipping toward east at the bottom to dipping toward north at the top of Caddo.
2. Stratigraphic interpretations are conducted by correlating the amplitude maps, isopach maps, and well logs. The isopach maps were generated for the Runway and Vineyard to show the thickness of the formations over the area of study. The horizon slices suggest some channels, point bars, and a mouth bar. Well log correlations were performed to verify the suggested stratigraphic features.

3. For the reservoir identification, RMS amplitude maps were generated for the Runaway and Vineyard Formations. In addition, petrophysical approaches were implemented to calculate the following reservoir properties: the gross, net pay, NGR, water saturation, shale volume, porosity, and gas formation factor. Integrated analysis of the depth maps, isopach maps, horizon slices, well logs, and petrophysical data, gives a good identification of the hydrocarbon spots for both targeted formations. Finally, volumetric prospect calculations were conducted to estimate the Recoverable Original Gas in-Place (ROGIP). The Runaway Formation prospect shows a potential gas amount of 989.44 MMSCF. The Vineyard Formation prospect shows a potential gas amount of 3.32 BSCF. These values of ROGIP for both formations suggest that the Boonsville field clastic formations of the Bend have a great potential for further production and development.

BIBLIOGRAPHY

- Asquith, G., and D. Krygowski, 2004, Basic well log analysis, second edition, *American Association of Petroleum Geologist and Society of Exploration Geophysics, Methods in Exploration*, 244 p.
- Carr, D. L., R. Y. Elphick, R. A. Johns, and L. S. Foulk, 1997, High-resolution reservoir characterization of mid-continent sandstones using wireline resistivity imaging, Boonsville (Bend Conglomerate) gas field, Fort Worth Basin, Texas, *The Log Analyst*, v. 38, p. 54–70.
- DeCelles, P. G., and K. A. Giles, 1996, Foreland basin systems, *Basin Research*, v. 8, p. 105–123, doi: 10.1046/j.1365-2117.1996.01491.x.
- Djebbar, T., and D. Erle, 2004, Petrophysics, second edition, *Elsevier Inc*, 890 p.
- Faust, L. Y., 1953, A velocity function including lithological variation, *Geophysics*, v. 18, p. 271 – 88.
- Galloway, W. E., 1989, Genetic stratigraphic sequences in basin analysis; I, Architecture and genesis of flooding-surface bounded depositional units, *AAPG Bulletin*, v. 73/2, p. 125-142.
- Hardage, B. A., 1996, Boonsville 3-D data set, *The Leading Edge*, v. 15, no. 7, p. 835–837, doi:10.1016/0191-8141 (85)90048-3.
- Hardage, B. A., D. L. Carr, D. E. Lancaster, J. L. Simmons Jr., R. Y., Elphick, V. M. Pendleton, and R. A. Johns, 1996a, 3-D seismic evidence of the effects of carbonate karst collapse on overlying clastic stratigraphy and reservoir compartmentalization, *Geophysics*, v. 61, p. 1336–1350, doi:10.1190/1.1444057.
- Hardage, B. A., D. L. Carr, D. E. Lancaster, J. L. Simmons Jr., D. S. Hamilton, R. Y. Elphick, K. L. Oliver, and R. A. Johns, 1996b, 3-D seismic imaging and seismic attribute analysis of genetic sequences deposited in low-accommodation conditions, *Geophysics*, v. 61, p. 1351–1362, doi:10.1190/1.1444058.
- Hardage, B. A., J. L. Simmons Jr., D. E. Lancaster, R. Y. Elphick, R. D. Edson, and D. L. Carr, 1996c, Boonsville 3-D seismic data set, *Austin, Texas, University of Texas at Austin, Bureau of Economic Geology*, 40 p.

- Hentz, T. F., J. A. Kane, W. A. Ambrose, and E. C. Potter, 2006, Depositional facies, reservoir distribution, and infield potential of the lower Atoka Group (Bend Conglomerate) in Boonsville field, Fort Worth Basin, Texas: New look at an old play (abs.), *AAPG Annual Convention Abstracts Volume*, v. 15, p. 46.
- Hentz, T. F., E. C. Potter, and M. A. Adedeji, 2007, Reservoirscale depositional facies, trends, and controls on sandstone distribution of the lower Atoka Group (“Bend Conglomerate”), Fort Worth Basin, Texas (abs.), *AAPG Annual Convention Abstracts Volume*, v. 16, p. 62.
- Hill, R. J., D. M. Jarvie, J. Zumberge, M. Henry, and R. M. Pollastro, 2007, Oil and gas geochemistry and petroleum systems of the Fort Worth Basin, *AAPG Bulletin*, v. 91, no. 4, p. 445–473, doi:10.1111/j.1365-3091.2004.00628.x.
- IHS Energy, Inc., 2011, U.S. production and well history control databases, *Englewood, Colorado*, CD-ROM.
- Maharaj, V. T., and L. J. Wood, 2009, A quantitative paleogeographic study of the fluvio-deltaic reservoirs in the Atoka interval, Fort Worth Basin, Texas, U.S.A., *Gulf Coast Association of Geological Societies Transactions*, v. 59, p. 495–509.
- Martin, C. A., 1982, Petroleum geology of the Fort Worth Basin and Bend Arch area, *Dallas Geological Society*, 442 p.
- McDonnell, A., R. G. Loucks, and T. Dooley, 2007, Quantifying the origin and geometry of circular sag structures in northern Fort Worth Basin, Texas: Paleocave collapse, pull-apart fault systems, or hydrothermal alteration?, *AAPG Bulletin*, v. 91, p. 1295–1318, doi:10.1306/05170706086.
- Pollastro, R. M., 2003, Geologic and production characteristics utilized in assessing the Barnett Shale continuous (unconventional) gas accumulation, Barnett-Paleozoic total petroleum system, Fort Worth Basin, Texas, *Barnett Shale Symposium, Ellison Miles Geotechnology Institute at Brookhaven College, Dallas, Texas, November 12–13, 2003*, 6 p.
- Pollastro, R. M., R. J. Hill, D. M. Jarvie, and C. Adams, 2004, Geologic and organic geochemical framework of the Barnett-Paleozoic total petroleum system, Bend arch–Fort Worth Basin, Texas (abs.), *AAPG Annual Meeting Program*, v. 13, p. A113, CD-ROM.
- Pollastro, R. M., D. M. Jarvie, R. J. Hill, and C. W. Adams, 2007, Geologic framework of the Mississippian Barnett Shale, Barnett-Paleozoic total petroleum system, Bend arch–Fort Worth Basin, Texas, *AAPG Bulletin*, v. 91, no. 4, p. 405–436, doi:10.1306/10300606008.

- Thomas, J. D., and W. Texas, 2003, Integrating synsedimentary tectonics with sequence stratigraphy to understand the development of the Fort Worth basin, *AAPG Search and Discovery*, Article #90023
- Thompson, D. M., 1982, Atoka Group (Lower to Middle Pennsylvanian), Fort Worth Basin, Texas: Terrigenous depositional systems, diagenesis, and reservoir distribution and quality, *University of Texas at Austin, Bureau of Economic Geology Report of Investigations*, v. 125, 62 p.
- Thompson, D. M., 1988, Fort Worth Basin, in L. L. Sloss, ed., Sedimentary cover—North American Craton: U.S., *Geological Society of America, Decade of North American Geology Series*, v. D-2, p. 347–352.
- Walper, J. L., 1982, Plate tectonic evolution of the Fort Worth Basin, in C. A. Martin, ed., Petroleum geology of the Fort Worth Basin and Bend arch area, *Dallas Geological Society*, p. 237–251.

VITA

Name: Aamer Alhakeem

Nationality: Saudi

Phone: +1(573)578-9136, +966541424004

Email: alhakeem.a@gmail.com

In 2013, I received a Master of Science degree in Geology and Geophysics at Missouri University of Science and Technology (MST). In 2007, I completed B.S. Degree in Geophysics from King Fahd University of Petroleum and Minerals (KFUPM).

During my Master degree, I have been doing a thesis research of 3D Seismic Interpretation of the Boonsville field using Kingdom Suite Software. At KFUPM, I was elected president of the Earth Science Student Committee. As a geosciences committee, we participated in many activities related to different fields such as, Geology, Geophysics, Environmental Sciences and Petroleum Engineering

My practical experience involved joining EniRepSa Gas Ltd. (Eni-50%, Repsol-30%, Aramco-20%). I worked in EniRepSa as Jr. Drilling Engineer after spending six weeks in ENI Indonesia earning drilling engineering courses. Moreover, I joined Saudi Aramco for summer training program, where I was exposed to the technical work environment of Geophysics and Geology.

